CYLINDRICAL THERMAL CONTACT CONDUCTANCE

A Thesis

by

GEORGE HAROLD AYERS

Submitted to the Office of Graduate Studies of
Texas A&M University
in partial fulfillment of the requirements for the degree of

MASTER OF SCIENCE

August 2003

Major Subject: Mechanical Engineering

CYLINDRICAL THERMAL CONTACT CONDUCTANCE

A Thesis

by

GEORGE HAROLD AYERS

Submitted to Texas A&M University
in partial fulfillment of the requirements
for the degree of

MASTER OF SCIENCE

Approved as to Style and Content by:

L. S. Fletcher (Chair of Committee)	N. K. Anand (Member)
J. A. Caton (Member)	Y. A. Hassan (Member)
D. L. O'Neal (Head of Department)	

August 2003

Major Subject: Mechanical Engineering

ABSTRACT

Cylindrical Thermal Contact Conductance. (August 2003)

George Harold Ayers, B.S., Arizona State University;

M.S., Arizona State University

Chair of Advisory Committee: Dr. L. S. Fletcher

Thermal contact conductance is highly important in a wide variety of applications, from the cooling of electronic chips to the thermal management of spacecraft. The demand for increased efficiency means that components need to withstand higher temperatures and heat transfer rates. Many situations call for contact heat transfer through nominally cylindrical interfaces, yet relatively few studies of contact conductance through cylindrical interfaces have been undertaken. This study presents a review of the experimental and theoretical investigations of the heat transfer characteristics of composite cylinders, presenting data available in open literature in comparison with relevant correlations.

The present investigation presents a study of the thermal contact conductance of cylindrical interfaces. The experimental investigation of sixteen different material combinations offers an opportunity to develop predictive correlations of the contact conductance, in conjunction with an analysis of the interface pressure as a function of the thermal state of the individual cylindrical shells. Experimental results of the present study are compared with previously published conductance data and conductance models.

ACKNOWLEDGMENTS

I would like to acknowledge my appreciation to the many people who assisted this thesis:

Mr. Gerry Harrison of TTI installed the strain gages on the test pieces. Mr. Gene Ripa and Mr. Dewey Christy of the Mahr-Federal, Inc. respectively facilitated and provided the necessary surface metrology data of the test pieces. Mr. Claude Davis of Corning, Inc. obtained the thermophysical properties of the Ultra Low Expansion Titanium Silicate glass used as thermal expansion standard. The engineers at National Instruments provided some much-needed advice and software for programming the data acquisition system. The TAMU Physics Machine Shop provided design advice and a couple of last-minute cylindrical shells. Dr. Thomas Walther of the TAMU Department of Physics made a gracious loan of diode laser equipment. Dr. Henry Taylor and Mr. Jong-Seo Lee of the TAMU Electrical Engineering Department loaned their expertise to the problem of measuring the interface pressure. Dr. Thomas Kozik of the TAMU Mechanical Engineering Department and Dr. Pedro Peralta of the ASU Department of Mechanical and Aerospace Engineering discussed the details of the interface pressure calculation. Ms. Heather Walker provided invaluable administrative assistance, as well as the occasional trip to the grocers. The faculty and staff of the Department of Mechanical Engineering offered cheerful advice and encouragement.

The students of the TAMU Conduction Heat Transfer Laboratory, Michael Lambert, Egidio Marotta, Srinivas Mirmira, Eric Simonson, Ivan Cavinall, Hugh Jamison, Matt Fischer, and others, offered advice, discussion, and comradeship. The present and former members of my advisory committee (Dr. Nagamangala Anand, Dr. Jerald Caton, Dr. Anne Chin, Dr. Leroy S. Fletcher, Dr. Yassin Hassan, Dr. George Peterson) gave me

advice and encouragement, as well as the commitment of time. I would like to especially thank my academic advisor, Dr. Leroy S. Fletcher, for his support and encouragement, as well as those lessons not taught in the classroom.

Bob and Peggy Holzweiss, David and Monique Reed, Ysidoro Ramirez, Hatcher Tynes, Ray Piazza, Kang-Hoon Ko, and other friends too numerous to mention, provided sound advice, a chance to experience the "other education," and the occasional clue-by-four. I would be a much poorer person without them. Deacon Bill and Estelle Scott went beyond the expected and opened their home and their hearts to me. My debt to them is beyond calculation. The community at St. Mary's Catholic Center in College Station, especially Fr. Michael Sis, Fr. David Konderla, Fr. Dean Wilhelm, Deacon Bill Scott, and Deacon David Reed provided an environment of faith, an opportunity to grow, and a place of fellowship.

My family, especially my mother and father, gave me moral support, encouragement, and a firm grounding in reality.

Finally, I thank the Creator for this life and the many possibilities it presents.

TABLE OF CONTENTS

CHAPTER Page

LIST OF FIGURES

Page

Page

LIST OF TABLES

Page

NOMENCLATURE

A	correlation constant; integration constant; macroscopic contour area
a	inner radius; microcontact spot radius
AA	interface pressure calculation term
B	correlation constant; radius of apparent macrocontact area
b	interface radius; least-squares intercept; microcontact flux tube radius
BB	interface pressure calculation term
C	integration constant
c	outer radius
CC	interface pressure calculation term
C_i	model parameter (cf. Madhusudana, 1986)
cp	specific heat
C_p	specific heat at constant pressure
C_v	specific heat at constant volume
D	integration constant
d	Vickers indention diameter
DD	interface pressure calculation term
DI	interface pressure calculation term
DII	interface pressure calculation term
d_o	tube outer diameter
E	Young's modulus; elastic modulus
E'	Hertzian elastic modulus
EE	interface pressure calculation term

F()	eigenfunction
f()	function; interface heat flux distribution (c.f. Wang and Nowak, 1982)
FF	interface pressure calculation term
fpi	linear fin density (typically fins per inch)
GG	interface pressure calculation term
h	conductance
H	microhardness
HH	interface pressure calculation term
I	tube expansion; interference
II	interface pressure calculation term
J_0	Bessel's function of the first kind, 0th order
JJ	interface pressure calculation term
k	thermal conductivity; eigenvalue
ka*	slope alignment parameter
KK	interface pressure calculation term
KM	Kline-McKlintock Operator (Appendix E)
L	fin collar length; length; load
l	length
LA	longitudinal thermal expansion calculation term
LB	longitudinal thermal expansion calculation term
LC	longitudinal thermal expansion calculation term
LL	interface pressure calculation term
m	asperity slope; least-squares slope
MM	interface pressure calculation term
n	expected number of contact spots

N_{uc}	joint conductance
P	pressure
Pr	Prandtl number
Q	heat rate
q	heat rate
q”	heat flux,
r	radius; radial position; radial displacement along surface from center of axisymmetric contact
R	thermal resistance; sphere radius; Pearson’s r
R_i	inside thermal resistance (including film and fouling)
R_o	outside thermal resistance (including film and fouling)
t	fin thickness
T	temperature
TIR	Total indicated reading,
T_o	fabrication temperature for fin and tube
u	mean plane separation
u(r)	radial displacement
u_c	initial interference at interface
w(z)	axial displacement, compliance or deformation due to load
x	arbitrary variable
XP	modified dimensionless pressure
XQ	modified dimensionless interface heat flux
y	arbitrary variable
Y	mean plane separation
z	axial direction

Greek

α	accommodation parameter; coefficient of thermal expansion; real effective contact radius
β	fluid parameter
δ_i	casing thickness; flatness deviation
δr_i	nominal interface clearance
ε	strain
Φ	difference of thermal expansion integrals
Φ_L	longitudinal thermal expansion term
ϕ_a	contact spot half-angle (c.f. Wang and Nowak, 1982)
ϕ_b	half-angle > ϕ_a (c.f. Wang and Nowak, 1982)
φ	thermal constriction parameter
Λ	molecular mean free path
λ	eigenvalue; thermal conductivity
μ	parameter (cf. Gardner and Carnavos, 1960)
ν	Poisson's ratio
θ	circumferential; circumferential position, circumferential distance
ρ	density; parameter (c.f. Gardner and Carnavos, 1960); radius of curvature
σ	roughness; stress
τ	shear stress
ξ	waviness number (c.f. Thomas and Sayles, 1974)
ψ	thermal constriction parameter
Ψ_G	plasticity index (c.f. Greenwood, 1967)
ζ	elastic conformity modulus (c.f. Clausing and Chao, 1964)

Subscripts, Superscripts, and Accents

¯	averaged
^	thermally deformed
‘	deformed; Effective; contour
°	zero-flux condition
a	ambient; inside radius of inner cylinder; actual; average
A	outer cylindrical shell
app	apparent
atm	atmospheric
b	fin base; interface radius
B	inner cylindrical shell
c	outside radius of outer cylinder, contact
e	effective
f	fin
gap	interstitial gap
go	gas gap thermal conductivity
i	inside, interior, interface
I	Case I
II	Case II
III	Case III
j	joint
L	longitudinal; large scale
M	Mechanical
m	Meyer (microhardness)
NIST	National Institute of Standards and Technology

o	original (fabrication); outer; outside
ps	pre-stressed
r	radial
rad	radiation
rms	root mean square
s	harmonic mean
S	reference state; small scale
T	thermal
t	tube
T/C	thermocouple
v	Vickers (microhardness)
x	derivative with respect to x
z	Axial/Longitudinal direction
α	thermal expansion coefficient
θ	circumferential

CHAPTER I

INTRODUCTION

The conduction of heat through homogeneous, isotropic materials has been well understood since the time of Fourier (1822). The conduction of heat across interfaces formed by contacting surfaces is less understood, especially since this phenomenon has received little attention until the investigations of Holm (1929) and Roess (1948). In many circumstances the rate of heat transfer through contacting components must be known and controlled to facilitate reliability and to prolong component life.

Thermal contact conductance is highly important in such applications as heat rejection from electronic components, cooling gas turbine blades, enhancement of heat transfer through duplex and shrink-fit finned tubes, and thermal management of space-borne systems. In many cases, the demand for increased efficiency means that components need to withstand higher temperatures and heat transfer rates. Gas turbines operate more efficiently at higher gas temperatures, so effective control of blade temperatures without the costs incurred by actively cooling the blades is very important. Nuclear power generators operate more efficiently at higher heat rates, so enhancing the rate of heat transfer across the junction of the fuel and sheathing allows these higher heat rates to be sustained without the risk of melting or cracking the fuel. Integrated circuits, which are becoming more and more densely packed, have higher power requirements and rely on contact conduction to transfer waste heat from internal components to external surfaces where it can be dissipated. While spacecraft rely upon radiation heat transfer to reject excess heat, conduction heat transfer is the primary means of moving heat to the

---

This thesis follows the style and format of the *Transactions of the ASME: Journal of Heat Transfer*.

thermal radiation systems to maintain appropriate temperature levels for component and personnel modules. Modern artillery and cannon barrels, made of shrink-fit composite cylinders, must withstand the transient pressures and high temperatures of firing and conduct waste heat through the cylindrical shells to the ambient air quickly enough to maintain strength and component life (Throop, et al. (1982), Underwood, et al. (1988), Endersby, et al. (1996)).

THERMAL CONTACT CONDUCTANCE

Surfaces that appear to be smooth are actually composed of microscopic asperities and depressions that deviate from an apparently smooth surface (Figure 1.1). Generally, the microscopic deviations are termed roughness and the macroscopic deviations are termed waviness. When two surfaces are in contact with each other, the actual area of contact is much smaller than the apparent area of contact. These areas of actual contact occur where the asperities of one surface are in contact with the asperities of the other surface. The number of these contact spots is further reduced when surface waviness and errors in form are taken onto account. Typically, there is some material or fluid in the interstitial spaces between the contacting surfaces, and heat is transferred through this interstitial material. If there are no interstitial materials or fluids, then most of the heat

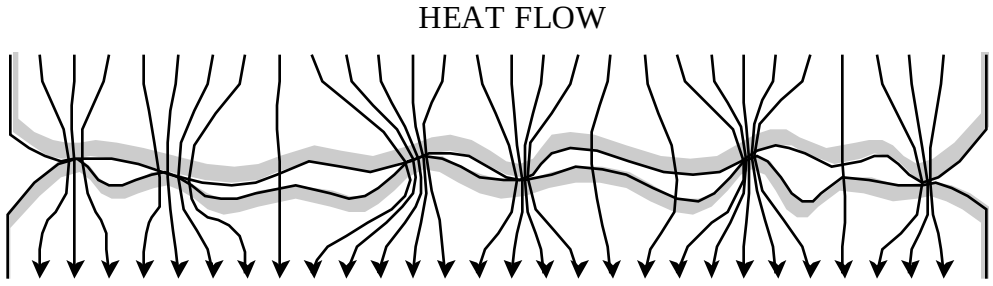

Figure 1.1 – Constriction of heat flow through an interface formed by two materials.

transferred across the interface formed by the two surfaces is transferred through these small contact spots. The amount of actual contact area is also dependent on the physical properties of the contacting materials. If one of the materials is softer than the other, then the asperities of the harder material are likely to penetrate the surface of the softer material and increase the contact area. At higher pressures, one would expect that the penetration of these asperities would increase. In the case of materials of nearly the same hardness, the asperities would deform, and one might expect that the amount of deformation would increase with pressure. Interfaces with a higher mean thermal conductivity would be expected to have a lower resistance to heat transfer than those interfaces that have lower mean thermal conductivities.

This limited contact area constricts the flow of heat to a few channels at the interface between the materials, making the temperature distribution in the vicinity of the interface complex and three-dimensional. An approximation to this complex temperature

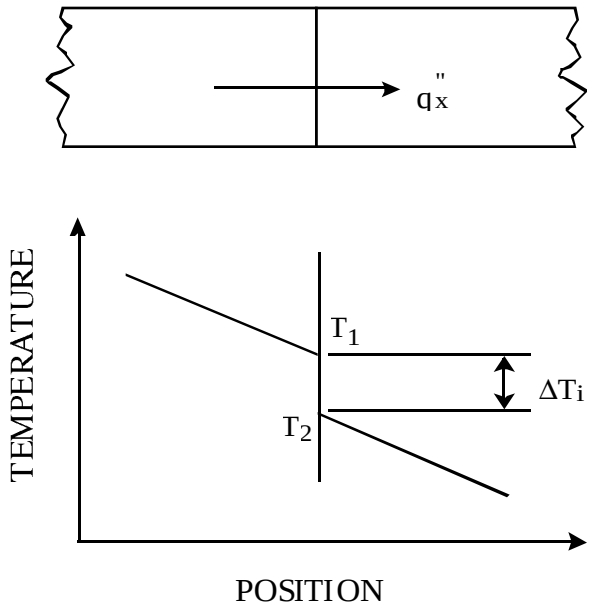

Figure 1.2 – Effect of constriction resistance on one-dimensional temperature distribution for flat interfaces.

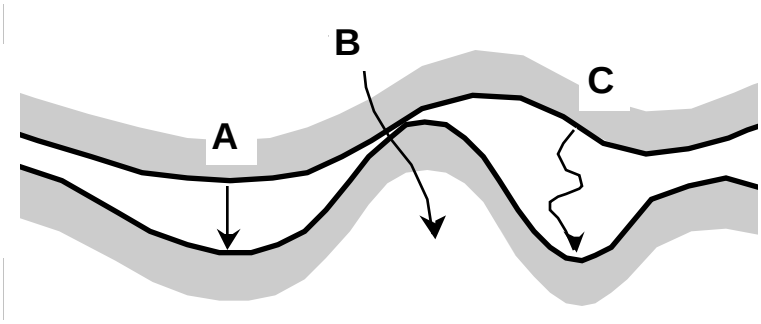

Figure 1.3 – Heat transfer paths at an interface: A) conduction through interstitial material, B) conduction at contact spot, C) radiation across interstitial space.

distribution is to assume a temperature discontinuity at the interface, with the associated temperature drop determined by the temperature distribution on either side of the interface (Figure 1.2). This temperature discontinuity is proportional to the heat flux through the interface, with the proportionality constant called the thermal contact conductance, h_c, defined in terms of the temperature drop across the interface and the heat flux through the interface. The phenomenon is further complicated when the surfaces that form the interface are not conforming, flat, or smooth.

Heat is transferred across interfaces formed by contacting surfaces through some combination of three paths (Figure 1.3): conduction through contacting spots, conduction across the interstitial space through interstitial material (if any), and radiation across the interstitial spaces (provided that the interstitial material is not opaque to thermal radiation). Convection within the interstitial fluid is not generally taken into account, as the thickness of the interstitial space is on the order of roughness and does not lend itself to bulk fluid motion. Thus, we express the heat transfer rate through the joint as the sum of the heat transferred through the contact spots and the heat transferred through the interstitial gap:

$$q_j = q_c + q_{gap} + q_{rad} \tag{1.1}$$

The radiative heat flux across the interface may be neglected if the interstitial material is opaque to infrared radiation or if the interface temperature level is less than 300 ˚C (Madhusudana, 1996). This is justified since even moderate temperature differences at that temperature level yield radiative heat rates that are much smaller than the total heat transfer through the joint.

Neglecting the contribution of thermal radiation, the heat transfer rates in Equation 1.1 can be linked to the temperature difference between the two surfaces by means of proportionality constants, or conductances:

$$h_j \equiv \frac{q_j}{A_{app}\,\Delta T_j}, \quad h_c \equiv \frac{q_c}{A_{app}\,\Delta T_j}, \quad h_{gap} \equiv \frac{q_{gap}}{A_{app}\,\Delta T_j} \tag{1.2}$$

Thus, the total heat transfer across the junction (Equation (1.1)) can be expressed as:

$$Q_j = h_j\,A_{app}\,\Delta T_j = \left(h_c + h_{gap}\right) A_{app}\,\Delta T_j \tag{1.3}$$

These conductances are often nondimensionalized with the harmonic mean roughness, the effective conductivity of the joint, and the average slope of the asperities of the rougher surface.

An appropriate predictive model of the thermal contact conductance should take into account the geometry of the interface. Thus, in addition to the thermophysical properties of the materials that define the interface, geometric parameters must be considered. These include microscopic scale parameters like roughness, waviness, and asperity shape (in the form of the asperity slope), and macroscopic parameters such as the radius of curvature at the macroscopic contact spots.

Additionally, the model should take into account the effects of the mechanical and thermal state at the interface (Fletcher, 1971). The conductance should approach an infinite vale as pressure increases to infinity and approach a zero value as the pressure decreases to

zero. The conductance should increase as the mean junction temperature rises, and as heat transfer rate increases.

CYLINDRICAL JOINTS

While studies dealing with thermal contact conductance between flat surfaces are common, studies dealing with cylindrical contacts are limited, and those deal primarily with specific applications. Cylindrical contacts occur in such diverse applications as composite cylindrical tanks, space structures, power transmission lines, electronic devices, nuclear fuel elements, air conditioning systems, and pipelines. As a consequence, conduction through cylindrical contacts is an important phenomenon to understand. While there are more studies devoted to thermal conduction through cylindrical contacts than there were a decade ago, this phenomenon is still rather under represented in the literature when one considers that cylindrical contacts are relatively common. In reviews of contact conductance literature (Fletcher (1988) and Madhusudana and Fletcher (1985)), approximately 5% of the contact conductance articles deal with cylindrical contacts.

Figure 1.4 illustrates the four different composite cylinder combinations of thick and thin shell geometries that can form a cylindrical interface. From a strength of materials point of view, a thin shell is defined as one whose thickness is less than one tenth the nominal radius (Shigley, 1972). Thin cylindrical shells are commonly found in such places as the cladding of superconducting wires, tension-wound finned tubes, and large diameter pipes. Thick cylindrical shells (including solid composite cylinders) may occur in such applications as nuclear fuel rods and composite pipes.

Cylindrical joints behave differently than flat joints. For heat transfer through flat contacts, pressure (although dependent on interface heat flux, interface temperature level, heat flow direction, interstitial fluid, surface condition, and the thermophysical properties of the materials that compose the joint) can be monitored and controlled independently of the

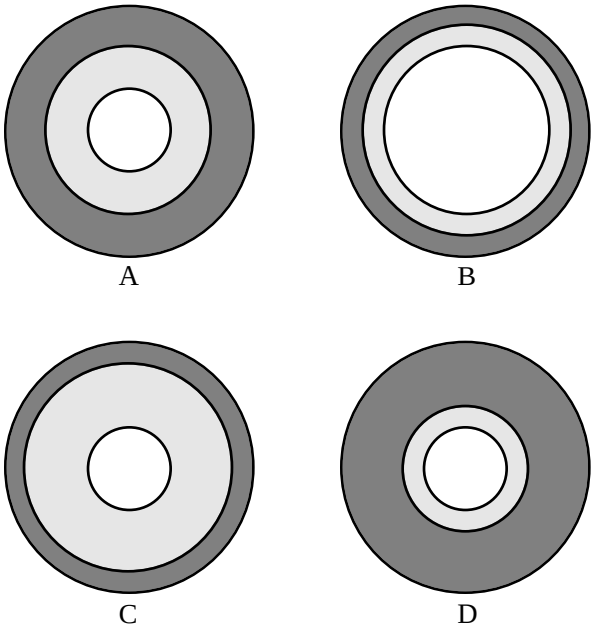

Figure 1.4 – Four different types of composite cylinders with inner-outer shell thickness combinations of: A) thick-thick, B) thin-thin, C) thick-thin, and D) thin-thick.

heat flux through the interface, and results are often presented in terms of conductance as a function of interface pressure. For cylindrical contacts (in addition to the aforementioned factors that influence interface pressure for flat surfaces) the interface pressure is also dependent on the initial degree of fit, the differential expansion of the cylinders due to the temperature difference at the interface, and the temperature distribution within the individual cylindrical shells.

The interface pressure, temperature distribution throughout the cylindrical shells, and the thermal contact conductance are interdependent – they all depend on the interface heat flux. Therefore, the heat flux is far more influential for cylindrical contacts than it is for flat contacts. Of the possible experimental test parameters, only the heat flux through the joint may be independently controlled. As a consequence, the experimental thermal contact conductance results for cylindrical contacts are often presented as a function of

interface heat flux, a function of calculated interface pressure, or a function of the temperature difference across one of the cylindrical shells.

In addition to surface irregularities such as waviness and roughness, conduction through cylindrical contacts involves other parameters such as out-of-roundness. Furthermore, placement of instrumentation for studies involving cylindrical contacts is more difficult than it is for flat contacts. It is probable that these additional complexities discourage investigations into thermal contact conductance of cylindrical contacts.

Additional parameters need to be considered in modeling as well. Since the pressure at the interface is not independent of the temperature distribution within the cylindrical shells, initial clearance/interference must be taken into account. Rather than depending on an assumption of isotropic roughness and waviness, the axial and circumferential roughness and waviness should be measured and geometrically averaged. Large-scale errors in form (cylindricity and roundness) should be accounted for when calculating the influence of the macroscopic contact spots.

Nevertheless, conduction through cylindrical contacts is increasingly important, and additional studies are warranted. The present study provides an overall review of the analytical and experimental studies of the thermal contact conductance of composite cylinders and associated configurations, and provides a comparison of existing experimental data and correlations, insofar as possible. Tabulations of previously published correlations, and figures demonstrating the range of available data in these categories are also presented.

OBJECTIVE

The objectives of this investigation include

- a review of current literature and models for cylindrical contact conductance,

- the development of empirical correlations of the cylindrical contact conductance as functions of interface heat flux and interface pressure,
- an experimental measurement of the thermal contact conductance between several selected pairs of cylindrical shells,
- an analysis of the coupling between the stress and thermal states of the cylindrical shells, in order to ascertain the pressure at the interface between the contacting cylindrical shells, and
- a comparison of the empirical correlations obtained in the present study with previously published and present experimental data.

CHAPTER II

LITERATURE REVIEW

Before making predictions of the thermal contact conductance at interfaces, it is necessary to have an adequate understanding of the mechanical and thermal phenomena affecting the thermal contact conductance. This chapter reviews some of the investigations of the thermal contact conductance of cylindrical interfaces, examining both theoretical models that illuminate the relevant phenomena, and experimental studies that provide results for comparison. Cylindrical contact studies are divided into two groups. Some studies are more theoretical in nature, dealing primarily with fundamental issues, and are broadly classified as General Cylindrical Studies. Others are experimentally based, and are classified as Applied Cylindrical Studies. A brief review of General Contact Conductance Studies (chiefly papers that deal with contact conductance theory for rough surfaces) follows. Papers in this section define parameters of interest and provide a basis of comparison of experimental results and theories. Correlations of interest are presented in tabular form for each section, and experimental data are compared to each other.

Thermal rectification, a phenomenon associated with contact conductance between dissimilar materials such as the different metals used in this study, has been studied by many investigators, with relatively few publications concerning predictive models. Further, this present study does not lend itself to the recognition of thermal rectification, since it is highly unlikely that identical mechanical and thermal conditions at the interface would exist for different material combinations. Therefore, thermal rectification will not be considered as it is outside the scope of this study.

Madhusudana, et al. (1990) reviewed studies of theoretical and experimental investigations of heat transfer in compound cylinders, categorizing these studies as

application oriented (and appropriate to specific materials and tubing) or fundamental (utilizing idealized surfaces and geometries). They found that there are significant holes in the state of knowledge of heat transfer through cylindrical contacts, and that only a modest effort has been made to fill these gaps. They conclude that there are several important shortcomings in the literature: contact resistance is measured indirectly from total resistance and computed material resistances; contact resistance is assumed to be constant (neglecting the effects of differential expansion); fundamental studies consider idealized surfaces that bear little resemblance to engineering surfaces; and that application oriented studies generally refer to specific conditions and materials. Furthermore, they recognize that there is a dearth of data that can be used to confirm theoretical models.

Hrnjak and Sheffield (1990) produced a similar review of plate-fin heat exchanger studies. The investigations reviewed were concerned with the junctions formed between the tubes and the fins. They identify thermal contact conductance between the fin and the tube as a neglected phenomenon, as far as most heat exchanger studies are concerned. They concluded that only a limited amount of experimental data is generally available, and that many parameters important to current contact conductance theories are not reported.

GENERAL CYLINDRICAL STUDIES

General studies of thermal contact conductance through cylindrical contacts consist of investigations dealing with composite cylinders and cylindrical shells. For the most part, the heat flow through composite cylinders is assumed to be axisymmetric and radial. While some of these studies are for specific materials and applications, it is fairly easy to extend their results to more general cases.

Brutto, et al. (1959) conducted a study of compound tubes in a vacuum environment. Their study was motivated by the problem of extracting heat from clad cylindrical nuclear fuel elements at interface heat fluxes between 3.0E5 and 9.0E5 W/m^2.

The experimental thermal contact conductance results are presented as a function of the temperature of the water surrounding the fuel elements, and cannot be compared to other published results of theories. They found that the cladding process (i.e. how the cladding is bonded to the fuel) had a significant effect on the thermal behavior of the interface, due to the existence of metallurgical bonding, plastic deformation of tube layers, and contact pressure due to residual elastic strain. The authors suggest surface roughness at the interface as a contributing factor to the contact resistance. They also recommend that the method of joining the cladding to the fuel be taken into account when making studies in this field, suggesting further that a metallic bond between the fuel and the cladding material is superior to a mechanical bond.

Cohen, et al. (1960) studied the conductance between cylindrical uranium-dioxide pellets and thin stainless steel cladding. They performed in-pile experiments, measuring the centerline temperature of the fuel pellet from 100 °C to nearly 1200 °C. They obtained experimental thermal contact conductance data as a function of contact pressure, which was calculated from the relative thermal expansion of the pellet and the cladding. They identified operating factors that influence the interface pressure (including fuel cracking, initial clearance, and assembly method). Among the interesting phenomenon observed was the variation of thermal contact conductance with the each startup and as a function of time during the operating cycle. The lack of surface metrology and the poor repeatability make the presented data of limited use for the purposes of the current study.

Williams and Madhusudana (1970) identified some basic problems associated with studies of conductance in cylindrical contacts, and presented the experimental results of two geometries – partial cylindrical contacts (included angle less than 20°) and full cylindrical contacts. The experimental thermal contact conductance data were obtained over a range between 1.0E5 and 5.0E5 W/m^2 with both air and vacuum as interstitial fluids. Some of the problems they encountered include difficulty in obtaining truly cylindrical

contacts, and facilitation of a uniform heat flux through the interface. They reported that partial cylindrical contacts behave very similarly to flat contacts, so much so that they may be simplified as such for many cases. Full cylindrical contacts were found to be very susceptible to small out-of-roundness deviations in the interfacial area. They recommend interference fits to enhance the conduction through the joint – in fact they state in their conclusions that the thermal resistance through such interfaces was too small to be accurately determined in their study. There is insufficient surface metrology and cylinder geometry to determine the interface pressure or to use current contact conductance models.

Novikov, et al. (1972) conducted a study of the heat transfer between coaxial cylindrical casings in vacuum, and determined that the contact pressure is strongly related to the ratio of thermal expansion coefficients, the initial stress state of the composite tube, and the thermal load. One of their conclusions is that when the thermal expansion coefficient of the outer casing is greater than that of the inner cylinder, the interface pressure will decrease and that contact resistance will increase with increasing, radially outward thermal load. Their model takes into account the thermophysical and mechanical properties of the cylindrical casings, but neglects surface conditions and imperfections. The experimental data used for their model development is not available for comparison.

Tam (1976) and Hsu and Tam (1979) conducted experiments with composite cylinders in air, varying the heat flux and surface roughness of one side of the interface. They identified phenomena that might explain the difference in the thermal contact conductance behavior of materials in cylindrical contacts and flat contacts. Predictions of contact conductance calculated by modified flat contact models (derived from Ross and Stoute (1962), and Shlykov and Ganin (1964)) are much lower than the experimental data of Hsu and Tam (1979). They propose as a possible explanation the lateral expansion of flat contacts, which would reduce the thermally induced strain at the interface and increase the associated micro-contact area. The slopes of the asperities may also be affected by the

lateral expansion, which would, in turn affect the actual contact area and thus the contact conductance. They also identify the effects of surface waviness, interfacial heat flux, oxidation, and radius of curvature as important parameters that should be accounted for in future correlations.

Madhusudana and Fletcher (1981) present results of thermal contact conductance tests for cylindrical interface heat fluxes between 8.0E3 W/m^2 and 4.2E4 W/m^2. They report that joints with an interference fit exhibit negligible thermal contact resistance (due to the negligible temperature discontinuity at the interface). They also report that the increase of the joint conductance in air compared to the increase in vacuum was of the same order of magnitude as the ratio of the thermal conductivity of air to the amount of initial clearance. They further assert that the primary factors of importance for predicting the thermal contact conductance are the initial fit, the differential expansion due to the temperature gradient within the cylindrical shells, and the differential expansion due to the temperature difference across the interface. They suggest that, as a result of the coupling between the contact resistance, interface pressure, and interface temperature difference, predictions of the contact conductance must be solved iteratively. They do not provide complete geometry data (only the interface radius is given) thermal data (temperatures are not given), or surface metrology.

Wang and Nowak (1982) conducted a theoretical analysis of the interface between duplex tubes where there is a sector at the interface where the tubes are not in contact with each other. Both isothermal and isoflux boundary conditions at the interface were studied through the use of an electrical analog tank and a computer model of a representative sector of the duplex tube. Results in the form of a predictive model for the contact resistance are presented, but no thermal contact conductance data is given in their study.

Srinivasan and France (1985) analytically studied heat transfer in prestressed duplex tubes. Their study, prompted by the erratic performance in the steam generator of

an experimental nuclear reactor, suggested that the multiple operating conditions were explained by the time relaxation of the initial prestress. Analytical models showed that sufficiently low prestresses at the interface of the duplex tube would lead to non-unique solutions. One suggested consequence of low prestress is the propagation of a non-contact region through the tube, leading to widespread separation of the layers of the tube. An increase in the temperatures throughout the tube and an increase in the heat flux in the contacting regions are also expected as a consequence of this separation. However, the results of the study cannot be compared with other published studies since the results are presented in arbitrary units.

Barber (1986a, 1986b) also studied the non-uniqueness of analytic solutions for the temperature distribution in prestressed duplex tubes studies by Srinivasan and France (1985). Specifically, he examined the influence of the phenomenon on the axial temperature variation in the duplex tubes, and the stability of the temperature distribution solutions. He found that there are always an odd number of solutions, alternating between stable and unstable, and that the phenomenon is sensitive to a number of conditions, including the initial stress state of the composite tube, the temperature level at the interface, and the thermophysical properties of the tube materials.

Madhusudana (1983, 1986, 1999) presents a predictive model for the thermal contact conductance through a cylindrical joint based on material properties, cylinder geometry, surface finish, and initial degree of fit. He illustrates the influence of thermal load, material combination, and interstitial fluid on interface pressure and contact conductance. In general, the model predicts that contact pressure increases with heat load. One interesting result of his model is that a material combination with a lower effective conductivity (defined as the harmonic mean of the two material thermal conductivities) may result in a higher contact conductance than a material combination of a higher effective conductivity, depending on the direction of the heat flow. He concludes (Madhusudana,

1986) that there is a strong relation between the contact pressure and material combination, and between conductance and the properties of the interstitial medium (especially at low thermal loads). He also states that there is a weak relation between the contact pressure and the properties of the interstitial medium. However, there are no comparisons with experimental data.

Lemczyk and Yovanovich (1987) offer a method for predicting the conductance of cylindrical contacts based on advanced models for conductance of flat contacts that considers contact pressure, microhardness, and surface roughness. The procedure is iterative in nature, and results are presented in the form of thermal contact conductance as a function of an estimated contact pressure. Good agreement is found with the data of Hsu and Tam (1976), although some surface properties (which were not provided) were estimated. Comparisons are made with modified flat contact models of Shlykov and Ganin (1964), Veziroglu (1967), and Ross and Stoute (1962), demonstrating that the method is more effective for predicting the contact conductance than the other three models. This is chiefly a result of the conforming surface model used, apparently from Yovanovich (1981). They recommend that, in future models, the difference between axial and circumferential roughness be taken into account. Their method assumes a plane-stress condition within the composite cylinder, and is developed for cases where there is an interference fit. Neither of these conditions apply to the facility used in the present study.

Danes and Simon (1990) used a modification of the transient method used by Bourouga and Bardon (1992) to determine the transient thermal contact resistance between two cylinders. They used several samples (constructed of an inner stainless steel cylinder and an outer tin cylinder) and determined an exponential correlation dependent on temperature. They report a reduction in the measurement error of 50%. However, Bourouga and Bardon (1992) cite an experimental uncertainty that is of the same order of magnitude as their measurement. Insufficient surface metrology information is provided to

use current conductance models and not enough geometric information is provided to determine the variation of interface pressure with experimental conditions.

Madhusudana and Litvak (1990) conducted an experimental study of conduction through a composite cylinder, focusing on the design, construction, and validation of an experimental test facility. The test facility consisted of a composite cylindrical shell (stainless steel 303 and aluminum 2011) which was heated on the interior by hot fluid and cooled on the exterior by cool fluid. They present the thermal contact conductance as a function of temperature difference across the interior cylinder, although they also give heat rates (and through calculation, interfacial heat fluxes). There is no mention of the clearance between the cylindrical shells or the surface characteristics (roughness and waviness). They call attention to the effect of the interstitial fluid and emphasize that the interface pressure can only be estimated, and should not be used to present data. They recommend that theoretical models be refined to take into account large scale irregularities (such as out-of-roundness and waviness) at the interface.

Artyukhin, et al. (1991) constructed a computational algorithm to determine the thermal contact resistance between nuclear fuel pellets and cladding by solving the inverse heat transfer problem, with the aim of using the model for non-steady experimental studies inside reactors. Their results suggest the optimal placement of temperature sensors within the fuel element and the means that may be used to analyze and process the data from non-steady thermal experiments.

Table 2.1 compares correlations that are more fundamental in nature, and have general applicability. These correlations borrow heavily from flat contact models, and have (for the most part) the familiar hardness, and roughness terms. Newer models for heat transfer through flat contacts may be modified to better account for out-of-roundness and longitudinal waviness.

Table 2.1 – General Cylindrical Conductance Correlations

Correlation	Comments/Conditions
Novikov, et al. (1972) $R_c = \frac{(P_c - P_{co})}{Q \alpha_1 r_1} \left\{ \frac{r_1^{3/2}\left[3(1-\nu_1^2)\right]^{1/4}}{E_1 \delta_1^{3/2}} + \frac{r_2^2\left[3(1-\nu_2^2)\right]^{1/4}}{E_2 \delta_2 (r_1 \delta_1)^{1/2}} \right\}$ $P_C \le$ yield stress	Semi-theoretical model for thin shells, power law correlations for resistance as a function of instantaneous interface pressure, dependence on thermophysical properties.
Wang and Nowak (1982) $R_c = \frac{2k}{\pi \phi_a} \left\{ \begin{array}{l} \frac{1}{\lambda_i} \sum_{n=1}^{\infty} \left[\frac{1}{n} F(k_n \phi_a) \left(\frac{\left(\frac{b}{a}\right)^{2k_n} - 1}{\left(\frac{b}{a}\right)^{2k_n} + 1} \right) \frac{\sin(k_n \phi_a)}{k_n \phi_a} \right] \\ + \frac{1}{\lambda_o} \sum_{n=1}^{\infty} \left[\frac{1}{n} F(k_n \phi_a) \left(\frac{\left(\frac{c}{b}\right)^{2k_n} - 1}{\left(\frac{c}{b}\right)^{2k_n} + 1} \right) \frac{\sin(k_n \phi_a)}{k_n \phi_a} \right] \end{array} \right\}$ where $F(k_n \phi_a) \equiv \int_0^{\phi_a} f(\phi) \cos(k_n \phi) \, d\phi$	Theoretical model for duplex tubes with spot contacts and an arbitrary heat flux $f(\phi)$, constant fluid temperatures, and steady, 2-D temperature distribution.
Madhusudana (1986) $h_c = \left(\frac{k}{\sigma}\right) \left[1.13 \tan\theta \left(\frac{P_c}{H} \right)^{0.94} + \frac{k_{go}}{3\sigma} \right]$	General theoretical cylindrical model derived from flat conductance model. Dependence on composite cylinder geometry, material properties, gas properties, and surface characteristics. Interface pressure arrived at through thermoelastic modeling.

CYLINDRICAL CONTACT APPLICATION STUDIES

A majority of the application studies deal with heat exchangers, including the installation of fins or extended surfaces. Thermal contact resistance accounts for a significant portion of the thermal resistance in plate finned heat exchangers. Typical finned-tube configurations are shown in Figure 2.1. From a geometric viewpoint, tension wound, footed fins have a dual nature. At the foot, they might be expected to behave as thin cylindrical shells. At the point where the fin rises from the foot, they might be expected to behave as thick cylindrical shells. Therefore, analysis of the heat transfer through the fin-tube interface requires careful consideration of the geometry.

The effects of the thermal resistance of the fin-tube bond are of considerable interest. Kim (1978) identified a major deficiency in the state of the art – specifically the lack of theoretical or empirical prediction techniques for the thermal contact resistance of all types of finned tubes. The memo describes the objectives of a proposed study: to

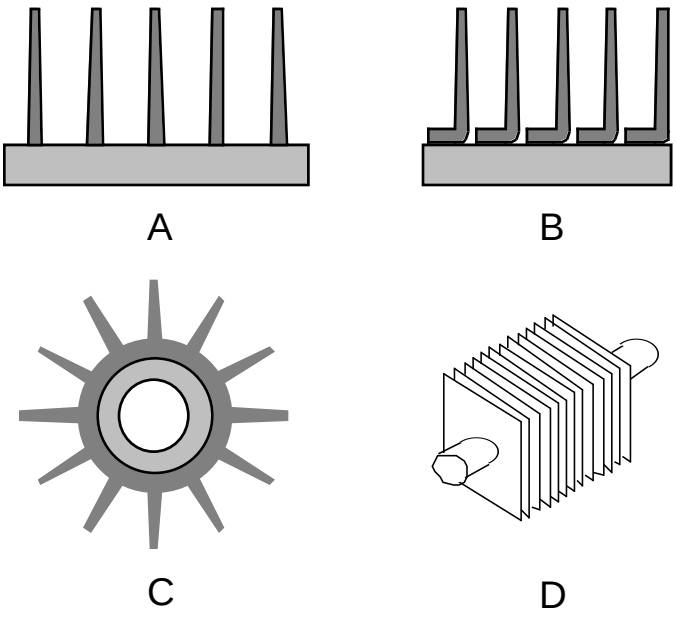

Figure 2.1 – Typical heat exchanger fin types: A) edge-wound 'I' fins, B) edge-wound 'foot' fins, C) extruded 'muff' fins, and D) plate fins.

investigate the effects of material properties, fin-tube geometry, and surface coating with the result of a correlation of joint conductance as a function of fin-tube geometry and mechanical properties.

Dart (1959) described a method of measuring the effect of fin bond on the heat transfer through the fin-tube contact and conducted a series of experimental tests to demonstrate the utility of the method. The method described in this seminal work was refined by Eckels (1974, 1977) and later by Abuebid (1984), and others. The method, which uses geometric parameters to predict the heat transfer through the bond, does not consider the effect of thermophysical properties.

Gardner and Carnavos (1960) presented a model for the thermal contact resistance of the bond between various types of fins on tubing, based on finned-tube geometry, material properties, and fluid temperatures. They observed that the interface pressure (due to elastic stresses in the tube and the fins) can be calculated with the method of Timoshenko and Goodier (1951). Experimental data include information from tests on tension wound fins and "muff-type" fins, but lack surface metrology and sufficient information regarding the interface geometry for broader application. They also proposed correlations to predict the gap resistance ("bond resistance") as a function of operating conditions, material properties and fabrication processes. They conclude that the "bond-resistance" of interference fit finned-tubes is negligible for air-cooled heat transfer equipment, but may be significant at extreme temperature level conditions. They also observe that the concentricity of the tube wall and the muff-fin base has little effect on the contact resistance – provided that the gap resistance is less than one fifth the overall resistance, and that the error introduced is less than three percent. They also observe that longitudinal variation of the interfacial diameters has a more dramatic effect on the thermal contact resistance.

Young and Briggs (1965) and Kulkarni and Young (1966) recognized that contact resistance can be a significant part of the overall thermal resistance in finned-tube heat exchangers. They produced design charts predicting the contact resistance as a function of air and fluid temperature operating conditions and classified them according to fin number and diameter. These charts assume an initial contact pressure and fabrication temperature, and were constructed from data for aluminum muff-type fins on steel tubes. Bond resistance (including contact resistance) is presented as a function of the temperature of the inside tube, which may not be uniform through the thickness or along the axis of the tube. Further, for different types of tubing or fin material, these charts may not be accurate, and they do not apply to different types of fin geometries such as tension wound fins. Further, no surface metrology information is given, and the data lack sufficient geometric information to calculate the variation of interface pressure with the temperature distribution. Insufficient information is present to fit the data into current predictive contact conductance models.

Smith, et al. (1966) utilized a single tube test rig to characterize the performance of steel and aluminum tubes with aluminum tension-wound and footed fins. Both steady and cyclic operation tests at tube temperatures between 330 °C and 375 °C. They found that there was an increase in thermal resistance with tube wall temperature, and that thin fins deform with temperature (changing the pressure distribution of the interface).

Eckels (1974, 1977) designed a test facility that used a large number of tube-fin interfaces in a tube coil to determine the average contact conductance between tubes and plate fins. The uncertainty of the thermal contact conductance values given by this technique was estimated to be on the order of 20%. Sheffield, et al. (1985b), Sheffield, et al. (1987), Sheffield, et al. (1989), and Sauer and Sheffield (1987) used this technique in the studies reviewed here. In a second study, Eckels (1977) utilized the previously designed test facility to obtain experimental values of the thermal contact conductance

through a dry, mechanically expanded plate-finned tube, and produced a correlation that is dependent on geometry alone. He found that the values of temperature, mass flow rate, and the fin resistance were the most significant sources of error in his relation, and that the error in the results increases with heat flux (approximately 15% at 5.676E3 W/m^2K, and 30% at 1.13E4 W/m^2K).

Kuntysh, et al. (1983) studied the thermal contact resistance of L-footed fins. They used two different tube boundary conditions in their investigation – constant tube wall temperature, and a varying tube temperature. They provide two power law correlations of contact resistance as a function of interface heat flux. Their correlation does not take into account the common thermophysical properties and surface characteristics that are considered in more recent thermal contact conductance theories, nor are these parameters presented in their study. Without these parameters, their data (thermal contact resistance as a function of heat flux) is difficult to use in any subsequent modeling without assuming too much information. Further, their correlation does not explicitly have any dependence on the boundary conditions in tests used to generate the empirical data.

Stafford (1983) and Sheffield, et al. (1989) used scanning electron microscopy to study the effects of expansion and other geometric parameters (such as waviness) on the characteristics of tube-fin interface surfaces. They determined that tube surface roughness decreases with decreasing fin number (fins per unit length), and increases with increasing tube expansion.

Christensen and Fernandes (1983) studied the contact and fouling resistances in pneumatically expanded finned tube heat exchangers, constructed of copper fins on copper, copper-nickel, or stainless steel tubes. They presented order of magnitude results that suggest that the contact resistance is greater than the fouling resistance. However, they report an uncertainty in the contact resistance results that is of the same order as the contact resistance. Their thermal contact resistance data are not presented as a function of interface

temperature, pressure, or heat flux. Further, they do not mention the influence of thermophysical properties or surface conditions on the thermal contact resistance.

Matal, et al. (1994) studied duplex tubes for use in a liquid sodium heated steam generator component of a nuclear power plant. The two tubes studied have either a set of grooves cut into the outer tube at the interface, or a set of three lands on the inner tube at the interface, to facilitate leak checking. Thermal contact resistance is given as a function of the temperature difference between the liquid sodium inside the tubes and the steam outside the tubes, and cannot be compared to other published results. Other results are given as a function of time. Many parameters are not reported, including surface finish, conductivity of the tube material, and interface heat flux. Further, in contrast to their figure relating thermal contact resistance to temperature difference, they claim to have "perfect" contact between the two tube layers.

Abuebid (1984) and Sheffield, et al. (1985a) used the method of Eckels (1974) to determine the contact conductance of plate-finned, mechanically expanded tubes. Although Sheffield, et al. (1985a) identify many parameters that are commonly accepted as being of importance in thermal contact conductance models, their correlation has no dependence on material properties, exhibits no influence of contact pressure or heat flux, and neglects surface roughness and out-of-roundness. The correlation is essentially a least squares fit through data for a specific geometry.

Ernest, et al. (1986), Sheffield, et al. (1987), Wood, et al. (1987a), Wood, et al. (1987b), Sheffield, et al. (1989), and Sauer and Sheffield (1987) conducted experimental studies investigating the thermal contact resistance of plate-finned tube coils in a vacuum. In their apparatus, the plate fins of several tubes were joined to form tube sheets. The apparatus circulated cold water through the outer banks of tubes and hot water through a center bank of tubes in the coil. They assumed that the tube conduction resistance and contact resistance are the same for both the hot tubes and the cold tubes.

However, since the contact resistance is dependent on the differential expansion of the contacting materials, it is indirectly dependent on the temperature.

Ernest, et al. (1986) investigated the quality of the mechanical bond between the fins and the tube – determining that a pull-out test is an appropriate measure of the strength of the bond, and thus the quality of the contact. The actual contact area, however, is dependent upon surface characteristics and fabrication process, therefore such a pull test may not be appropriate for all configurations. Sheffield, et al. (1987) describe a technique developed to test plate fin tube heat exchangers and to investigate the effects of varying geometry and manufacturing method.

Wood, et al. (1987a), (1987b) conducted experimental studies investigating the thermal contact resistance of plate-finned tube coils, and the effects of various tube coil parameters on the thermal contact resistance using the same apparatus of Sheffield, et al. (1985b). The results seem to imply that there is no dependence of the contact conductance on temperature, and roughly half of the results presented are within 20% of their experimental correlation. In their second study, Wood, et al. (1987b) conducted 32 experiments which examined the effects of the number of fins per inch, tube passes, fin conduction shape factor, fin-tube interference, and fin thickness on the contact conductance. They concluded that thermal contact conductance increases with interference, but decreases with tube diameter. Such conclusions are appropriate since interference fits increase the contact area and increased tube diameter generally involves more out-of-roundness and a non-uniform pressure distribution.

Sheffield, et al. (1989), and Sauer, and Sheffield (1987) conducted an experimental study investigating the thermal contact resistance of plate-finned tube coils in a vacuum. The apparatus was similar to that of Sheffield, et al. (1985a). They again assumed that the tube conduction resistance and contact resistance are the same for both the hot tubes and

the cold tubes. The correlation presented in this paper extends the range of the one presented in Sheffield, et al. (1985a).

Nho and Yovanovich (1989a), (1989b) experimentally studied the effects of surface condition on the thermal contact conductance of plate-finned tube heat exchangers. The method used was similar to that used by Sheffield, et al. (1989), except that the fins appeared to be instrumented with more thermocouples than in the study of Sheffield, et al. (1989). In addition to the same fin and tube parameters generally provided in this type of study, surface condition information including hardness, roughness, and asperity slope for both the tube and fin surfaces was provided. The hardness and conductivity of the oxide layer found on the contacting surfaces was also given, although no new correlation which uses this information was provided. They also examined the contact between the fin and the tube and found that the apparent contact area varies with the amount of expansion of the tube into the fin, causing the foot of the fin to either curl, buckle, or displace the heel of the adjacent fin foot. Each of these factors affects the contact area, and thus the conductance. The averaged conductance for each of the finned-tube units compares well with the model of Sheffield, et al. (1989), being within the uncertainty of the model for most of the finned tube units.

Egorov, et al. (1989) studied contact heat transfer resistance in finned-duplex tubes, which were manufactured by either drawing or pressing. They present results of contact conductance as a function of interfacial heat flux. They observed the effects of unstable contact between the tube layers, which was investigated in greater detail by Srinivasan and France (1985), and Barber (1986a, (986b). No surface metrology is provided, scant thermophysical property data (of interest due to the type of steel used) is given, and insufficient geometric information is given to calculate the variation of pressure with temperature.

Huang (1994) used a finite element technique to model the flow of heat between tubes connected by a plate fin to determine the conduction resistance associated with the geometry. This method can be used in conjunction with experimental data for plate-finned tube heat exchangers to determine the resistance due to contact between the tubes and fins. Previously, electrical analog techniques were used to determine the effect of the fin-tube geometry on the conduction resistance. The results of the method were compared with experimental data of Sheffield, et al. (1989). For seventeen of the thirty-two datasets used for comparison, Huang (1994) found that the average absolute error caused by measurement was 78%, and the average absolute error caused by the one-dimensional model was 68%. Further, his calculations for the same seventeen data sets show that while the one-dimensional model used in the experimental study results in a contact resistance of approximately 20% of the total resistance, a two-dimensional model results in a thermal contact resistance of approximately 11% of the total resistance, which indicates that analyses based on previous experimental studies have overestimated the fraction of the total thermal resistance due to contact resistance by about 9%. Huang (1994) concludes that his analysis would improve the experimental results because it does not assume a one-dimensional conduction between hot and cold tubes, and is able to avoid the error associated with that assumption.

Table 2.2 compares the available correlations for conductance through cylindrical contacts found in finned tubes and tube collars. Much of this work is empirical, and thus applicable only to specific geometries and material combinations. Of particular interest is the absence of hardness and surface characteristics such as roughness or waviness terms in the correlations. All correlations are dimensional.

Table 2.2 – Correlations for Conductance through Cylindrical Contacts in Finned Tubes and Tube Sheets

Correlation	Comments/Conditions
Gardner and Carnavos (1960) $R_c = \rho \left\{ \frac{(\alpha_f - \alpha_t)(T_h - T_o) - \mu p_{co}}{-\left[\alpha_f \left(1 - \frac{r_o}{R^* + R_g} \right) - \alpha_t \left(1 - \frac{r_i}{R^* + R_g} \right) \right] (T_h - T_a)} \right\}$ $P < 0.43(t/d - t)^{0.5}$	For interference fit finned-tubes, pressure based on elastic theory. Parameters ρ and μ defined in paper. Constant fluid temperatures, fin base and tube wall are concentric and smooth, effect of fluid pressure is negligible
Kuntysh, et al. (1983) a) $R_c = 0.552 q_c^{-0.304}$ b) $R_c = 0.004185 q_c^{1.115}$	Empirical curve fit, Air-Air heat transfer, co-axial circular find, interface heat flux between 2.5E4 and 7.0E4 W/m^2. a) Constant tube wall temperature, between 350 and 365 K b) Varying tube wall temperature, approximately linear from 345 K to 510 K
Eckels (1977) $h_c = 2.555 \times 10^6 \left[\frac{t}{d_o} \left(\frac{fpi}{t} - 1 \right)^{-2} \right]^{0.6422}$	Semi-theoretical, apropos to a specific geometry and material combination, no temperature or material property dependence.
Sheffield, et al. (1985b) $h_c = 2.815 \times 10^{23} \left(\frac{t}{d_o} \right)^{10.035} \left(\frac{I + 5.207 \times 10^{-4}}{L} \right)^{2.867}$ $6.73\% \le \text{error} \le 18.35\%$; $d_O = 0.009525$ m ; $6 \le N \le 20$; $0.001196 \text{ m} \le L \le 0.004219 \text{ m}$; $0.000165 \text{ m} \le I \le 0.000279 \text{ m}$	Mechanically expanded tubes and tube collars, minor dependence on material properties, no influence of contact pressure or heat load, apropos to a specific geometry and material combination, no temperature dependence,

Table 2.2 (continued)

Correlation	Comments/Conditions
Wood, et al. (1987a) $h_c = 5.67826 \exp\left\{6.092 + 2.889\left[\left(\frac{I\,fpi\,d}{d_o}\right)^{0.75}(t\,fpi)^{1.25}\right]\right\}$ $0.00635\ m \le d_O \le 0.015875\ m$; $6 \le fpi \le 18$; . $000114\ m \le t \le .000231\ m$; $0.000076\ m \le I \le 0.000191\ m$	Mechanically expanded, plate-finned tubes - copper tubes and aluminum fins, mechanically expanded tubes, apropos to a specific geometry and material combination, no temperature dependence, nearly one half of the coils tested fell within 20% of this correlation.
Sheffield, et al. (1989) $h_c = 5.67826 \exp\left\{7.828 + 2.889\left[\left(\frac{I\,fpi\,d}{d_o}\right)^{0.75}(t\,fpi)^{1.25}\right]\right\}$ $0.009525\ m \le d_O \le 0.015875\ m$; $6 \le fpi \le 18$; $0.000102\ m \le t \le 0.000231\ m$; $0.000076\ m \le I \le 0.000191\ m$	Mechanically expanded, plate-finned tubes, minor dependence on material properties, No influence of contact pressure or heat load – least-squares fit for data apropos to a specific geometry and material combination, No temperature dependence.

GENERAL CONTACT CONDUCTANCE STUDIES

Hertz (1881) made an analytical study of smooth contacting spheres. Hertzian contact theory assumes that each contacting sphere is smooth. While this makes the mathematics more tractable, real surfaces (which are not perfectly smooth) do not fall into this category. However, Hertzian contacts can be used as a limiting case and are at the base of many contact conductance models for non-conforming surfaces. Using Hertzian analysis for the contact between sphere and a plane (Timoshenko and Goodier, 1951), expressions for the contact area and pressure necessary to deform the sphere to form this area can be obtained. The Hertzian elastic modulus used in studies of the deformation of spheres is defined

$$E' = \left(\frac{E_1}{1-\nu_1^2} + \frac{E_2}{1-\nu_2^2} \right)^{-1} \tag{2.1}$$

Shlykov and Ganin (1964) semi-empirical model of contact conductance for nominally flat, rough metals, assumes that microcontact radius is constant and unaffected by roughness or contact pressure. The model further assumes that the contact hardness is three times the ultimate tensile strength.

Veziroglu (1967) correlated a significant amount of experimental data, identifying terms for effective interstitial gap thickness, gap conductance, but finding his effective gap thickness to be relatively insensitive to surface finish. Asperity slope and waviness parameters were not used due to lack of data. The correlation is difficult to implement due to its iterative nature.

Clausing and Chao (1964) considered non-flat surfaces, specifically relatively smooth spheres in contact. Assuming an elastic macrocontact deformation, they made use of the Hertzian contact model to determine the macrocontact size and pressure distribution and contact radius. The ratio of specimen size to the macrocontact radius was used to

determine the macroscopic constriction resistance. Assuming that the microcontact radii were constant and equal to the roughness, they developed a model for the microscopic constriction resistance. They defined a dimensionless group, termed the Elastic Conformity Modulus, representing the ratio of the elastic deformation of the macrocontact to the flatness deviation (approximately half the radius of curvature):

$$\zeta \equiv \left(\frac{P}{H_m}\right)\left(\frac{b_L}{2\rho}\right) \tag{2.2}$$

The Elastic Conformity Modulus provides a measure of the conformity of the mating surfaces under load and plays a large role in their macroscopic constriction model.

Greenwood (1967) defines a plasticity index indicating the mode of the microcontact deformation

$$\psi_G = \left(\frac{E'}{H}\right)m \tag{2.3}$$

For values of the index greater than 1, the micro-deformation is plastic, for values less than 0.7, the micro-deformation is elastic.

Cooper, et al. (1969) studied the contact conductance of rough, conforming metals experiencing light to moderate pressure. The model presumes that the microcontacts deform plastically.

Mikic (1970) developed models for the macroscopic and microscopic contact conductance that took into account non-uniform pressure distributions, but did not specify how the distributions were determined. The microscopic conductance model uses the plastic deformation model of Cooper, et al. (1969).

Thomas and Sayles (1974) studied the relative effects of waviness and roughness on thermal contact conductance. They observe that the total roughness of a specimen is related to its size. Defining a dimensionless waviness number,

$$\xi \equiv \frac{L}{E' \sigma b_L} \tag{2.4}$$

Thomas and Sayles (1974) identify the vicinity of $\xi \approx 0.7$ to be the point where roughness and waviness have equal influence over the contact conductance, and that the influence of waviness can be neglected for values greater than unity.

Yovanovich (1981) refined the model of Cooper, et al. (1969) for plastic deformation of microscopic contacts on conforming surfaces.

Lambert (1995) and Lambert and Fletcher (1997) developed a model for the thermal contact conductance of spherical rough metals that is valid in regions removed from the limiting cases of rough/flat, smooth/spherical surfaces. It is, however, a single macrocontact model, and requires loading on the macrocontact as well as the surface geometry of the contact. In multiple macrocontact situations, such as those encountered in large area contacts, it is difficult to estimate number of macrocontact, much less the loading on each macrocontact.

Table 2.3 lists the dimensional and non-dimensional contact conductance correlations reviewed in this section.

COMPARISON OF PUBLISHED RESULTS

Figure 2.2 shows a comparison between the conductance data of Hsu and Tam (1976) as a function of apparent contact pressure and the models of Ross and Stoute (1962), Shlykov and Ganin (1964), Veziroglu, (1967), and Lemczyk and Yovanovich (1987). Clearly, the model of Lemczyk and Yovanovich (using the effective hardness) fits the data well, while other models under-predict the data to varying degrees (between 20% for Ross and Stoute (1962) and 60% for Veziroglu (1967)). For flat and near flat contacts, pressure is often chosen as an independent experimental parameter. In the case of

Table 2.3 – Thermal Contact Conductance Models

Correlation	Comments/Conditions
Ross and Stoute (1962) $h_c = \dfrac{k_e P_c}{0.05 H \sqrt{\dfrac{\sigma_1^2 + \sigma_2^2}{2}}}$	Modified flat contact model, some dependence on thermo-mechanical properties.
Shlykov and Ganin (1964) $h_c = 4.2\times10^4 \dfrac{k_s P_c}{d_o(345\,\text{MPa})} + \dfrac{k_{go}}{\sigma_1 + \sigma_2}$	Modified flat contact model, some dependence on thermo-mechanical properties.
Clausing and Chao (1964) $\dfrac{h_{c,L} b_L}{k} = \dfrac{2}{\pi} \dfrac{a_{L,Hz}/b_L}{\psi(a_{L,Hz}/b_L)} = \dfrac{2}{\pi} \dfrac{1.285\chi^{1/3}}{\psi(1.285\chi^{1/3})}$ $\dfrac{h_{c,S}\sigma}{k} = \dfrac{\sigma}{m}\dfrac{2}{\pi}\dfrac{L/\pi a_{L,Hz}^2}{C_1 H}\dfrac{1}{a_S \psi(a_S/b_S)}$ $\dfrac{R_{c,L}}{R_{c,S}} = \dfrac{L/\pi a_{L,Hz}^2}{C_1 H}\dfrac{\psi(1.285\chi^{1/3})}{1.285\chi^{1/3}}\dfrac{b_L}{a_S\psi(a_S/b_S)}$	Spherical smooth surfaces elastic macroscopic deformation, plastic microscopic deformation $\chi \equiv \dfrac{L/\pi b_L^2}{E_h}\dfrac{b_L}{\delta_1+\delta_2}$ $a_{L,Hz} = (0.75 L \rho / E')^{1/3}$ $0 \le C_1 \le 1$, is elasto-plastic deformation correction factor, 1=plastic deformation
Veziroglu (1967) $N_{uc} = \dfrac{B^+ C^+}{\eta^+ \tan^{-1}\left[\left(\dfrac{1}{C^+}\sqrt{1-\dfrac{1}{N_{uc}}}\right)-1\right]}$	Modified flat contact model, some dependence on thermo-mechanical properties. $B^+ \equiv 0.335(C^+)^{0.315(1_c/l)^{0.137}}$ $C^+ \equiv \left(\dfrac{P_c}{H_m}\right)^{\frac{1}{2}}; \quad \eta^+ \equiv k_{go} k_s$

Table 2.3 (continued)

Correlation	Comments/Conditions
Cooper, et al. (1969) $\frac{h_c \sigma}{k m} = 1.45 \left(\frac{P}{H_v} \right)^{0.98}$ $3.6E\text{-}4 \le P/H_v \le 1E\text{-}2$ $1.0\ \mu m \le \sigma \le 8.0\ \mu m$ $0.08 \le m \le 0.16$	Nominally flat, rough surfaces.
Mikic (1970) For axisymmetric pressure distribution P(r): $\frac{h_{c,S} \sigma}{k m} = 2.90 \int_0^1 \frac{r}{b_L} \left(\frac{P}{H} \right)^{0.985} d\left(\frac{r}{b_L} \right)$ $\frac{h_{c,L} b_L}{k} = \left\{ 8 \sum_{n=1}^{\infty} \frac{\left[\int_0^1 \frac{r}{b_L} \left(\frac{P}{H} \right)^{0.985} J_0 \left(\lambda_n \frac{r}{b_L} \right) d\left(\frac{r}{b_L} \right) \right]^2}{\lambda_n J_0^2(\lambda_n)} \right\}^{-1}$ For unidirectional pressure distribution P(x): $\frac{h_{c,S} \sigma}{k m} = 1.45 \int_0^{\infty} \left(\frac{P}{H} \right)^{0.985} d\left(\frac{x}{b_L} \right)$ $\frac{h_{c,L} b_L}{k} = \left\{ 4 \sum_{n=1}^{\infty} \frac{1}{n} \left[\int_0^{\infty} \left(\frac{P}{P_{avg}} \right)^{0.985} \cos\left(\frac{n \pi x}{b_L} \right) d\left(\frac{x}{b_L} \right) \right]^2 \right\}^{-1}$	Applicable for spherical and cylindrical contacts, respectively P(r) and P(x) undefined

Table 2.3 (continued)

Correlation	Comments/Conditions
Yovanovich (1981) $h_c = 1.25\frac{k_s m}{\sigma}\left(\frac{P_c}{H_e}\right)^{0.95} + \frac{k_{go}}{Y + \alpha_a \beta \Lambda}$	Nominally flat, rough surfaces, Modification of Cooper, et al. (1969) $\beta = \left(2\frac{c_p/c_v}{c_p/c_v + 1}\right)\frac{1}{Pr}$ $1x10^{-5} \le P_e/H_e \le 1x10^{-2}$ $2.34 \le Y/\sigma \le 4.26$ $0.14\ \mu m \le \sigma \le 14\ \mu m$ $9.33\ \mu m \le \sigma/m \le 40\ \mu m$ $0.015 \le m \le 0.35$ $0.001 \le \Lambda_o/\sigma \le 1.5$ $1 \le \beta \le 2$ $0.04\ \mu m \le \Lambda_o \le 0.19\ \mu m$ $1x10^{-4} \le k_{go}/k_s \le 2x10^{-2}$
Lambert (1995) $h_c^* = \frac{1}{R_{c,S}^* + R_{c,L}^*}$ $R_{c,S}^* = \frac{\left(\frac{R_{c,S} k m}{\sigma}\right)\left(\frac{L}{H_v \rho \sigma}\right)^{0.95}\left(\frac{P_0}{P_{0,Hz}}\right)^{0.67}}{\left(\frac{b_L}{a_L}\right)^2 f_S\left(\frac{b_L}{a_L}\right)}$ $= 6.15\left(L^*\right)^{0.484}$ $R_{c,L}^* = \frac{\left(\frac{R_{c,L} k L}{\rho \sigma E'}\right)}{\left(\frac{P_0}{P_{0,Hz}}\right)^{0.20}\left(\frac{b_L}{a_L}\right)^2 f_L\left(\frac{b_L}{a_L}\right) g\left(\frac{b_L}{a_L}, L^*\right)}$ $= 1.44\left(L^*\right)^{0.954}$	Rough, spherical contacts $L^* = \frac{2L}{\sigma E' \sqrt{2\rho\sigma}}$ $1E\text{-}2 \le L \le 1E10$ $19.3\ GPa \le E \le 386\ GPa$ $0.8556\ MPa \le Hc \le 2567\ MPa$ $0.1\ \mu m \le \sigma \le 10\ \mu m$ $0.0316 \le m \le 0.316$ $1E\text{-}2\ m \le \rho \le 1E6$

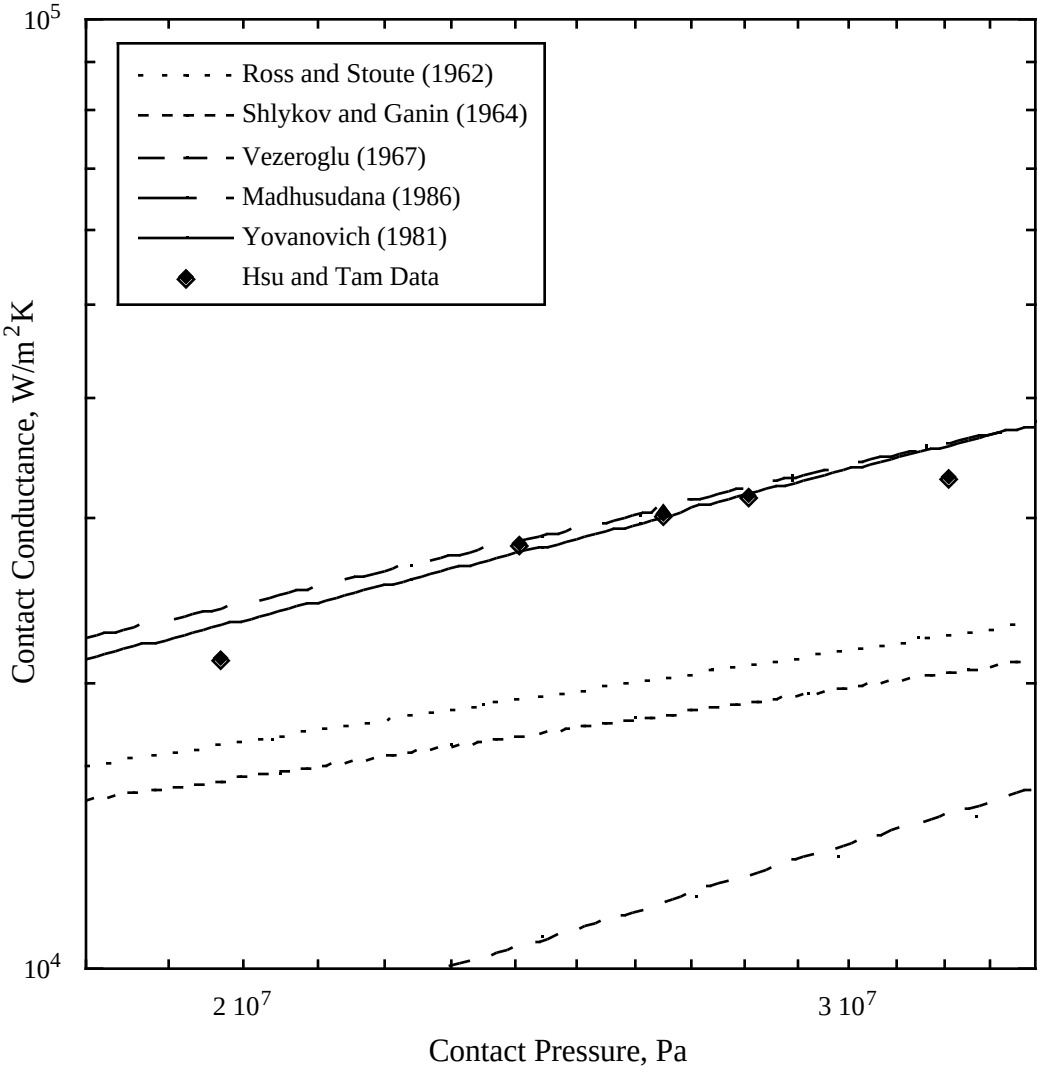

Figure 2.2 – Comparison between experimental data of Hsu and Tam (1976) for AL-2011 shell inside SS-304 shell (σ_e = 5.100 μm) and the models of Ross and Stoute (1962), Shlykov and Ganin (1964), Veziroglu (1967), Madhusudana (1986), Lemczyk and Yovanovich (1987), and Yovanovich (1981).

cylindrical contact conductance phenomenon, contact pressure is not easily measured, much less independently controlled.

Published experimental data are shown in Figure 2.3 to demonstrate the range of available information as a function of interface heat flux. While heat flux is of relatively little influence for flat and near flat contacts, it appears to be very influential in cylindrical contact conductance phenomenon. The conductance-interface heat flux data fall in families, which can be nondimensionalized.

Figure 2.4 presents dimensionless thermal contact conductance as a function of dimensionless interface heat flux. Heat flow is assumed to be radially outward through an interface formed by two thick cylindrical shells. The terms selected to form the dimensionless heat flux were chosen to form meaningful groupings:

$$h^* \equiv \left(\frac{h_c \sigma}{k m}\right)$$
$$q^* \equiv \left(\frac{q_i'' \alpha \sigma}{k}\right)\left(\frac{E}{H}\right)\left(\frac{\alpha_i}{\alpha_o}\right)^3\left[\frac{1}{2}\left(1+\frac{P}{P_{atm}}\right)\right]^2 \qquad (2.5)$$

The dimensionless conductance is the familiar dimensionless term used in flat contact studies, where contact conductance is nondimensionalized by the ratio of the effective roughness to the product of the effective conductivity and asperity slope. The first term in the dimensionless heat flux is a non-dimentionalization of the heat flux with effective (geometric mean) thermal expansion, effective surface roughness, and effective conductivity. The second term was chosen to account for the effects of effective hardness and elasticity, increasing hardness will diminish the conductance, while increased elasticity is expected to increase it. The ratio of the thermal expansions was chosen to account for the effect of the differential thermal expansion of the two shells. If the inner shell expands faster than the outer shell, then the interface pressure will increase, and so will the

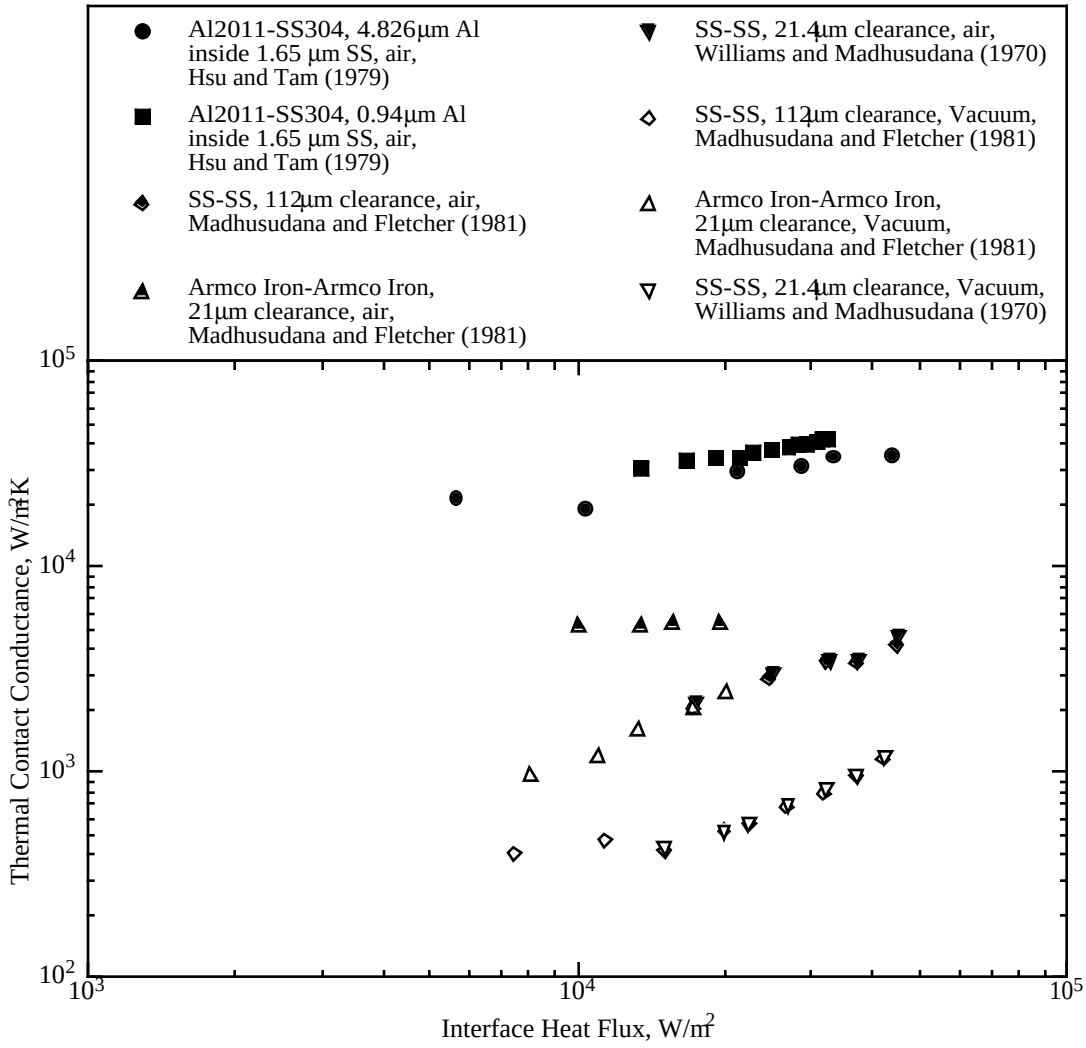

Figure 2.3 – Experimental thermal contact conductance data for cylindrical contacts as a function of interface heat flux.

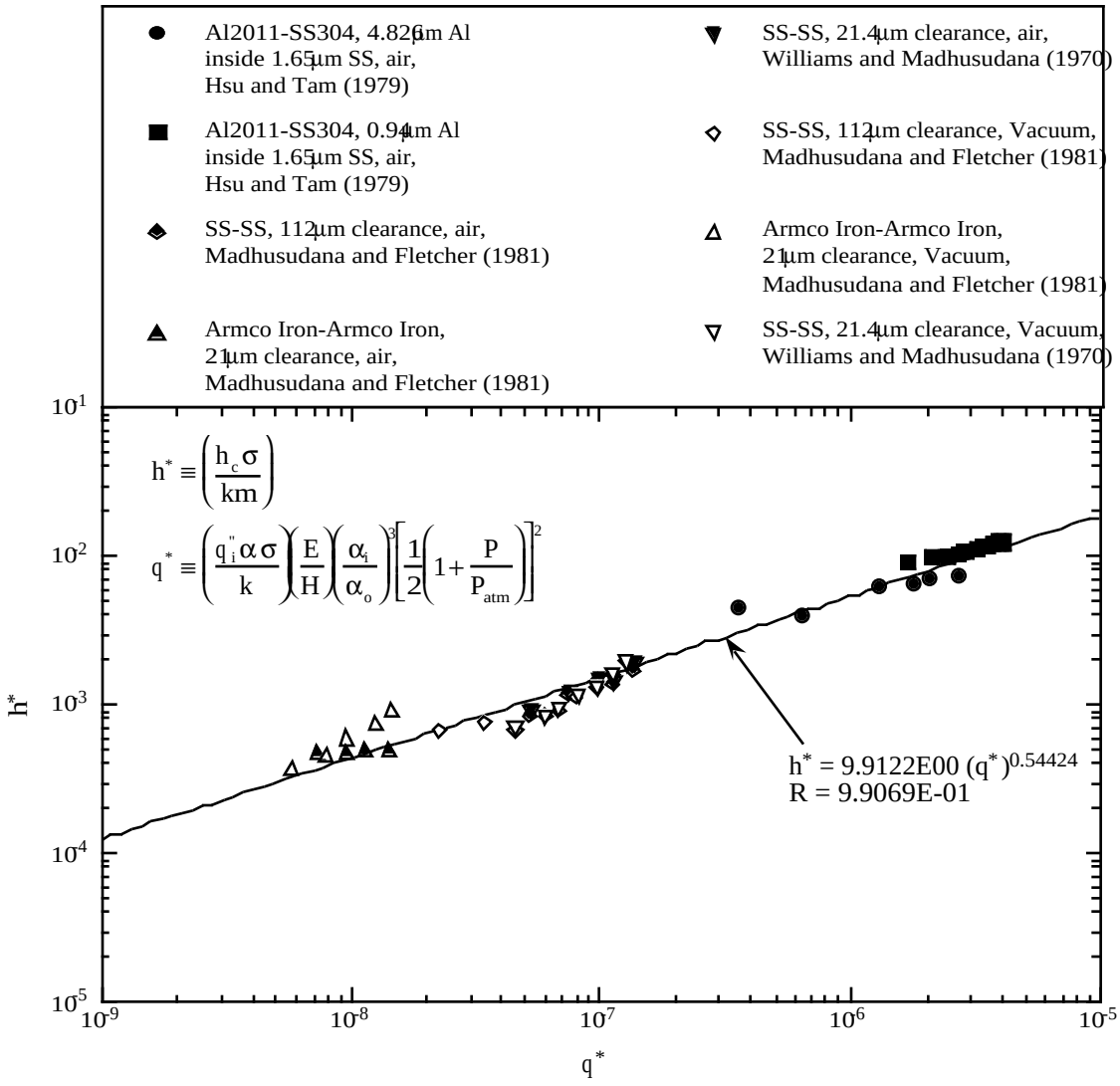

Figure 2.4 – Dimensionless thermal contact conductance data for cylindrical contacts as a function of dimensionless interface heat flux.

conductance. The fourth term is included to represent the effects of an interstitial gas. Conductance is expected to be higher when there is an interstitial gas. The whole number exponents of the third and fourth terms were selected to align the data. Since the calculation of the interface pressures is beyond the scope of this study, no attempt is made to account for their influence. As predicted by Madhusudana (1986), the effect of interface fluid on the conductance is smaller than that of the relative expansion of the cylinders that make the interface. A power law fit through the experimental data serves as a point of departure for further analytical studies:

$$h^* = 9.9122 \left(q^*\right)^{0.54424} \tag{2.6}$$

This correlation has a Pearson's r value of 9.907E-1, indicating a fairly good fit.

Figure 2.5 compares the relative fit of various plate-finned tube correlations with experimental data. Experimental data from the studies of Dart (1959), Eckels (1977), Sheffield, et al. (1987), and Nho and Yovanovich (1989a, 1989b) were compared with the values predicted by the correlations of Eckels (1977), Sheffield, et al. (1985b), Wood, et al. (1987a, 1987b), and Sheffield, et al. (1989) at the same conditions. The horizontal axis indicates the measured conductance value and the vertical axis indicates the conductance value predicted by the correlations. The data points in the figure are placed at the intersection of the experimental value and the predicted value for a specific set of conditions. A solid line at 45° to the horizontal indicates where the data points would fall if the experimental results were exactly predicted by a correlation. Straight lines parallel to the 45° solid line are a least-squares fit through the all of the data points for each of the four correlations, and indicate the average over prediction or under prediction of the corresponding correlation. Lines that are above the solid line indicate that the corresponding correlations over-predict the experimental data, while lines that are below the

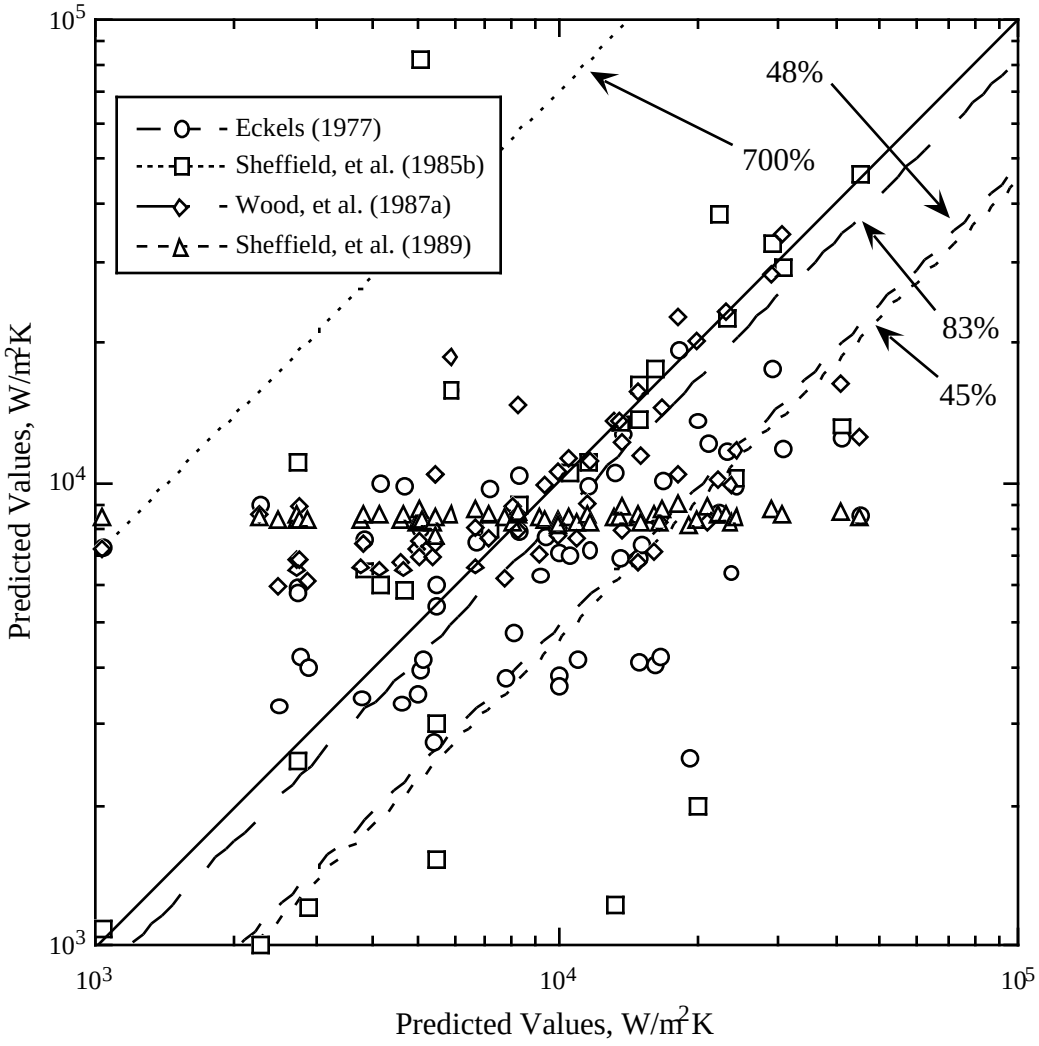

Figure 2.5 – Comparison of correlation predicted values of contact conductance with measured values for plate-finned tubes from studies of Dart (1959), Eckels (1977), Sheffield, et al. (1987), and Nho and Yovanovich (1989a, 1989b).

solid line indicate that the corresponding correlations under-predict the experimental data. The patterns made by the data on this figure are also of interest. While the data are scattered over the entire domain of the plot, a careful analysis of the data indicates that conductance values for finned tubes are generally low.

Examination of Figure 2.5 shows that the correlation of Eckels (1977) under-predicts the data by approximately 52%. The pattern formed by the data points is a wide band across the center part of the figure. The correlation of Sheffield, et al. (1985b) over-predicts the experimental values by approximately 700%. The correlation does not have a good correlation with the published experimental data (as exhibited by the wide scatter of corresponding data points). Further, the values predicted by this correlation span more than two orders of magnitude, while the experimental data spans slightly more than one. Some of the data points for this correlation lie near the bottom of the figure, while others lie near the top. This wide range of predicted values may be a result of the large exponent of the fin thickness–tube diameter ratio. The correlation of Wood, et al. (1987a) under-predicts the data by approximately 17%, and the associated data points exhibit a banded pattern across the lower part of the figure. The correlation by Sheffield, et al. (1989) under-predicts the data by an average of approximately 55%. The data points associated with the correlation exhibit a banded pattern across the middle part of the figure. The proposed correlations of Wood, et al. (1987a) and Sheffield, et al. (1989) have limited utility at low values of thermal contact conductance, since both have a lower bound inherent in the form of the correlation.

SUMMARY

Cylindrical contacts occur in many diverse applications. As a consequence, conduction through cylindrical contacts is an important phenomenon to understand. Cylindrical joints behave differently than flat joints. In flat contacts, interface pressure can

be monitored and controlled independently of the heat flux through the interface, and thermal contact conductance results are often presented as a function of interface pressure. In cylindrical contacts, the interface pressure is dependent on the initial degree of fit and the differential expansion of the cylinders (which is due to the temperature difference at the interface and to the temperature distribution within the individual cylindrical shells). As a consequence, the heat flux is far more important for cylindrical contacts than it is for flat contacts.

The present investigation provides a comparative study of the thermal contact conductance in cylindrical contacts for selected materials and conditions. While there are more studies devoted to thermal conduction through cylindrical contacts than there were six years ago, this phenomenon is still rather underrepresented in the literature. The available experimental data may not include all of the information required by current contact conductance models, including material designation, microhardness, or surface roughness and waviness (axially and circumferentially). There is a need, therefore, for more, quality experimental data. Sufficiently complex models may be able to more adequately predict the behavior of specific finned tube applications. Based on this review, it is evident that some areas of cylindrical thermal contact conductance have not been adequately investigated, including the effects of macroscopic eccentricities such as out-of-roundness and waviness. There are still many gaps in our understanding that need to be explored, hence the present investigation.

CHAPTER III

EXPERIMENTAL PROGRAM

Many factors influence experimental design. The design of the apparatus must balance the requirement of appropriate scale with the restriction of available resources. The apparatus must facilitate the measurements that need be made for calculation of the quantities of interest. Appropriate steps must be taken when designing an experiment to reduce the uncertainty of the experimental results. Some sort of control must be exerted on the experiment to ensure repeatability (which assures the reliability of the experimental results). Instrumentation and data acquisition equipment must be able to make accurate measurements over the expected range of experimental variables at the appropriate times. Precautions must be taken to ensure the safety of those involved and to prevent damage to the experimental facility. Additionally, in order to have reliable experimental results, the values of appropriate parameters must be known as a function of temperature. This chapter discloses and explains these details of the experimental design and the experimental procedure.

DESIGN OF APPARATUS

In order to evaluate the thermal contact conductance through cylindrical interfaces, an apparatus was designed to obtain data over a range of material and thermal conditions. The primary feature of the experimental apparatus is the assembly of co-axial cylindrical shells (each made from one of four different materials: CU-102, AL-6061, BR-360, or SS-304). These materials, with a wide range of thermophysical properties, were chosen so that the material properties part of a parametric study would have enough variability to be meaningful. These materials are also in relatively wide use, somewhat easy to machine, and

Table 3.1 – Nominal Material Properties at 300 K (from Touloukian and Ho, 1972)

	Copper Alloy 102	Aluminum Alloy 6061	Brass 360 70% Cu, 30% Zn	Stainless Steel Alloy 304
Thermal Conductivity,† k, W/m-K	401	154.9	110	16.3
Density, † ρ, kg/m^3	8933	2700	8530	7900
Specific Heat,† c_p, J/kg-K	385	962.9	380	502
Modulus of Elasticity, † E, GPa	110	70	110	193
Poisson's Ratio, † ν, unitless	0.35	0.33	0.35	0.27
Coefficient of Thermal Expansion, † α, 10^{-6} m/m-K	16.5	23.4	19.9	17.3

† Reported uncertainties in these values are within 3.5%.

readily obtainable. The nominal properties of the materials used in this investigation are listed in Table 3.1.

The dimensions of the cylinders were determined after considering the constraints of available space within the vacuum system, maximum available electrical power, mass of components, available instrumentation, and the desired range of interface heat fluxes. The cylindrical shell thicknesses were dictated by available metal stock sizes and the diameter of the heater. The nominal interface diameter, 0.0508 m, was chosen so that stock heaters could be used to produce a range of interface heat fluxes approaching those of previously published results. Shell clearances were selected to facilitate room-temperature assembly while providing appropriate contact pressures at operating temperatures. Future experiments should consider variation of the shell thicknesses and the interface clearance to fully investigate the effects of shell geometry on the contact conductance.

Heat was supplied to the assembly by a 0.1397 m long, 0.00127 m diameter, 1000 W cartridge heater placed along the axis of the inner cylinder. This provided a maximum heat flux of 4.93E4W/m^2 at the nominal interface diameter of 0.508 m. Thin, multi-layer, foil radiation shields were placed at the ends of the assembly to reduce heat losses due to radiation from the flat, end surfaces of the assembly, and to promote one dimensional, radial conduction through the cylinders. Heat is removed from the assembly by two cooling rings that are held onto the external surface of the outer cylinder with hose clamps. The cooling rings used in this investigation are shown in Figure 3.1.

Each of these cooling rings is constructed of three loops of 0.00635 m (0.25") copper tubing soldered onto two 0.0508 m (2") wide copper straps. Sufficient solder was used to completely fill the spaces formed by adjacent courses of tubing and the copper strap beneath them. Prior to soldering the tubes onto the straps, the straps were formed into arcs that would fit snuggly onto the outer cylinder. Relief arcs were formed in the tubing courses during fabrication to allow the rings to expand to facilitate assembly. The rate of coolant flow through the cooling rings (approximately 30 l/min) was assumed to be sufficient to maintain a near-uniform exterior surface temperature. In practice, the temperature difference between the supply and return legs of the coolant at the feed-through ring was negligible.

After assembly, the experimental apparatus was located within a vacuum enclosure to reduce the heat losses due to convection during testing. The apparatus was placed upon a four-point support to minimize heat losses due to conduction during testing. The vacuum within the chamber was maintained by an oil diffusion pump backed by a roughing pump.

Figure 3.1 shows partially assembled pair of cylindrical shells with attached cooling rings and a partially inserted heater. Eight of the sixteen thermocouples installed in the two cylinders are visible on the left side of the figure. The outer cylinder has been instrumented with strain gages at the mid-plane, between the two cooling rings. The tube-

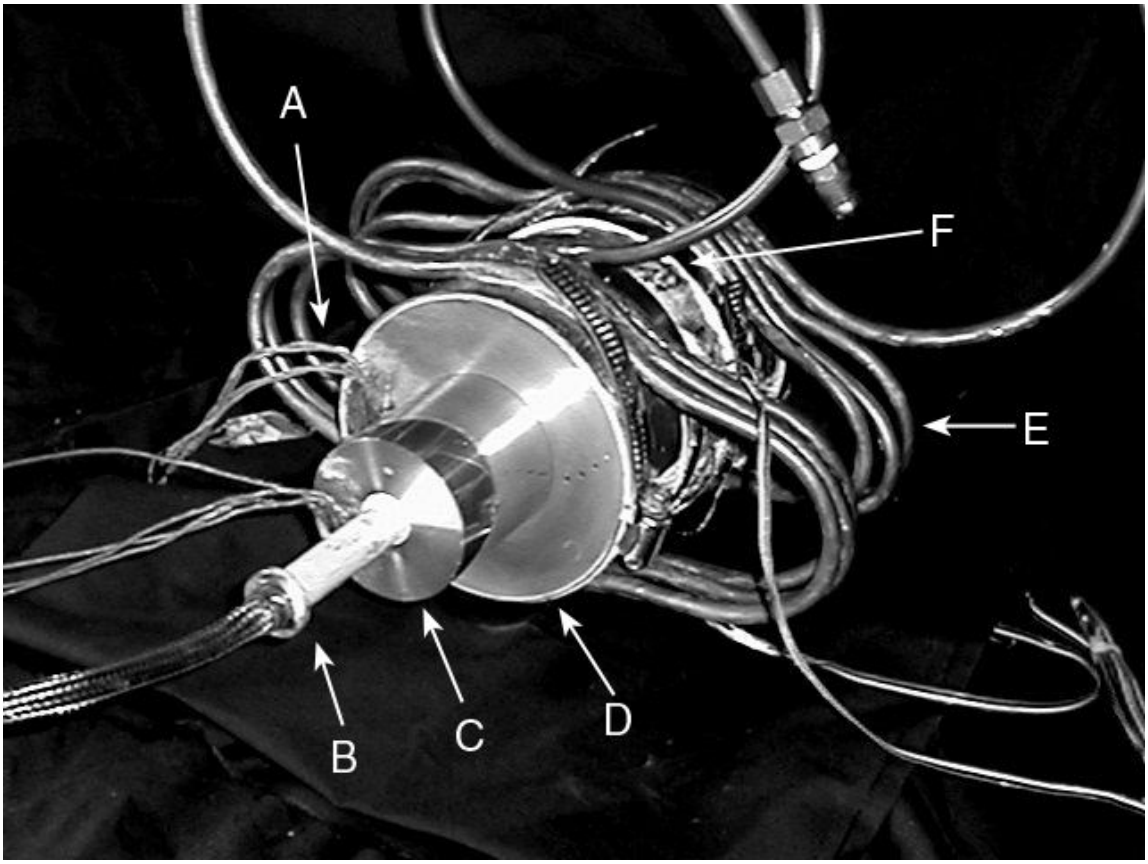

Figure 3.1 – Partially assembled test fixture. Indicated parts are (A) thermocouples, (B) 1000 W heater, (C) inner cylindrical shell, (D) outer cylindrical shell, (E) cooling rings, and (F) a strain gage rosette.

hose coupling at the top right of the figure is one of two the supply or return chilled water. Power leads for the heater and lead wires from the thermocouples and strain gages would be connected to appropriate feed-throughs within the vacuum chamber.

INSTRUMENTATION

In order to calculate the thermal contact conductance at the interfaces used in this investigation, it is necessary to have measurements of the temperature distribution within each of the cylinders. Also, since the pressures at the interface are of interest, some means of determining this empirically was desirable. All sensors were connected to an automated

recording and test control system to facilitate data acquisition. The data acquisition system also served to increase the repeatability of test results by providing a consistent criterion for the determination of steady state.

Thermocouples

The temperature distribution within each cylinder is monitored by eight fiberglass sheathed, AWG 36, special limit of error (SLE) grade, Chromel-Alumel (type K) thermocouples. The SLE grade thermocouples have a vendor-specified error of ± 1.1 K, and generally have a smaller error. Characterization testing of the wire used in the present study revealed an average error of ± 0.3 K for the wire from the same spool that was used for instrumenting the cylinders in this investigation. See Appendix E for details.

The thermocouples are located within each cylinder so that there are two thermocouples at each of four different, evenly spaced, radial locations, placed opposite to each other. The thermocouples were installed in holes drilled parallel to the central axis of the cylindrical shell, to different depths (varying from 0.01270 m to 0.02794 m, dependent on radial location), and offset 5° from each other circumferentially. These different depths and offsets were used to ensure that the thermocouple beads were located far enough away from each other that the distortion of the temperature distribution due to the presence of the other holes would be minimized. Small amounts of fine powdered copper were tamped into the holes prior to installation to assure that the thermocouples reported a reading representative of the temperature in the material around the holes. The SLE grade thermocouple leads were connected to extension grade wire (used in the feed-through ring) within a shielded isothermal block.

Strain Gages

Metal foil strain gages were evenly placed about the mid-plane on the exterior surface of the outer shells to facilitate the measurement of the average circumferential and

axial expansions of the outer cylinders. The places where the strain gages were to be mounted were slightly roughened with steel wool and cleaned prior to cementing the strain gages. Great care was taken to ensure alignment of the four dual-gage encapsulations with the mid-plane and main axis of each cylinder. Solder terminals for each of the gages were located near each encapsulation, and terminals for the gage array were located and fixed to the cylinder on the mid plane. Moderate pressure was applied to each encapsulation during the temperature curing process for the adhesive, at least 50 K above the expected service temperature for at least two hours (in accordance with Measurements Group Instruction Bulletin B-129, Measurements Group, Inc., 1999c).

The temperature distribution within the outer cylinder can be used with Lamé thermal stress relations to calculate the amount that the exterior surface should expand due to temperature. The difference between the measured and calculated expansion is presumed to be due to the pressure exerted on the outer cylinder by the inner cylinder at the interface. The relevant equations for this pressure calculation can be found in Appendices D and E. The uncertainty of the strain measurement ranged from 20% to 300%, while the uncertainty in the calculated pressure approximately ranged from 5% to 140%. Data that had excessively high uncertainties (greater than 30%) were not used in any of the correlations or figures in Chapter IV.

Data Acquisition and Control System

The devices used to monitor and record thermocouple and strain gage data are National Instruments FieldPoint modules, driven by software within a National Instruments LabView program. These 16 bit A/D devices have an effective resolution of 0.03125 K for the thermocouple modules, and 1.984E-6 VDC for the voltage measurement modules used to monitor strain gage output. Additional input/output channels are provided by the National Instruments PC/MIO E-series card mounted on the data acquisition

microcomputer. The 12 bit A/D input channels, used to measure the strain gage excitation voltage, have a resolution of 0.0051 VDC. The 12 bit A/D output channel, used to send a DC voltage to the heater op-amp, has a resolution of 0.00122 VDC, corresponding to a heater power resolution of 0.244 W. Control program operational details are covered later.

MATERIALS CHARACTERIZATION

As previously mentioned, the four materials used in this study were chosen for their machinability, their wide variation of thermophysical properties, and their availability. Of particular interest in this investigation are the thermal conductivity and coefficient of thermal expansion (CTE) of the test materials. Both of these properties strongly influence the thermally induced stresses within and at the interface between the cylinders, and the thermal conductivity obviously plays a large part in the conductance at the cylindrical joint. Other material properties (such as Young's modulus, Poisson's ratio, and thermal diffusivity) can be either obtained from thermophysical properties tables or derived from measured quantities with sufficient accuracy for the purposes of this investigation. The procedures used to determine these quantities are described below.

Coefficient of Thermal Expansion

The coefficient of thermal expansion (CTE) is typically measured by means of processes that adhere to ASTM Standard E 228-95 (ASTM, 2002). Processes that adhere to this standard utilize a sensitive dial indicator or electronic transducer to compare the expansion of cylindrical specimens of a quartz or vitreous silica expansion standard with the expansion of specimens of unknown coefficients of thermal expansion. However, making measurements with these dilatometers can be an exacting task, especially if there are no such facilities at hand with trained personnel. Micro-Measurements Technical Note TN-513-1 (Measurements Group, 1999a) describes a method to use metal foil strain gages to measure the coefficient of thermal expansion with acceptable accuracy. The method

makes use of unidirectional strain gages and a thermal expansion standard to provide a means of comparing the expansion of materials of interest to that of the known material. Since titanium silicate has a very low and well-characterized coefficient of thermal expansion, it was selected for use as the thermal expansion reference. The linear thermal expansion of the titanium silicate expansion standard is given in Figure 3.2, with data supplied by C. L. Davis of Corning, Inc. (2000).

The titanium silicate bar (0.1624 m x 0.0254 m x 0.00635 m) was instrumented with one Micro-Measurements WA-06-250BG-120 strain gage, a 120 ohm unidirectional, encapsulated gage. Cylindrical samples (0.0254 m diameter, 0.0762 m long) of each test material were each instrumented with a WA-06-250BG-120 strain gage. Each gage was located at the mid-plane of the specimen, aligned with the major axis of the specimen. An AWG 36, special limit of error (± 1.1 °C) Chromel-Alumel thermocouple was mounted 0.0191 m deep into one end along the axis of each of the metallic specimens. All sensors were connected to appropriate bridging equipment and to National Instruments FieldPoint data acquisition modules, driven by a microcomputer running a National Instruments LabView program. All strain gages and thermocouples used in these characterization tests were taken from the same package or reel, to minimize errors due to manufacturing inconsistencies.

Prior to characterization, the specimens were cycled between the maximum and minimum test temperatures three times to redistribute any residual stresses (which would make the measurements non-repeatable). During testing, all specimens were placed on a glass wool pad within a controlled-temperature furnace to reduce the resistance to expansion due to friction. The furnace was set to a desired temperature and the LabView program was started. The program monitored the temperatures reported by the thermocouples within the metal specimens. When steady state was achieved the voltage

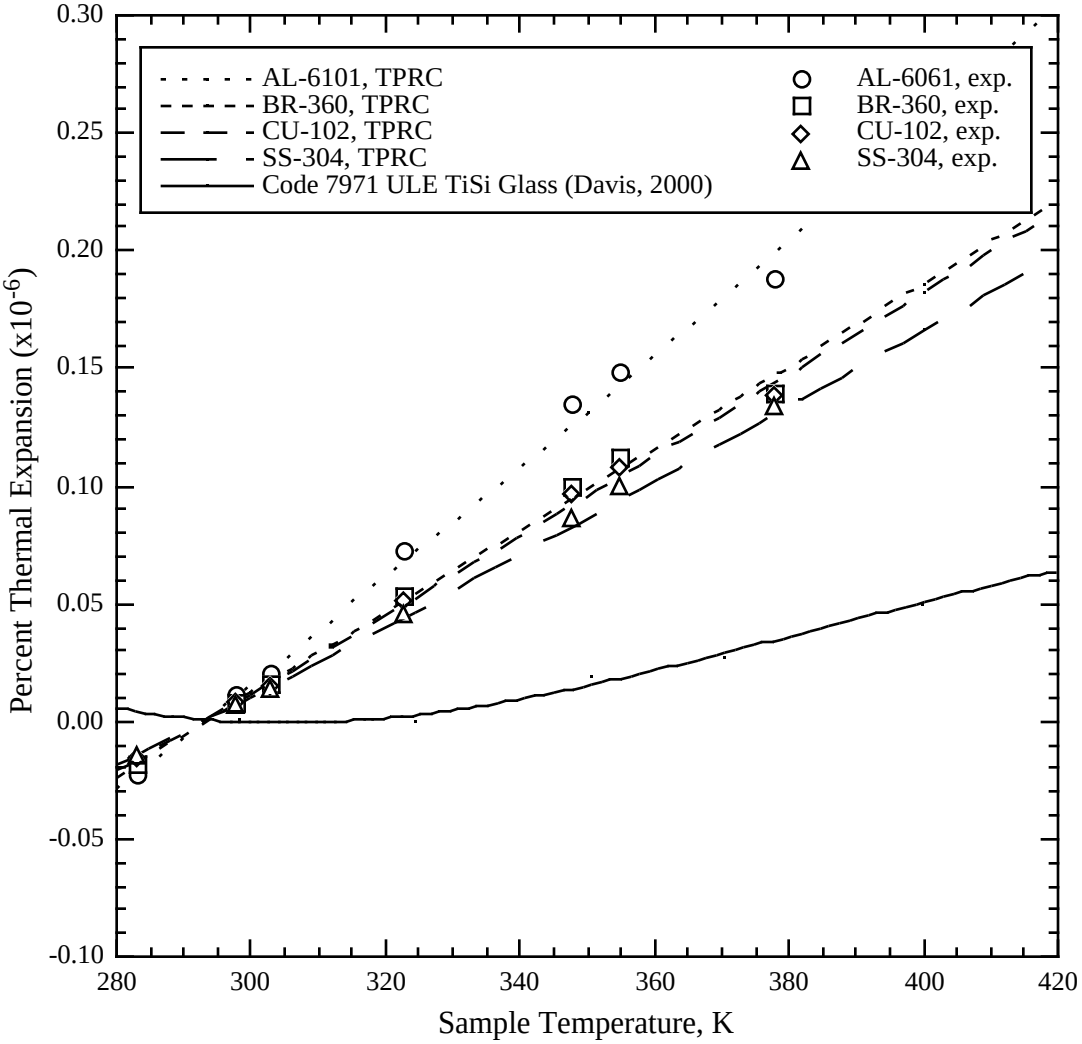

Figure 3.2 – Comparison of temperature dependent strain of test materials with polynomial curves recommended by the Thermophysical Properties Research Center (TPRC) obtained from Touloukian and Ho (1972), and temperature-dependent strain of Code 7971 Ultra Low Expansion Titanium Silicate expansion standard (Davis, 2000).

Table 3.2 – Polynomial Coefficients for Coefficient of Thermal Expansion (Touloukina and Ho, 1972)

$\alpha(T) = \sum_i a_i T^i$	AL-6061	BR-360	CU-102	SS-304
a_0	-1.5796E+01	4.5359E+01	-1.0837E+00	9.4031E+00
a_1	4.8889E-01	-2.9227E-01	1.3650E-01	2.1573E-02
a_2	2.4976E-03	1.1815E-03	-3.7885E-04	-1.3461E-05
a_3	6.1407E-06	-2.3416E-06	4.0396E-07	8.8909E-09
a_4	-7.0032E-09	2.2972E-09	-3.1051E-10	8.0024E-12
a_5	2.9983E-12	-8.7285E-13	7.2562E-14	2.7007E-15

across appropriate points of the bridge were recorded and converted to apparent strain. Since the thermocouple wire used to instrument the CTE specimens is of the same roll as the wire used in the other experiments in this investigation, a standard uncertainty of ± 0.3 K is assumed to be appropriate.

Following the procedure recommended in TN-513-1 (Measurements Group, 1999a), the strain of the reference specimen was subtracted from these apparent strains of the test materials, and the resulting values were plotted as a function of temperature and compared with the expected values obtained in Touloukian and Ho (1972). There experimentally obtained data have good agreement with the suggested handbook values, and due to the relatively small amount of data, the polynomial expressions for the coefficient of thermal expansion for these materials will be used. The coefficients for the polynomial expression of the coefficient of thermal expansion as a function of temperature given in Table 3.2 are the recommended values from Touloukian and Ho (1972).

Determination of Thermal Conductivity

The thermal conductivity of the materials used in this investigation was determined by means of the cut-bar method. This method, as employed in this investigation, imposes a flow of heat through a stack of instrumented cylindrical samples. Samples of known conductivity are placed on either side of a sample of unknown conductivity, and heat is introduced at one end of the stack and removed at the other. The heat flux through each sample of known conductivity (or heat flux meter) is calculated using Fourier's Law, the temperature dependent conductivity of the heat flux meter, and the temperature gradient within the heat flux meter. Similarly, given the average heat flux through the sample of unknown conductivity and the temperature gradient within the sample, the thermal conductivity of the sample can be calculated.

The experimental test facility (Figure 3.3) consists of a vertical frame with sliding plates which support a load cell, a pneumatic bellows, two source-sink holder assemblies, calibrated heat flux meters, and the test specimens. An axial force is applied to the test column by the pneumatic bellows and is monitored by the load cell. This force is transmitted through two hardened steel spheres to the source-sink holder assemblies, and thence to the test specimens. Since the steel spheres do not support a moment, this arrangement ensures a uniform pressure over the test surfaces. Heaters and integral coolant passages in both the top and bottom heat flux meter holding assemblies facilitate control of the temperature at the interface of interest or the average temperature of the specimen. The facility is housed in a vacuum bell jar to reduce the radial heat losses due to convection. Stack pressure and specimen temperature sensors are connected to a Hewlett-Packard 3497A data acquisition control unit, and then to the controlling microcomputer. Interface pressure and temperature are controlled by a test control program on the controlling microcomputer. Principal inputs to the test control program include the flux

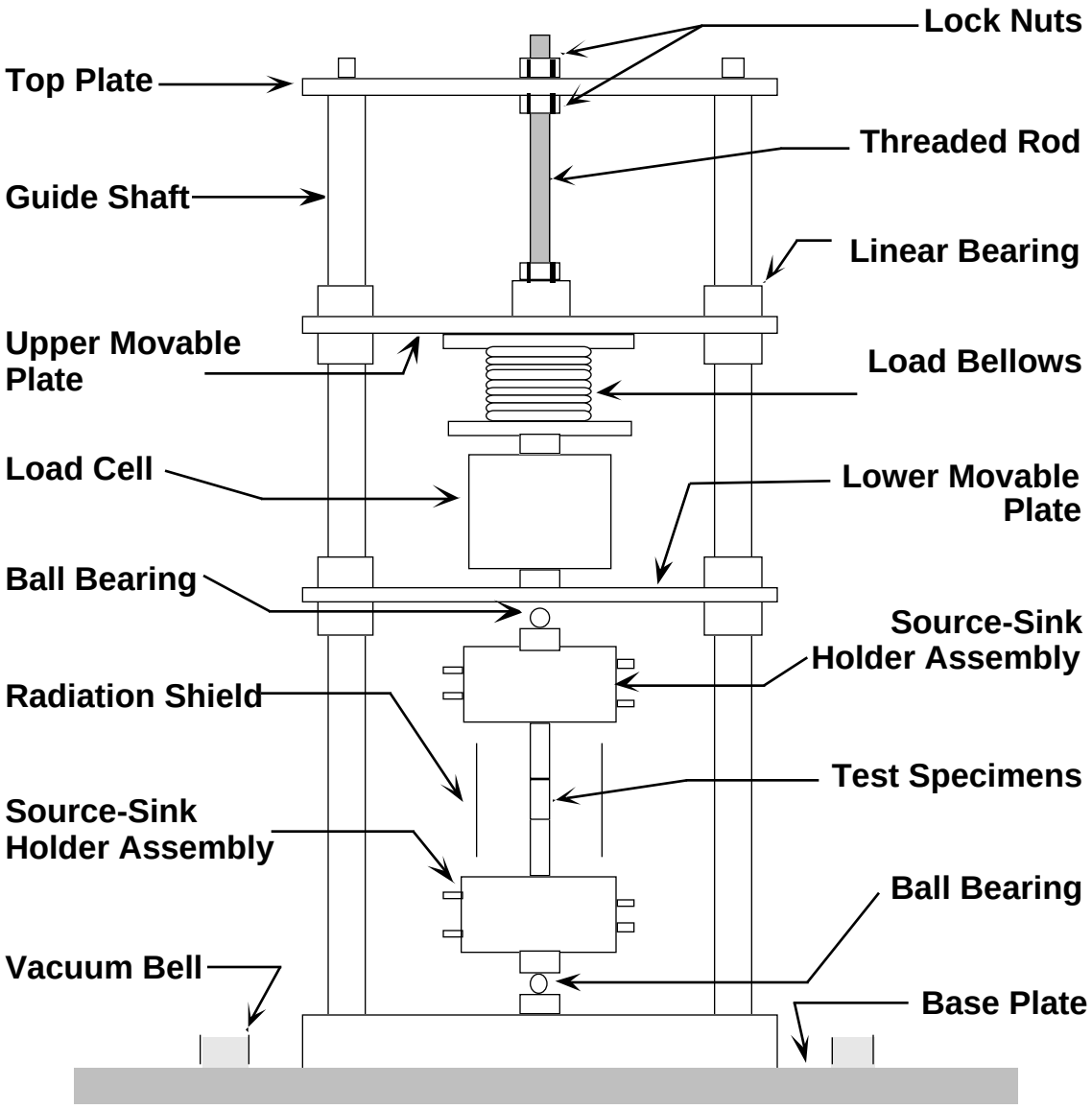

Figure 3.3 – Cut-bar thermal conductivity facility used in this investigation.

meter material, thermocouple placement and specimen geometry, desired test pressure, and an array of test temperatures.

The specimens and heat flux meters used in this experiment were 0.0254 m diameter cylinders, 0.0381 m long. The flux meters were made from NIST-supplied electrolytic iron, and the conductivity test specimens were made from the same material as the cylindrical contact conductance specimens. The roughness of the flat, circular surfaces was specified to be less than 25 μm to ensure good contact between the heat flux meters and the test specimens. The heat flux meters and test specimens were each instrumented with five fiberglass sheathed, special limit of error (± 1.1 K), Chromel-Alumel (type K) thermocouples at 0.00635 m intervals along their length. The thermocouples were installed in holes drilled to the axes of and at 0.00635 m intervals along the length of the flux meters and the specimens. Fine powdered copper was tamped into the holes to assure that the thermocouples reported a reading representative of the temperature in the material around the holes. Each thermocouple wires was wrapped around the flux meters or specimen (to minimize errors due to heat conduction away from the thermocouple beads).

Prior to installation within the test stack, the contacting surfaces of each specimen and flux meter were cleaned and coated with a thermally conductive grease and they were placed between the source/sink holders. The thermally conductive grease reduces the power required by the heater to maintain the test specimen at a desired temperature by reducing the temperature discontinuities at the interfaces between the specimens, heat flux meters, and source/sink holder assemblies. Alignment of the specimens with the heat flux meters was meticulously checked to avoid uncertainty errors in the macroscopic conduction area. A radiation shield was placed around the stack to minimize radial heat loss and the associated uncertainty in stack heat rate. After ensuring that all sensor and coolant connections were sound, the chamber was closed and evacuated. Tests were conducted at

chamber environmental pressures less than 0.13 Pa (5.00E-3 Torr), which were maintained by an oil diffusion pump backed by a two stage roughing pump.

The desired stack pressure and the different mean test specimen temperatures were then entered into the control software, along with the stack geometry, and testing was initiated. The test control program monitors and controls the interface pressure and the temperatures reported by the thermocouples, adjusting the power to the heater and pressure within pneumatic bellows to maintain the specified specimen temperature and interface pressure operating conditions within a consistent range (typically within 1% of the set point values). A nominal stack pressure of 1.379E6 Pa was used to ensure good contact between the test sample and the heat flux meters. The thermal conductivity of the test samples was evaluated over a range of temperatures from 300 K to 450 K. Sixteen temperatures were used to span this temperature range.

All conductivity measurements were taken while the specimens were at steady state. The control software ascertains that steady state has been reached when the variation of the control parameters and the measured value does not exceed the specified drift tolerance range for thirty minutes. Heat fluxes are obtained by using a least squares fit of the temperatures at known locations within the heat flux meters to determine the average heat flux through the test stack via Fourier's Law. The thermal conductivity of the test specimen is obtained by dividing the average heat flux by the averaged temperature gradient through the specimen. After the data have been recorded to disk, the program either proceeds to the next set of conditions or terminates power to the heater and ends the test, whichever is appropriate. Figure 3.4 shows the results of these thermal conductivity tests, along with other published data for similar materials, and Table 3.3 lists the fifth order polynomial coefficients of the least-squares line through the data.

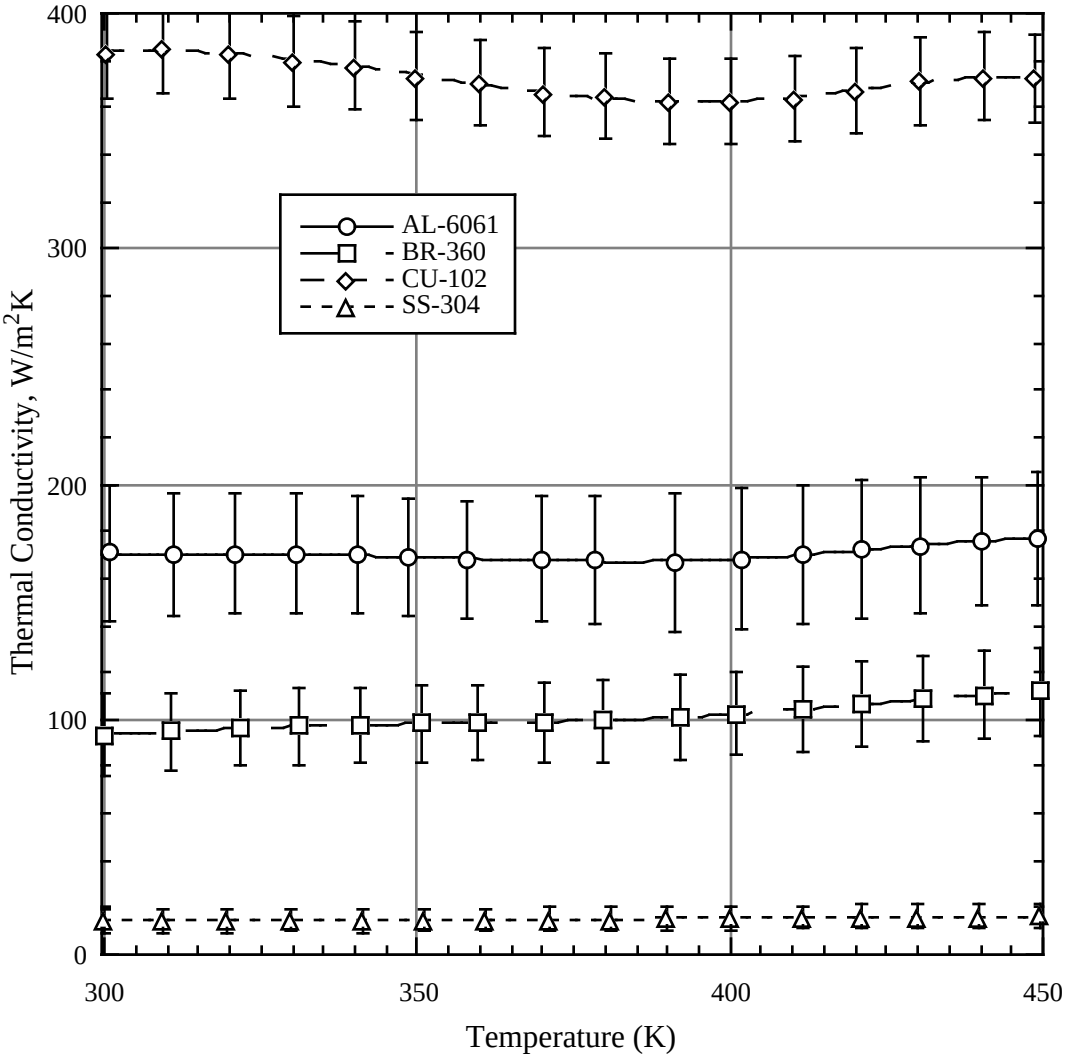

Figure 3.4 – Results of thermal conductivity testing of materials used in this investigation.

Table 3.3 – Experimentally Determined Polynomial Coefficients for Thermal Conductivity

$k(T) = \sum_i a_i T^i$	AL-6061	BR-360	CU-102	SS-304
a_0	2.4631E+04	1.4930E+04	3.8046E+04	-3.4083E+03
a_1	-3.4347E+02	-2.1185E+02	-5.4048E+02	4.5791E+01
a_2	1.9173E+00	1.2008E+00	3.0809E+00	-2.4336E-01
a_3	-5.3156E-03	-3.3771E-03	-8.7093E-03	6.4219E-04
a_4	7.3167E-06	4.7132E-06	1.2199E-05	-8.4147E-07
a_5	-3.9984E-09	-2.6105E-09	-6.7705E-09	4.3818E-10

Surface Characterizing

Prior to commencing the experimental investigation, the cylindrical shells to be used in the experiment were sent to the Mahr-Federal Corporation for surface characterization. Data obtained in this characterization are presented in Appendix C. In addition to the standard linear roughness and waviness parameters, the cylindricity, roundness, and circumferential waviness of the contact surfaces are also provided.

Some of these parameters (flatness, cylindricity, roundness) are related to geometric dimensioning and tolerancing terms, and are sometimes used interchangeably. Flatness is the condition where all points on a surface lie on the same plane. A flatness tolerance is the spacing between two parallel planes between which all points on the nominally flat surface must lie. A flatness tolerance zone is a space aligned with the specified surface bounded by the two parallel planes. Similarly, circularity (or roundness) is the condition where, on a cylinder or cone, all points on the surface intersected by a plane perpendicular to the axis are equidistant from the axis. A circularity tolerance is the spacing between two concentric circles between which all points on the surface intersected by a plane perpendicular to the

axis must lie. A circularity tolerance zone is the space between the two concentric circles. Cylindricity may be visualized as a combination of flatness and circularity, extended to an entire cylindrical surface. A cylindricity tolerance is the spacing between two concentric cylinders between which all points on a nominally cylindrical surface must lie.

Throughout the test program, surface characterization measurements of the contacting surfaces were made. Since circumferential measurements are beyond the capacity of the SurfAnalyzer 5000 available for use, only axial measurements could be checked over the course of the test program. The change in the axial roughness of the cylindrical surfaces over the course of testing was within the uncertainty of the SurfAnalyzer 5000 used. There were, however, small scratches on the surface where the parts rubbed against each other during assembly.

DETERMINATION OF THERMAL CONTACT CONDUCTANCE

As defined in Chapter I, thermal contact conductance is the ratio of the heat flux across an interface defined by two surfaces and the magnitude of the temperature discontinuity at that interface. The heat fluxes through the cylindrical interfaces examined in this study were calculated by dividing the average rate heat transferred through the inner and outer shells, as calculated through Fourier's Law, by the nominal interface area. Fourier's law is also used to relate the thermal conductivity and the known temperature distribution in each of the cylinders to the inner and outer interface temperatures, and thus to the magnitude of the temperature discontinuity at that interface.

With four different materials used to make the inner and outer shells, compound cylinders with sixteen different material combinations are available for testing. In addition to the effects of the different temperature-dependent thermophysical properties of the materials, different surface characteristics influence the heat transfer as an effect of each material combination. The surface roughness, asperity slope, and room-temperature

Table 3.4 – Test Interface Geometry Parameters

Outer Cylinder Material			Inner Cylinder Material: AL-6061	BR-360	CU-102	SS-304
	AL-6061	δr_i, m	1.799E-05	1.908E-05	2.193E-05	1.334E-05
		σ_e, m	6.896E-05	1.053E-04	8.835E-05	7.736E-05
		m_e	1.475E-01	1.475E-01	1.475E-01	1.475E-01
	BR-360	δr_i, m	1.156E-05	1.265E-05	1.549E-05	6.900E-06
		σ_e, m	7.595E-05	1.100E-04	9.391E-05	8.366E-05
		m_e	1.535E-01	1.535E-01	1.535E-01	1.535E-01
	CU-102	δr_i, m	4.233E-07	1.512E-06	4.360E-06	-4.233E-06
		σ_e, m	4.806E-05	9.295E-05	7.321E-05	5.950E-05
		m_e	1.984E-01	1.984E-01	1.984E-01	1.984E-01
	SS-304	δr_i, m	1.281E-05	1.389E-05	1.674E-05	8.149E-06
		σ_e, m	7.146E-05	1.069E-04	9.031E-05	7.960E-05
		m_e	1.605E-01	1.605E-01	1.605E-01	1.605E-01

interface clearance play a role in the contact conductance. Table 3.4 lists these test parameters.

Certain material combinations (such as aluminum/copper or aluminum/brass) are susceptible to galling or cold welding, so the time that the cylinder pairs are assembled was minimized. Galling and cold welding are welding processes that use molecular migration at room temperature to join metals. Galling is adhesion or welding during sliding contact. Since the assembly of the compound cylinders takes place manually and is followed immediately by a slight rotation of one cylinder with respect to the other, it is unlikely that any "sticking" of the shells together would pass unnoticed and the effects of galling are avoided. Cold pressure welding is the process where high contact pressures (1.4E6 – 5.6E6 Pa) break surface oxide layers to allow molecular bonding to take place between the

uncontaminated subsurface metals. Typically, ductile metals and alloys are good candidates for this process.

The selection of the heater settings is influenced by the maximum temperatures allowed. The thermocouple insulation has a maximum service temperature of 700 K and the stainless steel will start to undergo a phase transformation at 670 K. The elastic modulus of all materials will become nonlinearly variable at temperatures above 570 K and the solder has a maximum service temperature of 565 K. The epoxy used to pot the thermocouples softens at elevated temperature (at least, until it is completely out-gassed), but since no strain was applied to the wire this was not taken into account to determine the over-temperature condition. The temperature used to determine if an over-temperature condition existed was 550 K, ensuring that none of the components or instrumentation were damaged. Preliminary testing of the test facility and program revealed that maximum heater settings could be used without violating the over-temperature criteria. Therefore, all testing included the maximum heater setting.

Test Plan

For each of the sixteen material combinations used in standard conductance testing, at least twelve heater settings were used: 0 W, 300 W, 500 W, 600 W, 700 W, 750 W, 800 W, 850 W, 900 W, 950 W, 1000 W, 501 W, 1 W. More data points were collected at higher heater settings, since it was assumed that there would be better contact and thus more interesting information at those conditions. The initial, 0 W, setting provided an opportunity to check sensor connections, thermocouple uncertainty, and initial strain gage tare. The last two settings allowed some measure of test repeatability. The typical time from a change in heater set point to steady state was roughly one hour. At lower heat rates (300 W and lower), either the interface pressures were too low or the uncertainties in the contact conductance were too high to provide valid conductance data.

Some additional experiment test series were run to test experimental repeatability, using the same heater settings and coolant flow rates as initial experiments for a given pair of cylindrical shells. The cylindrical shells were aligned differently for each repeatability series, offset by at least 45° from the initial assembly alignment. In other experiments the heater settings were cycled between two values to examine the effect of repeat loading on the thermal contact conductance. One experiment was run to determine if hysteresis phenomena were of importance, but the differences between the increasing heat flux leg and the decreasing heat flux leg were lost in the uncertainty of the contact conductance and interface heat flux. These supplemental experiments were run after all other testing was completed.

Sample Preparation and Assembly

After the cylindrical shells were cleaned, the working order of every thermocouple in each cylinder was verified and the condition of their mounting was examined for potential failure. The resistance across each strain gage and both strain gage arrays were checked to verify that the gages were in good working order. Prior to cylinder assembly, the interior contacting surfaces of the cooling rings were coated with thermal grease, mounted onto the exterior surface of the outer cylinder, and connected to each other. The coolant ring and outer cylinder subassembly was then placed on the test stand. Coolant feed-through lines were attached to the inlet and outlet connectors of the coolant rings and fluid at 323 K was allowed to flow through the coolant loop. While the outer cylinder was being warmed by fluid, the contacting surfaces of the inner and outer cylinder were cleaned again with methanol.

The posterior thermocouple lead wires and connector plugs of the inner cylinder were carefully threaded through the opening in the outer cylinder. The inner cylinder was oriented so that the thermocouples on either the posterior or the anterior sides were not

aligned with the thermocouples on the outer cylinder. As the inner cylinder was gently inserted into the opening, the posterior lead wires, having been wrapped in lint-free tissue, were gradually pulled though so that they wouldn't contaminate the contacting surfaces. Axial alignment of the cylinders was verified by touch. In a few instances, the inner cylinder was slightly longer than the outer cylinder, but not more than 0.001 m. In these cases, the posterior surfaces of the cylinders were aligned and the discontinuity was allowed at the anterior end of the assembly. After the cylinders were aligned, the cartridge heater was coated with a thin layer of thermal grease and inserted with a rotary motion into the heater cavity at the axis of the inner cylinder. This was done to ensure an even coating of grease throughout the length of the cavity. Excess grease was wiped from the exposed surfaces of the cylinders and heater alignment was verified.

The thermocouple lead wires on both sides of both cylinders were placed so that they did not rest on any part of the heater, and their connector plugs were inserted into the appropriate sockets. The leads from the longitudinal and circumferential strain gage arrays were connected to the appropriate signal feed-through wires. The feed-through wires were connected to appropriate bridging equipment and to National Instruments FieldPoint data acquisition modules, monitored by a microcomputer running a National Instruments LabView program. The thermocouple and strain gage channels on the data acquisition system were observed to verify that the sensors were in working order. The heater power leads were threaded through the hole in the anterior radiation shield and the shield was mounted onto the test fixture. The heater power leads were then connected to the power feed-through and the power connection continuity was verified. Figure 3.5 shows the test fixture prior to heater insertion and assembly of the radiation shield.

After the cylinders were assembled and the thermocouple, strain gage, and heater power leads were connected, the test chamber was sealed and connected to the roughing pump. After the pressure sensor within the chamber registered less than 0.001 Torr, the

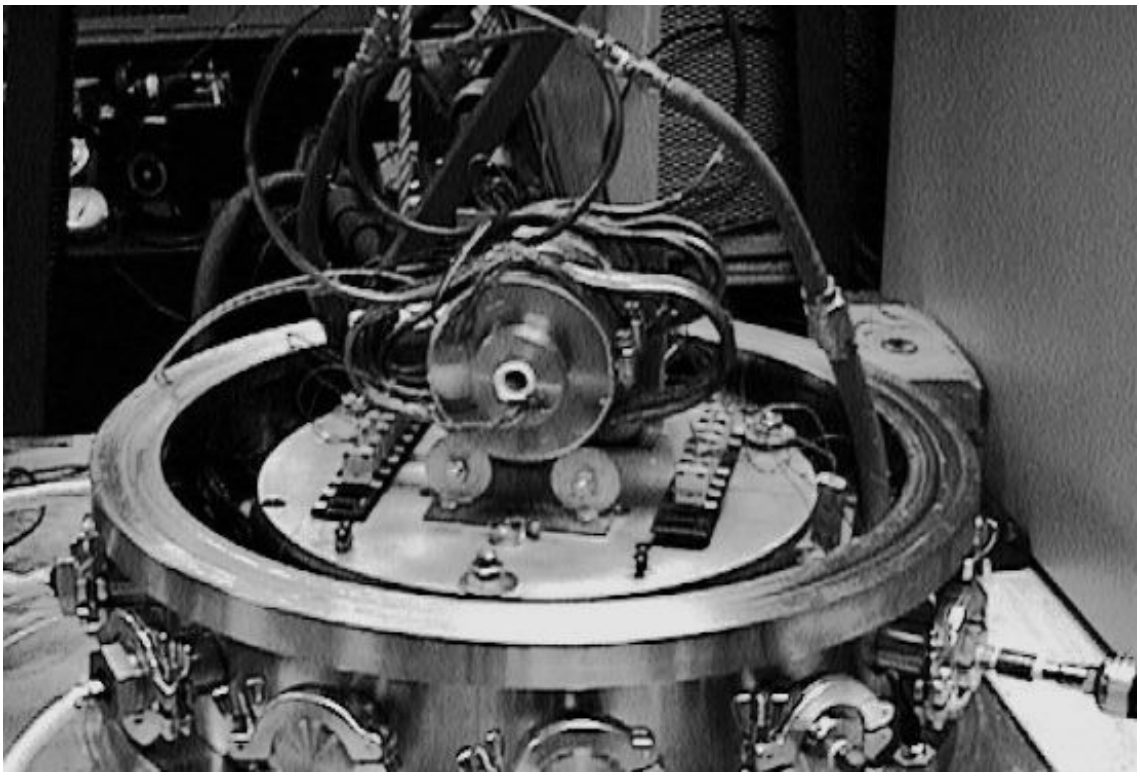

Figure 3.5 – Partially assembled test fixture on test stand.

constant temperature bath was disconnected, the chill water flow was introduced through the cooling rings, and the test assembly was allowed to come to a near-steady state while the chamber pressure continued to its maximum vacuum level. This was done so that there would not be any possibility of condensation contaminating the interfacial surfaces.

Control Program

At the heart of the data acquisition and control system used in this investigation was a microcomputer running the National Instruments LabView software package. The test control and data acquisition program was constructed using LabView's graphic interface, by essentially placing "components" and "wiring" them together. Since a complete reproduction of the various screens and windows of the program is meaningless to those

who are unfamiliar with the LabView system, a flow diagram and pseudocode of the program, detailing its operation, are found in Appendix B.

The desired heater power range array was populated by heater settings (essentially percentages of full power). When running, the program would deliver a 0-10 V DC signal to the op-amp such that the desired amount of power energized the heater. The op-amp operates on a five second, two-cycle time basis. For example, a 10 V DC signal to the op-amp would energize the heater with 120 V AC power for the full five seconds; a 5 V DC signal would energize the heater with 120 V AC power for two and a half seconds, followed by two and a half seconds without power; and a 1 V DC signal would energize the heater for a half second, followed by four and a half seconds without power.

At each heater power setting, thermocouple and strain gage outputs were monitored until steady state was achieved. It is important to be certain that the measurements are being done at steady state. Unless the assembly is at steady state, calculations of the average heat conduction rate through the cylinders will have unacceptably high uncertainties, of the same order of magnitude as the calculated value. These uncertainties will cascade through the data reduction, rendering the calculated values of the thermal contact conductance and interface temperature useless. Steady state is defined for the purposes of automated data acquisition when the variation of each of the measured and calculated temperatures is less than 0.15 K per half-hour. This value of allowable drift is related to the uncertainty in the interface heat flux (due to temperature drift) that varies with interface heat flux. An analysis of the influence of allowed temperature drift on the calculated value of the interface heat flux is given in Appendix E. When steady state was observed to have been achieved, the strain gage and thermocouple readings were taken and recorded, appropriate parameters calculated, and the next heater setting sent to the op-amp. At the end of the assigned tests for a test assembly, the control program sets the heater power to zero and stops running.

Data Reduction

While the test control program calculated the values of the interface heat flux and thermal contact conductance for the purposes of determining steady state, post-experimental processing was required to determine the interface pressure. A spreadsheet program was used to calculate these interface pressures, as well as the interface heat flux and interface temperatures. Relevant values are reported in Appendix C. The relevant data reduction and uncertainty algorithms are detailed in Appendix E.

CHAPTER IV

RESULTS AND DISCUSSION

Results of the experimental investigation and a discussion of those results are presented in this chapter. Sample calculation of results and an associated uncertainty analysis for a selected data point may be found in Appendix E. The results are presented dimensionally on a heat flux basis and on an interface pressure basis. The results are also presented non-dimensionally with previously published results, previously published correlations, and with empirically derived correlations. In this chapter, data sets are identified by a two-letter label. The first letter indicates the inner shell material (A – aluminum 6061, B – brass 360, C – copper 102, and S – stainless steel 304), and the second letter indicates the outer shell material. Similar nomenclature is used when presenting previously published results, insofar as it is possible.

Power law correlations are used to correlate conductance data from the present study, as well as previously published data, since log-log plots of the data appear to be linear. Power law correlations presume that one variable is proportional to another variable raised to some exponent. Compound power law correlations take this further, by relating one variable to the product of several variables, each raised to a different power, multiplied by some scaling factor.

Pearson's r, also known as the correlation coefficient or Pearson's correlation coefficient, has values between –1 and +1, inclusive. It indicates how well a linear best-fit line relates two paired variables, such as the contact conductance and interface pressure. A value of 0 indicates that neither variable can be predicted by the other with a linear equation, and values of 1 and –1 indicate a perfect linear relationships between the two variables

(-1 indicating an inverse relationship, 1 indicting a direct relationship). Pearson's r is defined for paired data (x, y) as:

$$R \equiv \frac{N\sum xy - \left(\sum x\right)\left(\sum y\right)}{\left[\left(n\sum x^2 - \left(\sum x\right)^2\right)\left(n\sum y^2 - \left(\sum y\right)^2\right)\right]^{\frac{1}{2}}} \tag{4.1}$$

Pearson's r is somewhat sensitive to extreme values in the data, and can be markedly reduced by outliers.

INTERFACE FLUX EXPERIMENTAL RESULTS

Dimensional Results, Heat Flux Basis

Figures 4.1–4.4 present the thermal conductance data from the present study on an interface heat flux basis. Figure 4.1 presents the thermal contact conductance for the experiments in the present study that involve the AL-6061 outer shell. Similarly, Figure 4.2 presents results for the brass-360 outer shell, Figure 4.3 presents results for the copper-102 outer shell, and Figure 4.4 presents results for the stainless steel-304 outer shell. All four figures show that the data are well behaved, as evidenced by the high values of Pearson's r for power-law fitted curves driven through each data set.

It is not difficult to convince oneself that the all of the data should be able to be described by a power law correlation, particularly in light of the clustering of data presented in Figure 4.5. In general, inner shells made of high conductivity materials have lower conductance values than low conductivity inner shells. While the power law curve fit through the aggregate data has an adequate correlation between the interface heat flux and the contact conductance, it should be possible to achieve a greater degree of correlation by using other parameters in addition to the heat flux. An analysis of the residuals of the correlation and the data shows that 95% of the data falls within 27% of the power law curve

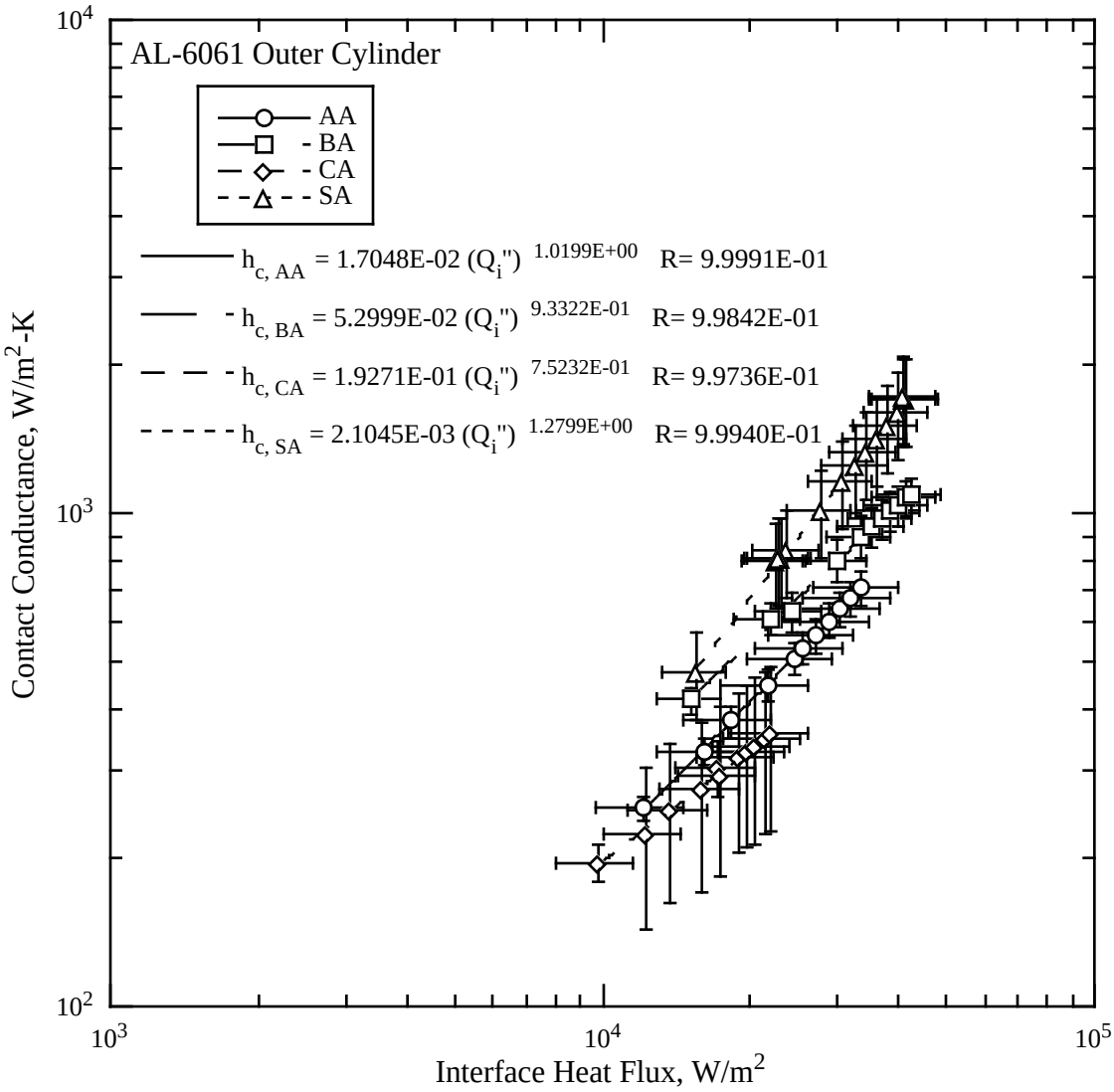

Figure 4.1 – Thermal contact conductance as a function of interface heat flux for aluminum outer shell experiments .

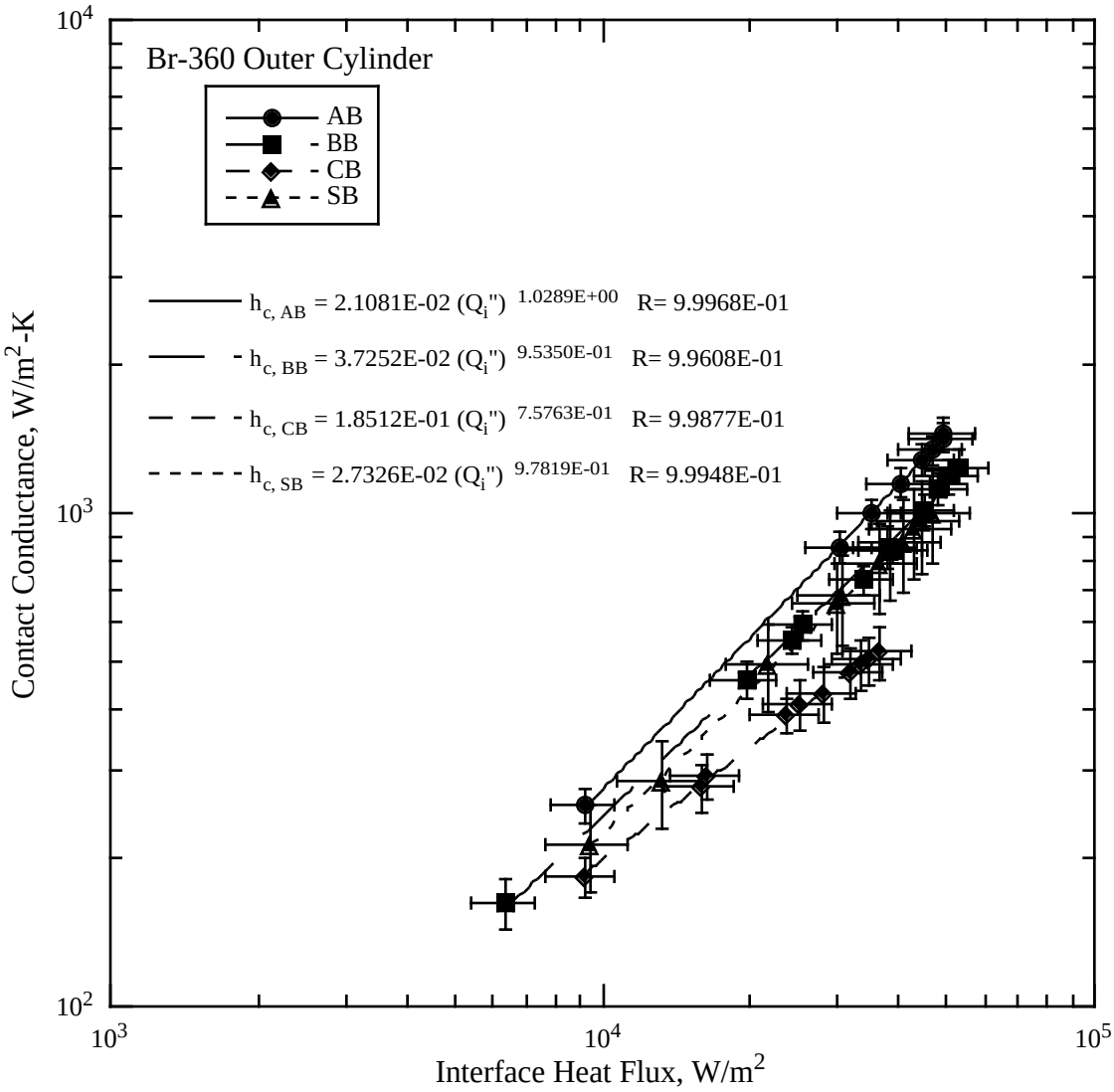

Figure 4.2 – Thermal contact conductance as a function of interface heat flux for brass outer shell experiments.

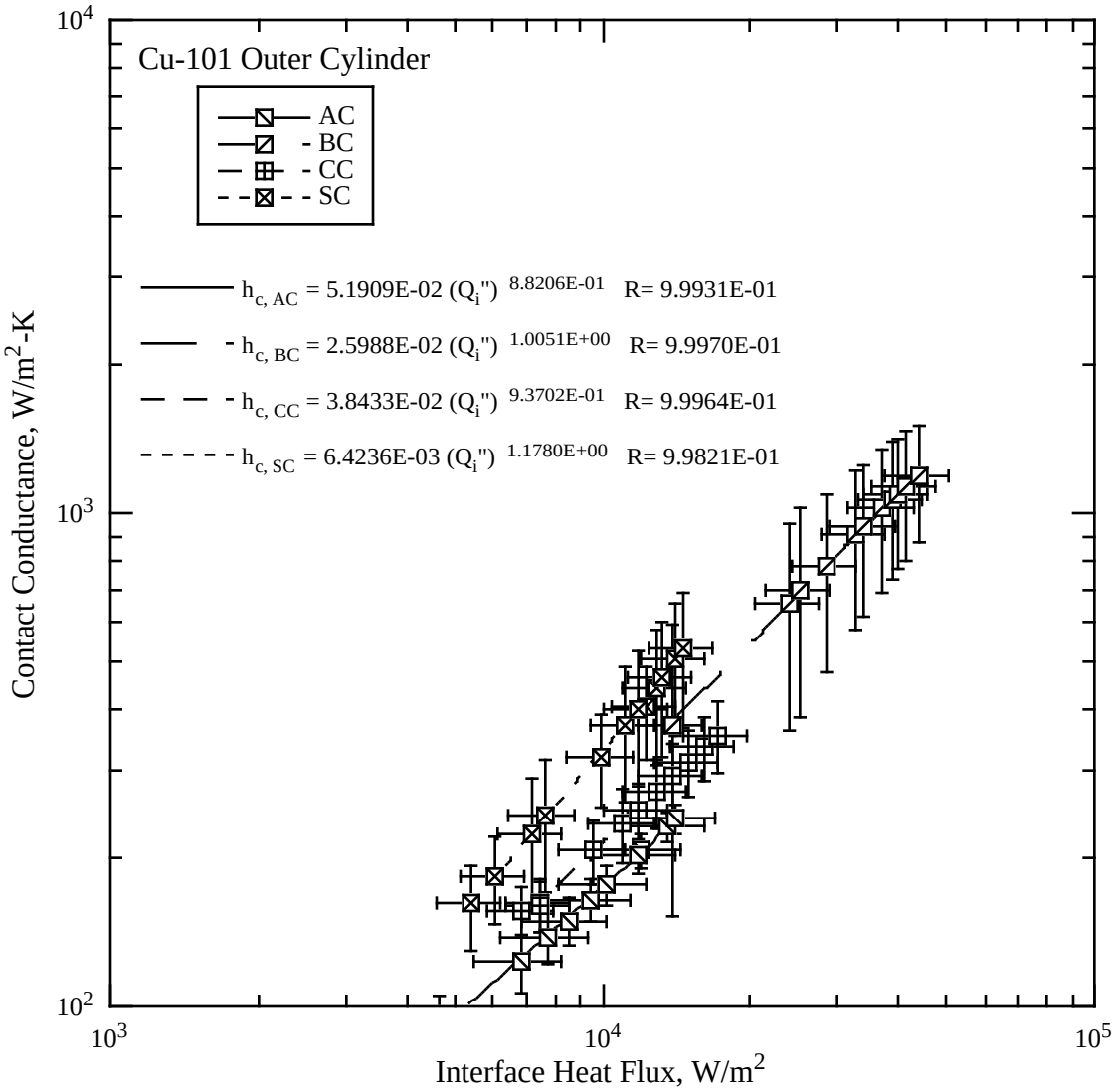

Figure 4.3 – Thermal contact conductance as a function of interface heat flux for copper outer shell experiments.

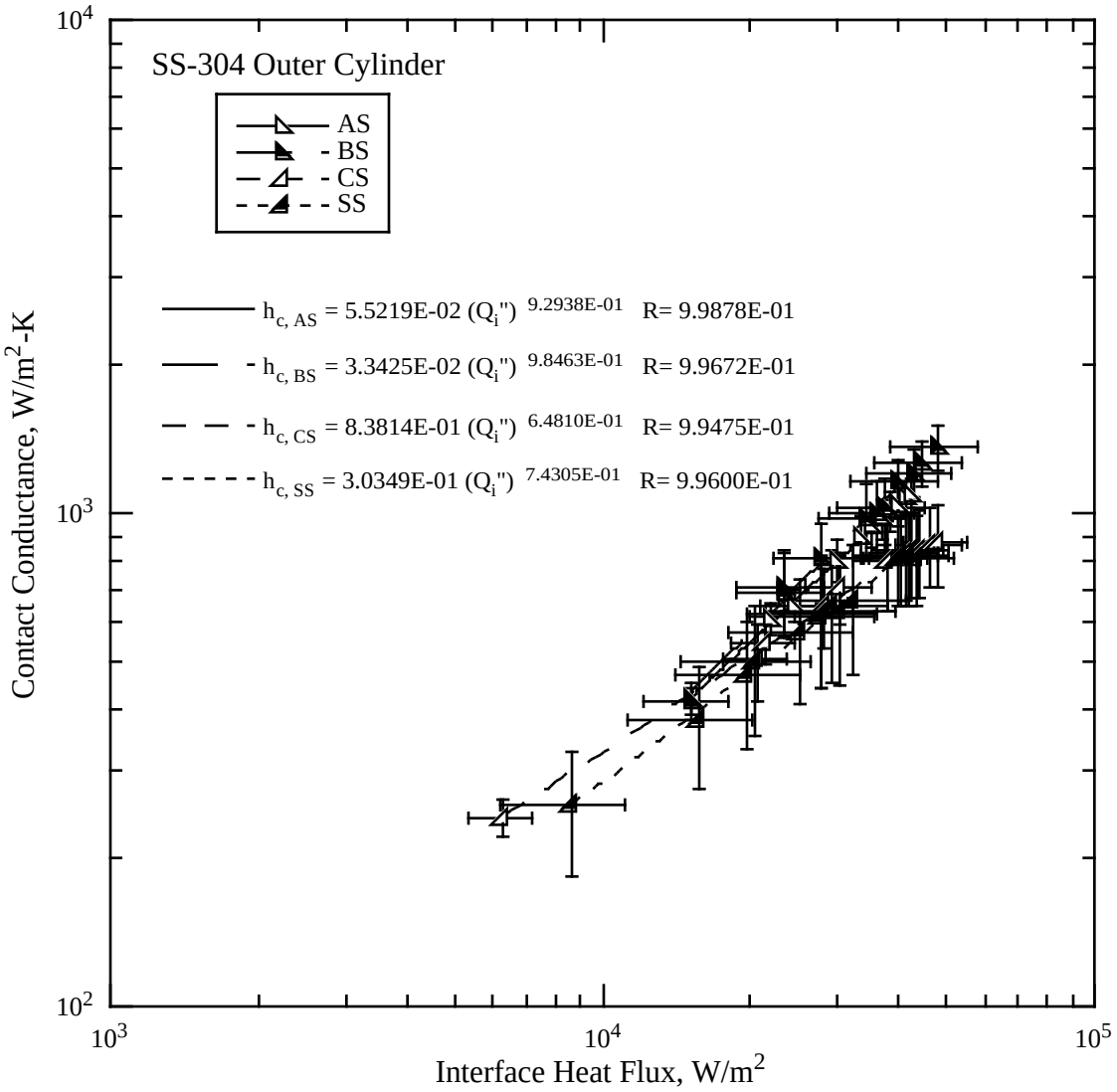

Figure 4.4 – Thermal contact conductance as a function of interface heat flux for stainless steel outer shell experiments.

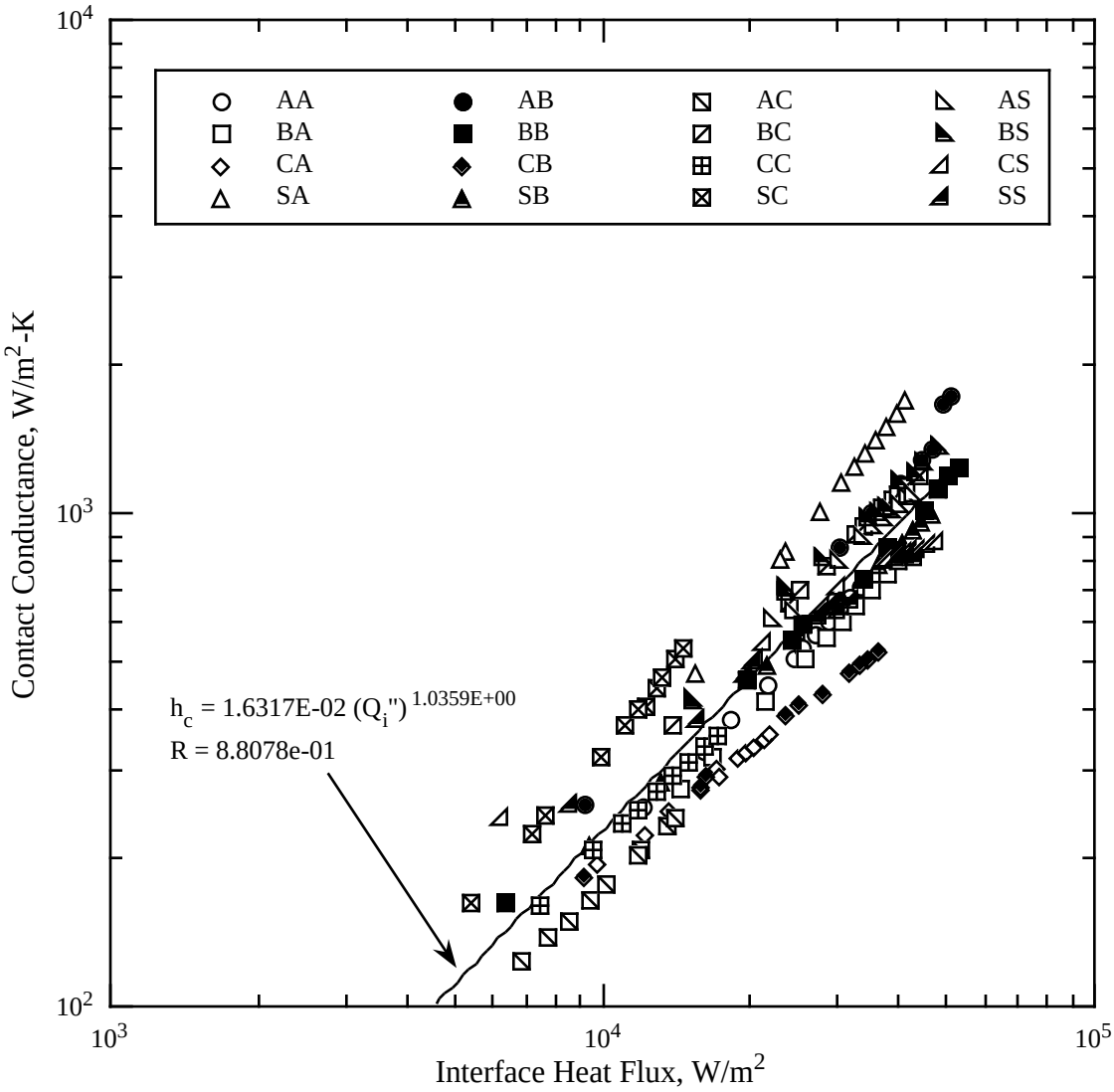

Figure 4.5 – Thermal contact conductance as a function of interface heat flux for all of the present experimental data.

fit through the data. A comparison of initial and retest data is found in Figure 4.6 for four cylindrical shell pairs. The close agreement of the retest data with the initial test data provides some assurance of the quality of the data.

Figure 4.7 presents a comparison of previously published data (from Figure 2.5) with selected results of the present study. The values from the present study are of nearly the same magnitude and slope as those of previously published results, particularly those of Madhusudana and Fletcher (1981) and Williams and Madhusudana (1970). Differences may be accounted for by the surface finish and initial clearance, in addition to the obvious enhancement effect of interstitial air. The designation Fe indicates tests where Armco Iron was used as a shell material.

Dimensionless Results, Heat Flux Basis

The method chosen to nondimensionalize the interface heat flux uses selected thermophysical properties of the shells to correlate the slopes of the individual power law curves for each shell combination. Selecting the familiar dimensionless conductance as the ordinate, the abscissa parameter was constructed of dimensionless groupings of interest, similar to a Buckingham's Pi analysis of the data. The dimensionless heat flux was constructed by dividing the interface heat flux by product of the interface temperature and effective joint conductivity and multiplying the result by the interface radius. The coefficient of thermal expansion ratio (the appropriate value for the outer cylinder divided by the value for the inner cylinder) was chosen because (from the analysis in Appendix D) the interface pressure is expected to be dependent on this parameter. The thermal conductivity ratio, while important, did not have a high degree of correlation with the data and is indirectly used in the effective conductivity and the exponent of the dimensionless heat flux. The interface separation is nondimensionalized by the interface radius. Definitions of these parameters can be found in the Nomenclature section. Surface

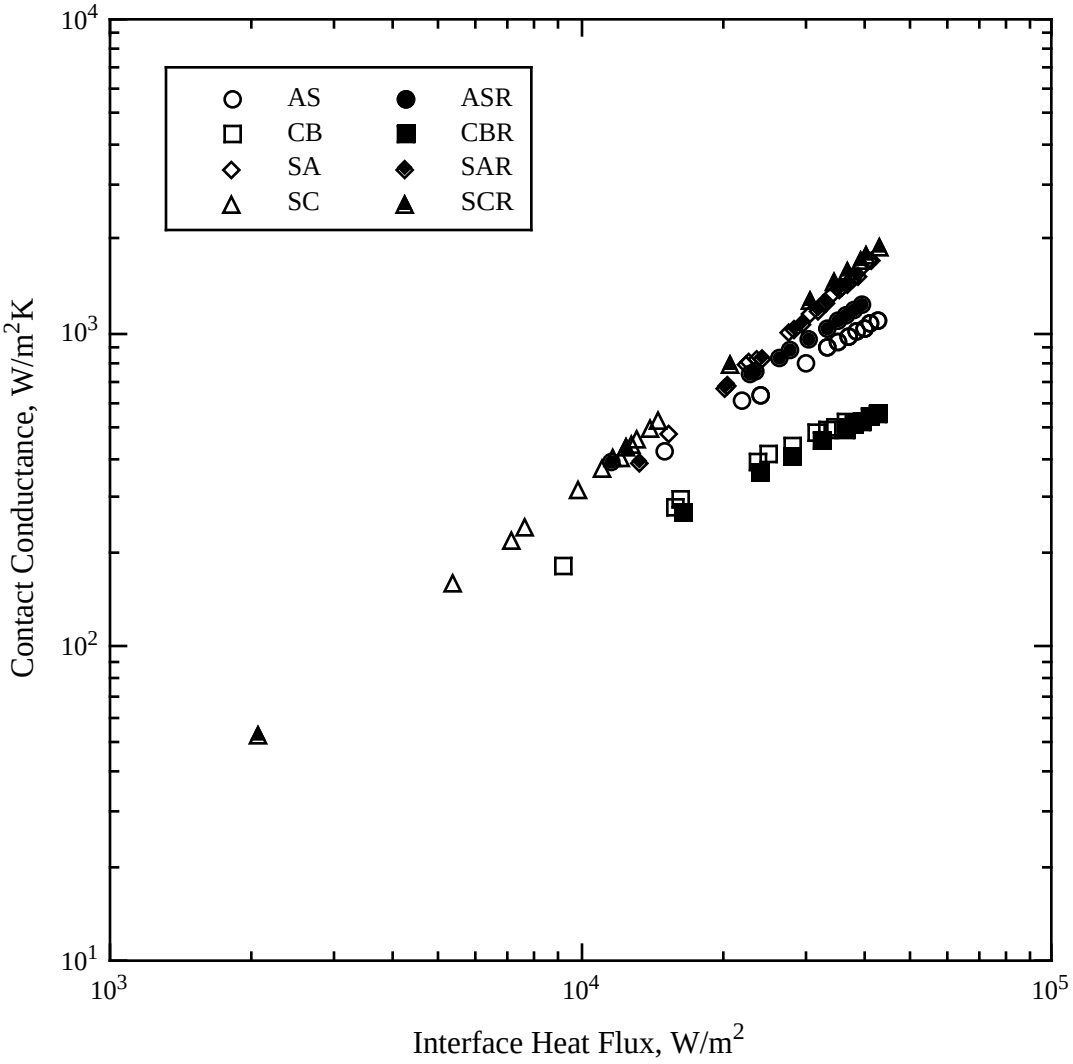

Figure 4.6 – Comparison of conductance as a function of interface heat flux for initial (open symbols) and retest (filled symbols) experiments.

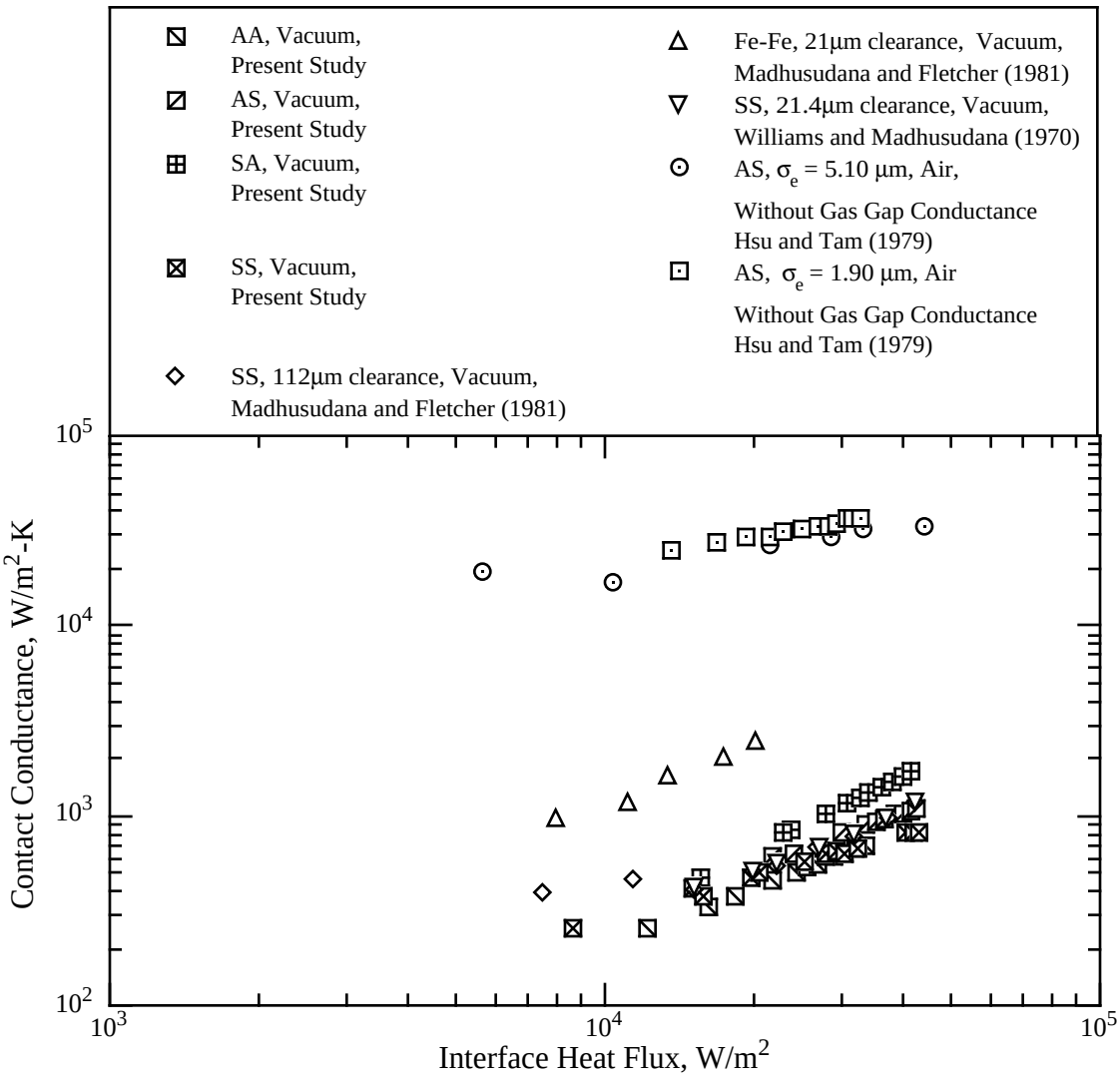

Figure 4.7 – Comparison of results of conductance as a function of interface heat flux for selected experimental data of the present study and previously published studies.

roughness and asperity slope are used to nondimensionalize the contact conductance, and do not significantly improve the correlation when incorporated in the abscissa parameter.

The crude slope matching technique has limited effectiveness for the harder outer shell materials (steel and brass), but the inclusion of a hardness parameter had a negligible effect on the slope parameter ka*. The negative exponent associated with the dimensionless interface gap reflects the intuitive perception that the conductance will increase as the gap decreases (or the interference increases). Similarly, the positive exponent of the ratio of coefficients of thermal expansion reflects the idea that the inner cylindrical shell will expand into the outer cylindrical shell under the conditions of radially outward heat flow.

Only a few published correlations that relate interface thermal state (of heat flux or axial temperature distribution) to the contact conductance. These are power law relations of heat rate only, and are applicable to particular circumstances. With this reasoning, no other correlations or data are depicted in Figure 4.8. All of the dimensionless data fall within 42% of the correlation, and 95% of the data are within 28% of the correlation.

INTERFACE PRESSURE EXPERIMENTAL RESULTS

Dimensional Results, Pressure Basis

Dimensional conductance presented as a function of calculated pressure is presented in Figure 4.9. Initial observation reveals that several of the datasets have extremely steep slopes. Not unexpectedly, these material combinations have relatively small mean interface gaps combined with large thermal conductivities in one or both shells and low elastic modulus in one or both of the shells. These factors lead to the conclusion that while contact between the shells is established early, the contact pressure doesn't change much and the increase in conductance through the interface is chiefly a factor of the increased interface heat flux

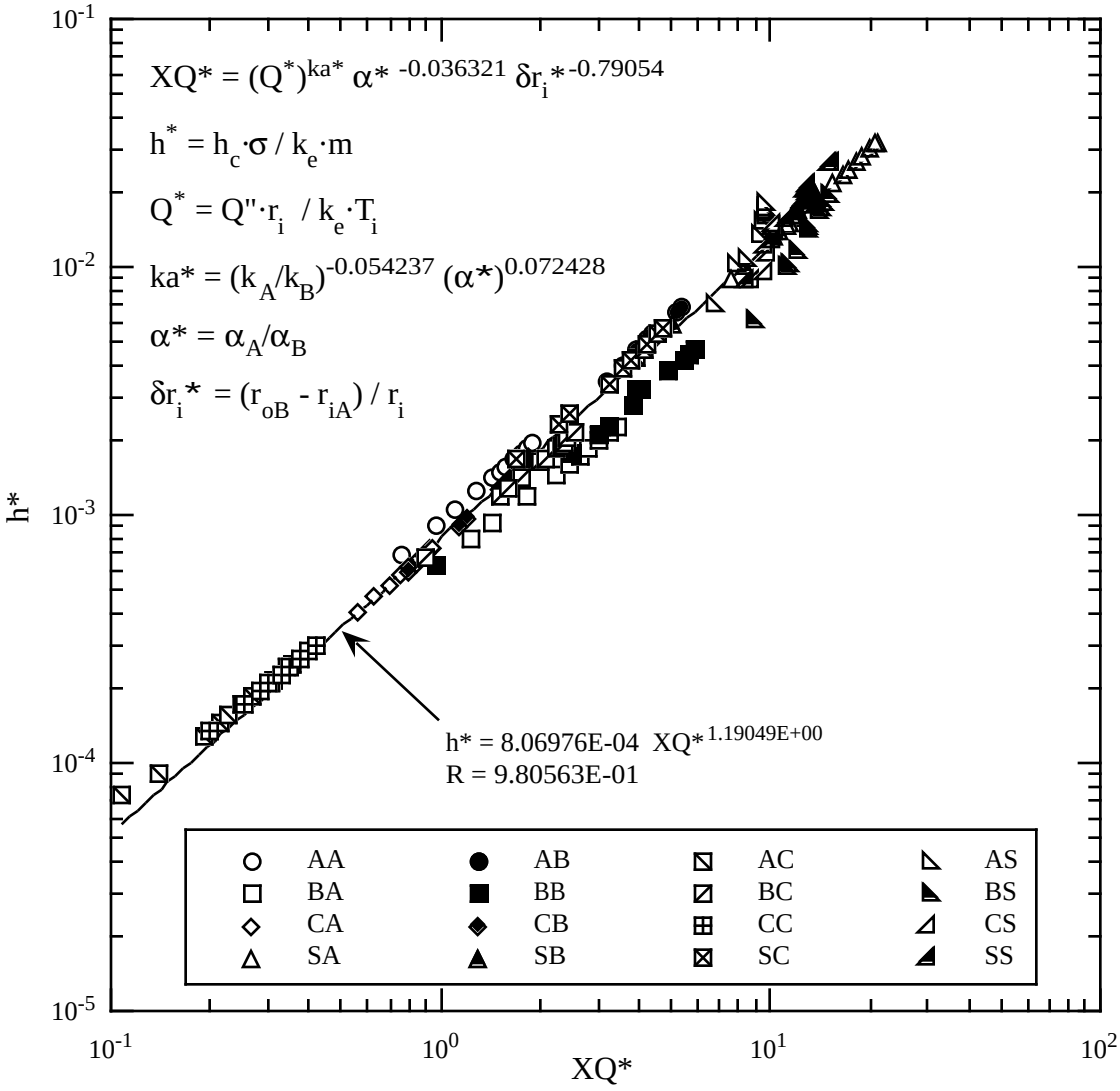

Figure 4.8 – Dimensionless heat flux correlation for results of present study.

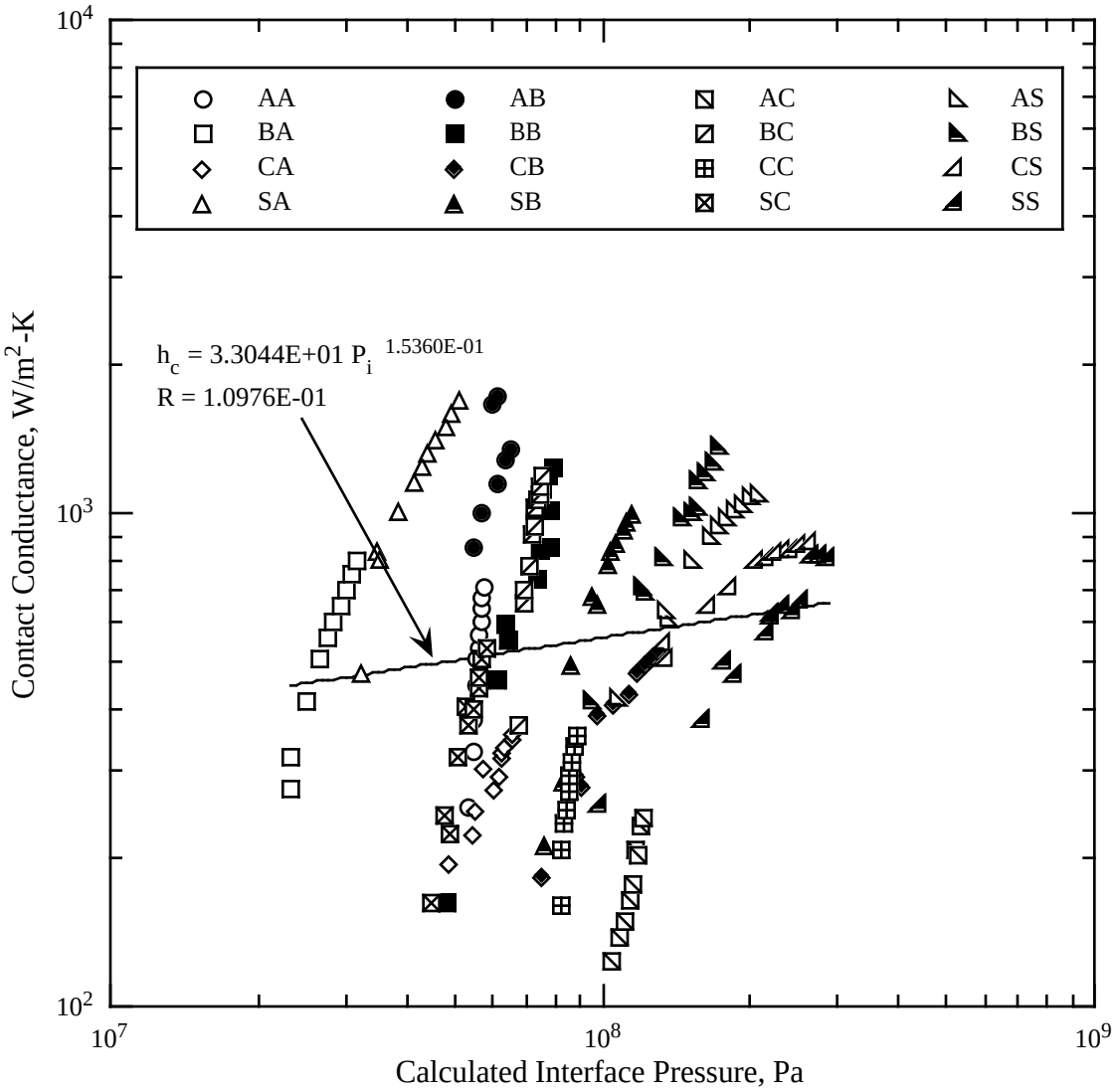

Figure 4.9 – Thermal contact conductance as a function of calculated interface pressure for all of the present experimental data.

Dimensionless Results, Pressure Basis

Figure 4.10 presents the familiar dimensionless contact conductance as a function of the dimensionless interface pressure for all test data.

In Figure 4.11, the dimensionless conductance-dimensionless interface pressure data are compared to the models of Yovanovich (1981) and Lambert and Fletcher (1997).

The Yovanovich model is valid for conforming surfaces, and has been at the heart of many of the theoretical and experimental studies of cylindrical thermal contact conductance. It is not surprising that it over-predicts the conductance of the cylindrical interfaces used in the present study since the cylindrical surfaces of interest are not conforming.

The model of Lambert and Fletcher (1997) was developed for surfaces with a single macro-contact. Simplifying assumptions used to implement the model include:

- Surface waviness can be expressed as the superposition of perpendicular sine waves, which leads to tractable expressions relating the waviness amplitude, slope of the macroscopic asperities, and radius of the macroscopic flux tube (Appendix E),
- Vicker's microhardness is an appropriate measure of the contact microhardness, and
- Contact load is estimated as the average calculated contact pressure multiplied by the area of the macroscopic flux tube.

Details of the model are more completely covered in Lambert and Fletcher (1997) and Lambert (1995).

In general, high quality pressure results are not available for use in the construction of a predictive model. One of the assumptions in the thermoelastic method used to calculate the interface pressure is that the shells are in perfect mechanical contact with each

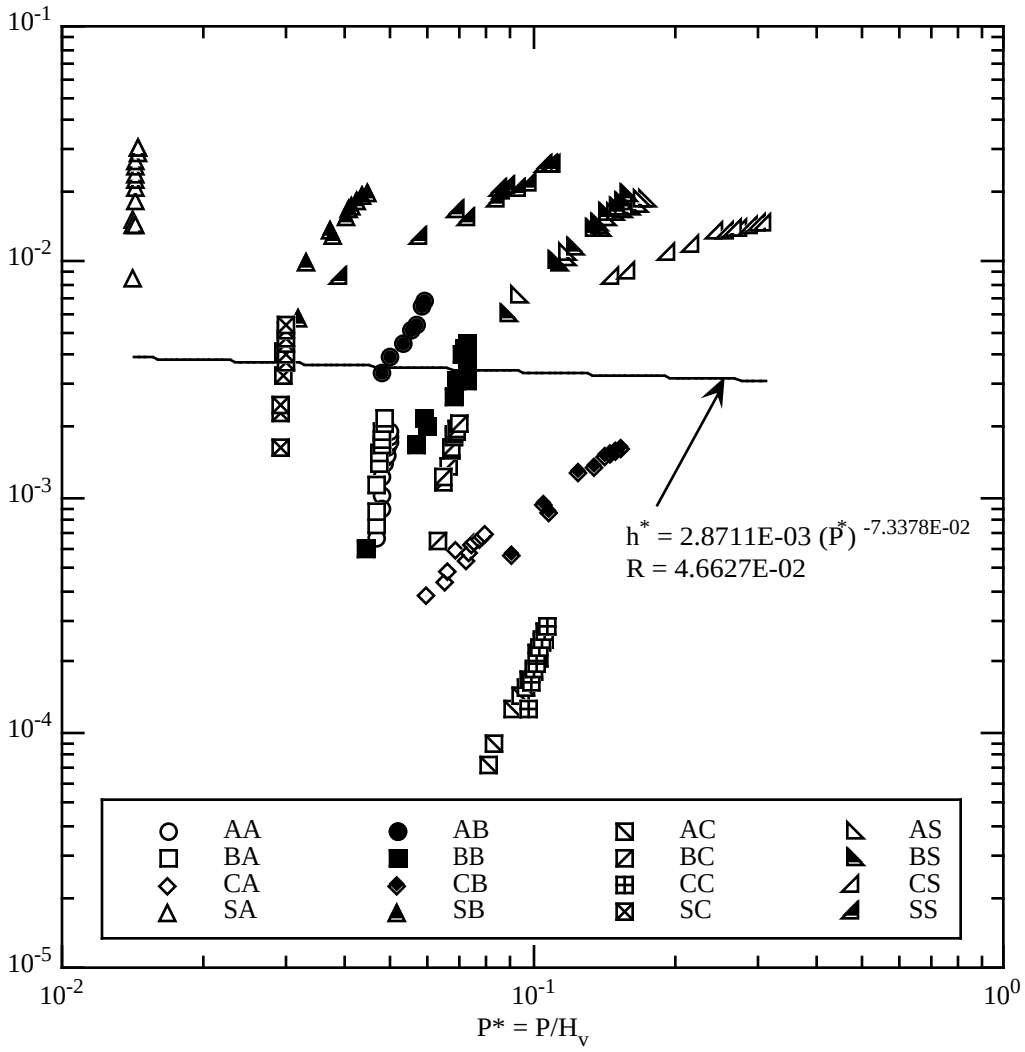

Figure 4.10 – Dimensionless contact conductance as a function of dimensionless calculated interface pressure for all experimental data.

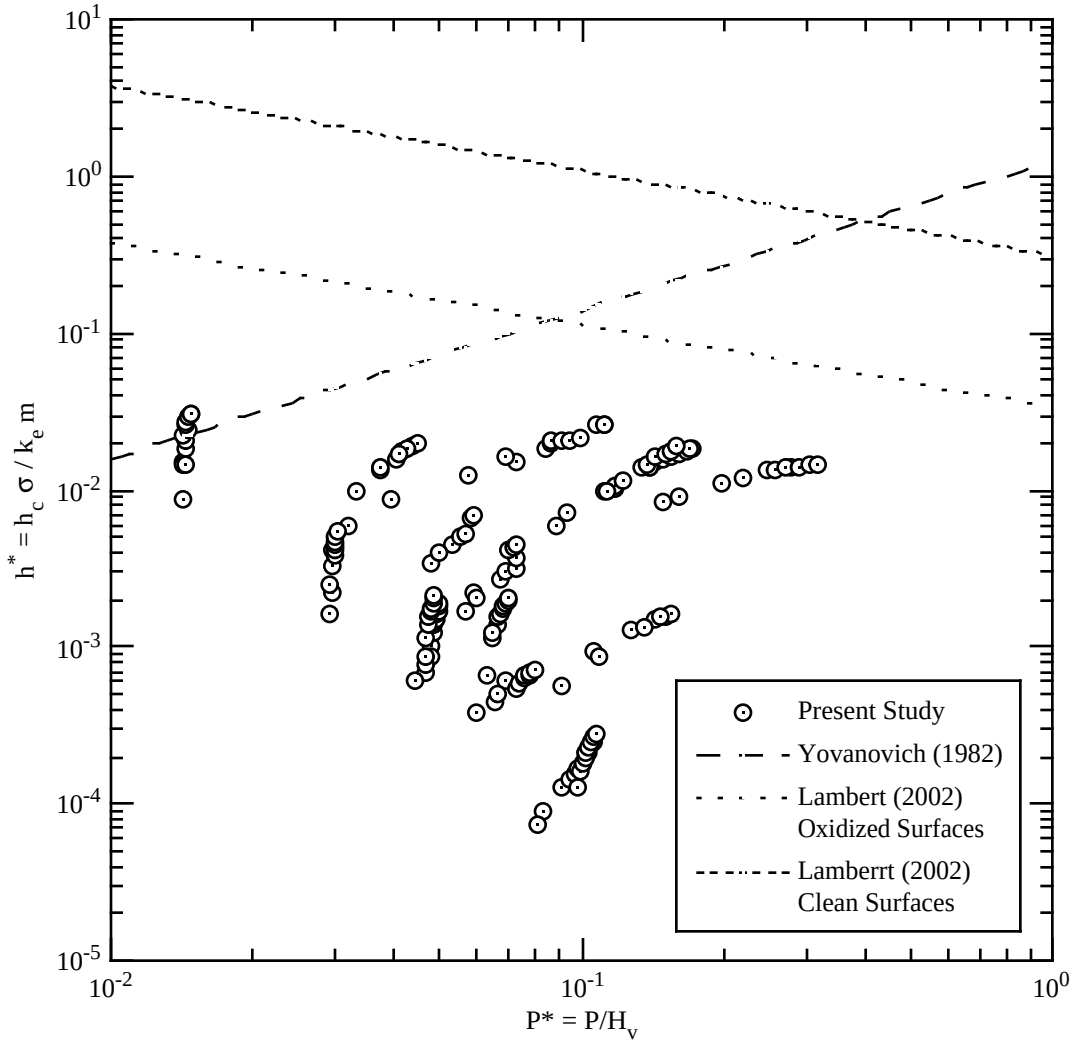

Figure 4.11 – Comparisons of dimensionless contact conductance as a function of dimensionless calculated interface pressure of the present study with the correlations of Yovanovich (1981) and Lambert (1995).

other and exert a uniformly distributed stress upon each other at the interface. Since the contact surfaces of the experimental cylindrical shells have discernable waviness, this is not the case. Strain gage results were not reliable because of several factors. An unquantified strain gage misalignment with the mid-plane and the axis of rotation, easily facilitated by the small sizes of the gage rosettes and the outer cylindrical shells, may have introduced an uncertainty in the reported strain. Gage output voltage signals were somewhat noisy, allowing the uncertainty due to signal variation to become the dominant uncertainty in the measured output voltage. Insufficient compensation for gage thermal response resulted in calculated interface pressures that were either negative or much lower than expected.

Probable causes for the over-prediction of the conductance by the Lambert and Fletcher model include insufficient knowledge of the surface waviness and uneven pressure distribution. The surface waviness is not isotropic, as evidenced by the surface characterization results. The longitudinal waviness and the circumferential waviness quite different, and the effect of the cylindrical surface is probably not adequately modeled by mapping the two wavinesses to a plane surface. Further, the model presumes that the macro-contacts are spherical, at least in the vicinity of the contact. While the sinusoidal surface model makes the relation between various parameters tractable, it has the effect of enlarging the macroscopic flux-tube radius. This is not a problem for single macro-contacts where the actual size of the flux tube is measurable. It is likely that the random nature of the surfaces is manifested in there being a few macro-asperities that are higher than others and bearing the load on a much smaller contact area. This would result in a greater constriction of the heat flow on the macro-scale, which would not be predicted by the model.

CHAPTER V

CONCLUSIONS AND RECOMMENDATIONS

CONCLUSIONS

An experimental facility for the investigation of the thermal contact conductance of cylindrical interfaces has been designed and fabricated. Sixteen thermocouples and eight analog channels were monitored, and two analog output channels were used to control heaters and to automate valves.

An experimental procedure for determining the variation of the contact conductance of composite cylinders in a vacuum was developed and implemented. While the outer shells of the composite cylinders were instrumented with strain gages, data of insufficient quality was obtained. Repeat tests were performed to provide some measure of data reliability.

A comparison of dimensional conductance results with previously published data on both the heat flux and interface pressure bases were favorable. Cylindrical thermal contact conductance was of appropriate magnitude for both the heat flux and contact pressure levels at the interface. Repeat testing provided some assurance of data quality. Data analysis shows that the calculated interface pressure is quite sensitive to uncertainties in interface geometry and shell temperature distribution. Dimensionless conductance and dimensionless heat flux have very good correlation, while dimensionless conductance and dimensionless interface pressure have relatively poor correlation (due to inadequate surface characterization, large contact pressure uncertainties, and poor understanding of multiple macro-contact conductance phenomenon).

RECOMMENDATIONS

The present study has provided data for the contact conductance of a single composite cylinder geometry with a variety of material combinations and somewhat more limited variety of surface conditions. Further investigation into cylindrical thermal contact conductance should take into account the following recommendations to foster a better understanding of (and consequently better predictive models for) thermal contact conductance of cylindrical interfaces.

Composite Cylinder Geometry

In future studies, it is recommended that the length of the composite cylinder should be more then five times the average shell thickness, to ensure that end effects have no influence on the temperature and strain (pressure) measurements done in the vicinity of the centerline.

It is suggested that different composite cylinder geometries be used in future experiments, to study the effects of varying the shell thickness, interface radius, and ratio of interface radius and nominal interface clearance (or interference). Longer cylinders will make interference fit cylindrical shells difficult to assemble and disassemble, but will produce results more appropriate to conditions found in radial thermal control situations.

Some attempt should be made to transform the presently available contact conductance models from the Cartesian coordinate system to a curvilinear coordinate system.

Contact Pressure

Techniques for directly measuring the pressure at the interface should be investigated. Such techniques should be able to withstand the temperatures and pressures at the interface and should be relatively insensitive to ambient pressure in order to give valid results for experiments in vacuum and other conditions.

Equivalent Isotropic Waviness

The cylindrical shells have roughness and waviness in both the axial and circumferential directions. A more rigorous means of determining an equivalent isotropic waviness should be investigated in order to use the simplified conductance models.

Radial Cylindrical Heat Channel

A different macroscopic constriction parameter should be developed for a non-conforming surface model of the thermal contact conductance through cylindrical interfaces. Similar to parameters in use for nominally flat interfaces, the radial-cylindrical constriction parameter should take into account the asymmetric nature of the heat flux channel on either side of the interface.

Macrocontact Pressure Distribution

Due to the difference in waviness wavelengths and amplitudes in the longitudinal and circumferential directions, it is unlikely that the macrocontact spots will be circular, and the pressure within the macrocontact area can not be described as a unidirectional function of Cartesian or polar coordinates. The effect of the nominal cylindrical interface geometry on macrocontact radius and pressure distribution should be investigated.

Multiple Contact Interaction

Greenwood (1966) describes the interaction between clusters of contacts based on the spacing of the contacts and their sizes. He describes the resistance to be a function of the mean contact area and the Holm radius of the contacts. With further consideration and refinements, similarity arguments can be made for larger-scale contacts and a similar interaction parameter can be constructed for the macroscale portion of the contact resistance.

REFERENCES

Abuebid, M. A., 1984, *A Thermal Contact Conductance Correlations for Mechanically Expanded Finned Tube Heat Exchangers*, MS Thesis, Department of Mechanical and Aerospace Engineering, University of Missouri-Rolla, Rolla, MO.

Artyukhin, E. A., Nenarokomov, A. B., Tryanin, A. P., Utenkov, S. A., and Yakovlev, V. V., 1991, "Identification of Contact Thermal Resistances in Nuclear Reactor Fuel Elements. 1. Development of Algorithms," *Inzhenerno-Fizicheskii Zhurnal*, Vol. 60, No. 3, March, pp. 478-487.

ASTM, 1997, "Test Method E 92-82 Standard Test for Vickers Hardness of Metallic Materials," *Annual Book of ASTM Standards*, Vol. 03.01, pp. 208-216.

ASTM, 2002, "Test Method E 228-95 Standard Test Method for Linear Thermal Expansion of Solid Materials with a Vitreous Silica Dilatometer," *Annual Book of ASTM Standards*, Vol. 14.02, pp. 70-76.

Barber, J. R., 1986a, "Non-Uniqueness and Stability for Heat Conduction Through a Duplex Heat Exchanger Tube," *Journal of Thermal Stresses*, Vol. 9, No. 1, pp. 69-78.

Barber, J. R., 1986b, "The Influence of Interface Thermal Contact Resistance on the Heat Transfer Performance of Duplex Tube," *International Journal of Heat and Mass Transfer*, Vol. 29, No. 5, pp. 761-767.

Boley, B. A., and Weiner, J. H., 1997, *Theory of Thermal Stresses*, Dover Publications, Minneola, NY.

Bourouga, B., and Bardon, J. P., 1992, "Mesures des Résistances Thermiques Superficielle et de Contact au Moyen de la Constante de Temps Fondamentale," *International Journal of Heat and Mass Transfer*, Vol. 35, No. 2, February, pp. 361-373.

Brutto, E., Casagrande, I., and Perona, G., 1959, "Thermal Contact Resistance Between Cylindrical Metallic Surfaces," *Energia Nucleare*, Vol. 6, No. 8, August, pp. 532-540.

Christensen, R. N., and Fernandes, H. V., 1983, "Contact and Fouling Resistances in Finned Tube Heat Exchangers," ASME Paper 83-HT-39.

Clausing, A. M., and Chao, B. T., 1964, "Thermal Contact Resistance in a Vacuum Environment," *Transactions of the ASME Journal of Heat Transfer*, Paper No. 64-HT-16, September, pp. 1-8.

Cohen, I., Lustman, B., and Eichberg, J. D., 1960, "Measurement of Thermal Conductivity of Metal Clad Uranium Rods During Irradiation," U.S. Atomic Energy Commission, Bettis Atomic Power Laboratory, Report WAPD-228, West Mifflin, PA, August.

Cooper, M. G., Mikic, B. B., and Yovanovich, M. M., 1969, "Thermal Contact Conductance," *International Journal of Heat and Mass Transfer*, Vol. 12, No. 3, March, pp. 279-300.

Danes, F. E., and Simon, G., 1990, "Study of Thermal Contact Resistance in a Closed Cylindrical Geometry," *Science of Heat: Progress and Actual Challenges*, Vol. 2, Societé Française des Thermiciens 90: Science of Heat Colloquium: Progress and Actual Challenges, Nantes, France, May 16-17, pp. 217-220.

Dart, D. M., 1959, "The Effect of Fin Bond on Heat Transfer," *ASHRAE Journal*, Vol. 1, May, pp. 67-71.

Davis, C. L., 2000, Personal Communication, Corning, Inc., 8 May.

Eckels, P. W., 1974, "Design of a Contact Conductance Experiment for Plate Finned Tube Heat Exchangers," Westinghouse Research Labs. Document 73-1E9-HEATA-M3, Pittsburgh, PA.

Eckels, P. W., 1977, "Contact Conductance of Mechanically Expanded Plate Finned Tube Heat Exchangers," Westinghouse Research Laboratories Document 77-1E9-SURCO-P1, Pittsburgh, PA.

Egorov, E. D., Nekrasov, M. I., and Pikus, V. Y., 1989, "Investigation of Contact Heat-Transfer Resistance in Two-Layer Finned Tubes," *Energomashinostroenie*, Vol. 13, No. 6, pp. 17-19.

Endersby, S. N., Parker, A. P., Bond, T. J., and Underwood, J. H., 1996, "Stress Concentration, Stress Intensity and Fatigue Lifetime Calculations for Shrinkfit Compound Tubes Containing Axial Holes within the Wall," *Fatigue and Fracture Mechanics, ASTM STP 1321*, Underwood, J. H., MacDonald, B. D., Mitchell M. R., editors, American Society for Testing and Materials.

Ernest, T. L., Sheffield, J. W., and Sauer, H. J., Jr., 1986, "Finned Tube Contact Conductance: Characterizing the Integrity of the Mechanical Bond," *ASHRAE Transactions*, Vol. 91, Part 2, pp. 85-98.

Fletcher, L. S., 1971, "Criteria for the Prediction of Thermal Contact Conductance," *Proceedings of the Third Canadian Congress of Applied Mechanics*, University of Calgary, Canada, May, pp. 667-68.

Fletcher, L. S., 1988, "Recent Developments in Contact Conductance Heat Transfer," *Transactions of the ASME: Journal of Heat Transfer*, Vol. 110, November, pp. 1059-1070.

Fourier, J. B. J., 1822, *Theorie Analytique de la Chaleur*, Chez Firmin Didot, Père et Fils, Paris, France.

Gardner, K. A., and Carnavos, T. C., 1960, "Thermal Contact Resistance in Finned Tubing," *Transactions of the ASME, Journal of Heat Transfer*, Vol. 82, November, pp. 279-93.

Greenwood, J. A., 1966, "Constriction Resistance and the Real Area of Contact," *British Journal of Applied Physics*, Vol. 17, pp. 1621-1632.

Greenwood, J. A., 1967, "The Area of Contact Between Rough Surfaces and Flats," *Transactions of the ASME: Journal of Lubrication Technology*, Vol. 89, No. 1, January, pp. 81-91.

Hertz, H., 1881, "On the Contact of Elastic Bodies," *Journal fur die rein undo angewndte Mathmatic*, Vol. 92, pp. 156-171

Holm, R., 1929, "On Metallic Contact Resistance," *Wissenschaftliche Veröeffentlichungen aus den Siemens-Werken*, Vol. 7, p. 217-271.

Hrnjak, P. S., and Sheffield, J. W., 1990, "Contact Resistance in Plate Finned Tubes Heat Exchangers: State-of-the-Art," *Proceedings of the Ninth International Heat Transfer Conference*, Hemisphere Publishing, New York, Vol. 5, pp. 9-14.

Hsu, T. R., and Tam, W. K., 1979, "On Thermal Contact Resistance in Composite Cylinders," AIAA Paper 79-1069, 14th AIAA Thermophysics Conference, Orlando, FL, June 4-6, 1979.

Huang, M. M., 1994, *Contact Resistance of Round Tube and Plate Heat Exchangers Using Finite Element Analysis*, M.Phil. Thesis, Department of Mechanical and Manufacturing Engineering, University Brighton, United Kingdom.

Kim, H. C., 1978, "Fin Bond – ASHRAE Project," Interoffice Memo, Gulf Western Manufacturing Company, Bohn Group, February 28.

Kline, S. J., and McClintock, F. A., 1953, "Describing Uncertainties in Single-Sample Experiments," *Mechanical Engineering*, Vol. 75, No. 1, pp. 3-8.

Kozik, T., 2001, Personal Communication, Texas A&M University, 8 September.

Kulkarni, M. V., and Young, E. H., 1966, "Bimetallic Finned Tubes", *Chemical Engineering Progress*, Vol. 62, July, pp. 68-71.

Kuntysh, V. B., Toporkova, M. A., and Girishin, V. P., 1983, "Heat Exchange in Tube Banks with L-Shaped Profiled Fins," *Energomashinostroenie*, Vol. 7, No. 4, pp. 1-6.

Lambert, M. A., 1995, *Thermal Contact Conductance of Spherical, Rough Metals*, Ph.D. Dissertation, Department of Mechanical Engineering, Texas A&M University, College Station, Texas.

Lambert, M. A., and Fletcher, L. S., 1997, "Thermal Contact Conductance of Spherical Rough Metals," *Transactions of the ASME: Journal of Heat Transfer*, Vol. 119, November, pp. 684-690.

Lemczyk, T. F., and Yovanovich, M. M., 1987, "New Models and Methodology for Predicting Thermal Contact Resistance in Compound Cylinders and Finned Tubes," *Heat Transfer Engineering*, Vol. 8, No. 2, pp. 35-48.

Madhusudana, C. V., 1983, "Contact Heat Transfer Between Coaxial Cylinders of Similar or Dissimilar Materials," *Proceedings of the ASME/JSME Thermal Engineering Joint Conference*, Honolulu, HI, Vol. III, March, pp. 317-322.

Madhusudana, C. V., 1986, "On Heat Flow Across Cylindrical Joints," *Proceedings of the Eighth International Heat Transfer Conference*, Hemisphere Publishing, New York, Vol. 2, pp. 651-658.

Madhusudana, C. V., 1996, *Thermal Contact Conductance*, Springer, New York.

Madhusudana, C. V., 1999, "Thermal Conductance of Cylindrical Joints," *International Journal of Heat and Mass Transfer*, Vol. 42, No. 27, pp. 1273-1287.

Madhusudana, C. V., and Fletcher, L. S., 1981, "Thermal Conductance of Cylindrical Contacts," *Proceedings of the Eighth Canadian Congress of Applied Mechanics*, University of Moncton, Moncton, New Brunswick, Canada, June, pp. 755-756.

Madhusudana, C. V., and Fletcher, L. S., 1985, "Contact Heat Transfer—The Last Decade," AIAA Journal, Vol. 24, No. 3, February, pp. 510-523.

Madhusudana, C. V., and Litvak, A. L., 1990, "Thermal Contact of Composite Cylinders: An Experimental Study," *AIAA Journal of Thermophysics and Heat Transfer*, Vol. 4, No. 1, January, pp. 79–85.

Madhusudana, C. V., Fletcher, L. S., and Peterson, G. P., 1990, "Thermal Conductance of Cylindrical Contacts – A Critical Review," *AIAA Journal of Thermophysics and Heat Transfer*, Vol. 4, No. 2, April, pp. 204-211.

Matal, O., Tomas, Z., Simo, T., and Konecny, A., 1989, "Experimental Investigation of Duplex Tubes for Sodium Heated Steam Generator," *NURETH-4 Proceedings of the Fourth International Topical Meeting on Nuclear Reactor Thermal-Hydraulics*, American Nuclear Society, LaGrange Park, IL, Vol. 2, pp. 1402-1406.

Measurements Group, Inc., 1999a, *Measurement of Thermal Expansion Coefficient Using Strain Gages*, Tech Note TN-513, October.

Measurements Group, Inc., 1999b, *Strain Gage Thermal Output and Gage Factor Variation with Temperature*, Tech Note TN-504, April.

Measurements Group, Inc., 1999c, *Surface Preparation for Strain Gage Bonding*, Instruction Bulletin B-129.

Mikic, B. B., 1970, "Thermal Constriction Resistance Due to Non-Uniform Surface Conditions; Contact Resistance at Non-Uniform Interface Pressure," *International Journal of Heat and Mass Transfer*, Vol. 13, No. 9, September, pp. 1497-1500.

Nho, K. M., and Yovanovich, M. M., 1989a, "Effect of Oxide Layers on Measured and Theoretical Contact Conductances in Finned Tube Heat Exchangers," Presented at the A. L. London Symposium on Compact Heat Exchangers, Stanford University, March 23-24.

Nho, K. M., and Yovanovich, M. M., 1989b, "Measurement of Contact Resistance in Finned Tube Heat Exchangers," *ASHRAE Transactions,* Vol. 95, Part 1, pp. 370-378.

Novikov, I. I., Kokorev, L. S., and Del'vin, N. N., 1972, "Experimental Heat Exchange Between Coaxial Cylinders in Vacuum," *Atomnaya Énergiya,* Vol. 32, No. 6, pp. 474-475.

Omega Engineering, Inc., 1995, *The Pressure, Strain and Force Handbook*, Omega Engineering, Inc., Stamford, CT.

Popov, E. P., 1978, *Mechanics of Materials*, Prentice-Hall, Englewood Cliffs, NJ.

Roess, L. C., 1948, "Theory of Spreading Conductance," Appendix to Weills, N. D., Ryder, E. A., 1948, "Thermal Resistance Measurements on Joint Formed Between Stationary Metal Surfaces," presented at Semi-Annual ASME Heat Transfer Division Meeting, Milwaukee, Wisconsin.

Ross, A. M., and Stoute, R. L., 1962, "Heat Transfer Coefficient Between UO_2 and Zircaloy-2," Atomic Energy of Canada, Ltd., Report CRFD-1075, Ottawa, Ontario, Canada.

Sauer, H. S., and Sheffield, J. W., 1987, "Finned-Tube Contact Conductance Studies," *ASHRAE Journal*, Vol. 29, November, p. 48.

Sheffield, J. W., Abu-Ebid, M. A., and Sauer, H. J., Jr., 1985, "Finned Tube Contact Conductance: Empirical Correlation of Thermal Conductance," *ASHRAE Transactions*, Vol. 91, Part 2A, pp. 100-117.

Sheffield, J. W., Sauer, H. J., Jr., and Wood, R. A., 1987, "An Experimental Method for Measuring the Thermal Contact Resistance of Plate Finned Tube Heat Exchangers," *ASHRAE Transactions*, Vol. 93, Part 2, pp. 776-795.

Sheffield, J. W., Stafford, B. D., and Sauer, H. J., Jr., 1985, "Finned-Tube Contact Conductance: Investigation of Contacting Surfaces," *ASHRAE Transactions*, Vol. 91, Part 1, No. 3242, pp. 442-452.

Sheffield, J. W., Wood, R. A., and Sauer, H. J., Jr., 1989, "Experimental Investigation of Thermal Conductance of Finned Tube Contacts," *Experimental Thermal and Fluid Science*, Vol. 2, pp. 107-121.

Shigley, J. E., 1972, *Mechanical Engineering Design*, 2nd ed., McGraw-Hill , New York.

Shlykov, Y. P., and Ganin, Y. A., 1964, "Thermal Resistance of Metallic Contacts," *International Journal of Heat and Mass Transfer*, Vol. 7, No. 8, pp. 921-929.

Siegel, R., and Howell, J. R., 1992, *Thermal Radiation Heat Transfer*, 3rd ed., Hemisphere Publishing Corporation, Washington, D.C.

Smith, C. E., Gunter, A. Y., and Victory, S. P., 1966, "Fin Tube Performance," *Chemical Engineering Progress*, Vol. 62, No. 7, pp. 57-67.

Srinivasan, M. G., and France, D. M., 1985, "Non-uniqueness in Steady Heat Transfer in Prestressed Duplex Tubes," *Journal of Applied Mechanics*, Vol. 52, June, pp. 257-262.

Stafford, B. C., 1983, *Investigation of Important Surface Characteristics of a Finned Tube Heat Exchanger*, M.S. Thesis, Department of Mechanical and Aerospace Engineering, University of Missouri-Rolla, Rolla, MO.

Tam, W. K., 1976, *On Thermal Contact Resistance of Compound Cylinders*, M.S. Thesis, Department of Mechanical Engineering, University of Manitoba, Winnipeg, MB, Canada.

Thomas, T. R., and Sayles, R. S., 1974, "Random-Process Analysis of the Effect of Waviness on Thermal Contact Resistance," *Heat Transfer with Thermal Control Applications*, Yovanovich, M. M., editor, Progress in Astronautics and Aeronautics, Vol. 39, pp. 3-20.

Throop, J. F., Underwood, J. H., and Leger, G. S., 1982 "Thermal Relaxation in Autofrettaged Cylinders," in *Residual Stress and Stress Relaxation*, Kula, E., and Weiss, V., editors, Plenum, New York.

Timoshenko, S. P., and Goodier, J. N., 1951, *Theory of Elasticity*, McGraw-Hill Book Company, New York, New York.

Touloukian, Y. S., and Ho, C. Y. (editors), 1972, *Thermophysical Properties of Matter*, Plenum Press, New York, Vol. 1-13.

Underwood, J. H., Fujczak, R. R., and Hasenbein, R. G., 1988, *Elastic, Strength, and Stress Relaxation Properties of A723 Steel and 38644 Titanium for Pressure Vessel Applications*, Technical Report ARCCB-TR-88011 US Army ARDEC, Close Combat Armaments Center, Picatinny Arsenal, New Jersey.

Veziroglu, T. N., 1967, "Correlation of Thermal Contact Conductance Experimental Results," *Progress in Astronautics and Aeronautics: An American Institute of Aeronautics and Astronautics series*, Academic Press, New York, Vol. 20, pp. 879-907.

Wang, J. C. Y., and Nowak, E. S., 1982, "A Study of Thermal Construction Resistance at the Interface of Double Tubes," *Proceedings of the Seventh International Heat Transfer Conference*, Hemisphere Publishing, New York, Vol. 2, pp. 87-92.

Williams, A., and Madhusudana, C. V., 1970, "Heat Flow Across Cylindrical Metallic Contacts," *Heat Transfer 1970*, Elsevier, Amsterdam, the Netherlands, Paper Cu 3–6.

Wood, R. A., Sheffield, J. W., and Sauer, H. J., Jr., 1987a, "Thermal Contact Conductance of Finned Tubes: A Generalized Correlation," *ASHRAE Transactions*, Vol. 93, Part 2, No. 3103 (RP-446), pp. 786-797.

Wood, R. A., Sheffield, J. W., and Sauer, H. J., Jr., 1987b, "Thermal Contact Conductance of Finned Tubes: The Effect of Various Parameters," *ASHRAE Transactions*, Vol. 93, Part 2, pp. 798-810.

Young, E. H., and Briggs, D. E., 1965, "Bond Resistance of Bimetallic Finned Tubes," *Chemical Engineering Progress*, Vol. 61, No. 7, pp. 71-79.

Yovanovich, M. M., 1981, "Thermal Contact Correlations," AIAA Paper No. 81-1164, AIAA 16th Thermophysics Conference, Palo Alto, California, pp. 35-45, June 23-25.

SUPPLEMENTAL SOURCES CONSULTED

Ayers, G. H., Fletcher, L. S., Madhusudana, C. V., 1997, "Thermal Contact Conductance of Composite Cylinders," *Journal of Thermophysics and Heat Transfer*, Vol. 11, No. 1, pp. 72–81, January–March.

Barber, J. R., 1999, "Thermoelasticity and Contact," *Journal of Thermal Stresses*, May-July, Vol. 22, No. 4-5, pp. 513-525.

Cook, R. D., Young, W. C., 1985, *Advanced Mechanics of Materials*, 1st ed., Macmillan , New York.

Gatewood, B. E., 1948, "Note on the Thermal Stresses in a Long Circular Cylinder of m+1 Concentric Materials," *Quarterly of Applied Mathematics*, Vol. 6, No. 1, pp. 84-86.

Greenwood, J. A., and Tripp, J. H., 1967, "The Elastic Contact of Rough Spheres," *Transactions of the ASME: Journal of Applied Mechanics*, Vol. 89, No. 1, March, pp. 153-159.

Greenwood, J. A., and Williamson, J. B. P., 1966, "Contact of Nominally Flat Surfaces," *Proceedings of the Royal Society of London*, A295, April, pp. 300-319.

Gromovoi, G. P., 1994, "Solution of Three-Dimensional Static Problems of Thermoelasticity," *International Applied Mechanics*, Vol. 30, No. 3, pp. 184-192.

Hocker, G. B., 1979, "Fiber-Optic Sensing of Pressure and Temperature," *Applied Optics*, Vol. 18, No. 9, May, pp. 1445-1448.

Imoto, I, Yoshizawa, N., Sakai, J. I., and Tsuchiya, H., 1980, "Birefringence in Single-Mode Optical Fiber due to Elliptical Core Deformation and Stress Anisotropy," *IEEE Journal of Quantum Electronics*, Vol. QE-16, No. 11, November, pp. 1267-1271.

Jamison, H. J., Mirmira, S. R., and Fletcher, L. S., 1999, "Thermal Contact Conductance of Dissimilar Metallic Interfaces," AIAA Paper 99-0472, AIAA 37th Aerospace Sciences Meeting, Reno, NV, January 11-14.

Lee, C. E., and Taylor, H. F., 1998, "A Fiber-Optic Pressure Sensor for Internal Combustion Engines," *Sensors*, March, pp. 20-26.

Madhusudana, C. V., and Fletcher, L. S., 1981, "Gas Conductance Contribution to Contact Heat Transfer," AIAA Paper No. 81-1163, AIAA 16th Thermophysics Conference, Palo Alto, California, June 23-25.

Mentes, A., Veziroglu, T. N., Samudrala, R., and Sheffield, J. W., 1981, "Effects of Interface Gases on Contact Conductance," AIAA Paper No. 81-0214, AIAA l9th Aerospace Sciences Meeting, St. Louis, Missouri, January 12-15.

Mikic, B. B., and Rohsenow, W. M.,1966, "Thermal Contact Resistance," Technical Report No. 4542-41, Department of Mechanical Engineering, Massachusetts Institute of Technology, Cambridge, Massachusetts, September.

Naraghi, M. H. N., and Antonetti, V. W., 1993, "Macro-constriction Resistance of Distributed Contact Contour Areas in a Vacuum Environment," *Enhanced Cooling Techniques for Electronics Applications, ASME HTD Vol. 263, Proceedings of the 1993 Winter Annual Meeting*, Garimella, S. V., Greiner, M., Yovanovich, M. M., and Antonetti, V. W., editors, New Orleans, Louisiana, November 28 – December 3, pp 107-114.

Pople, J., 1982, "Errors and Uncertainties in Strain Measurement," *Strain Gauge Technology*, Window, A. L., Holister, and G. S. editors, Applied Science, Englewood, NJ, pp. 209-264.

Salerno, L. J., and Kittel, P., 1997, "Thermal Contact Conductance," *NASA TM-110429*, February.

Strub, R. A., 1953, "Distribution of Mechanical and Thermal Stresses in Multilayer Cylinders," Transactions of the ASME, Vol. 75, No. 1, pp. 73-82.

Swartz, E. T., and Pohl, R. O., 1989, "Thermal Boundary Resistance," *Reviews of Modern Physics*, Vol. 61, No. 3, July, pp. 605-668.

Timoshenko, S. P., 1956, *Strength of Materials: Part II – Advanced Theory and Problems*, D. Van Nostrand Company, Princeton, New Jersey, 3rd ed, March.

Wahid, S. M. S., and Madhusudana, C. V., 2000, "Gap Conductance in Heat Transfer," *International Journal of Heat and Mass Transfer*, Vol. 43, No. X, pp 4483-4487.

Yovanovich, M. M., 1971, "Thermal Contact Resistance: Theory and Applications," Presented at University of Tennessee Space Institute, April 26-28, Knoxville, TN.

Yovanovich, M. M., 2000, "Thermal-Mechanical Models for Non-Conforming Surface Contacts," Kromann, G. B., Culham, J. R., and Ramakrishna, K., editors, *ITHERM 2000: Proceedings of the Seventh Intersociety Conference on Thermal and Thermomechanical Phenomena in Electronic Systems*, 23-26 May 2000, Las Vegas, NV, pp. 290-295.

APPENDIX A

FACILITY DRAWINGS

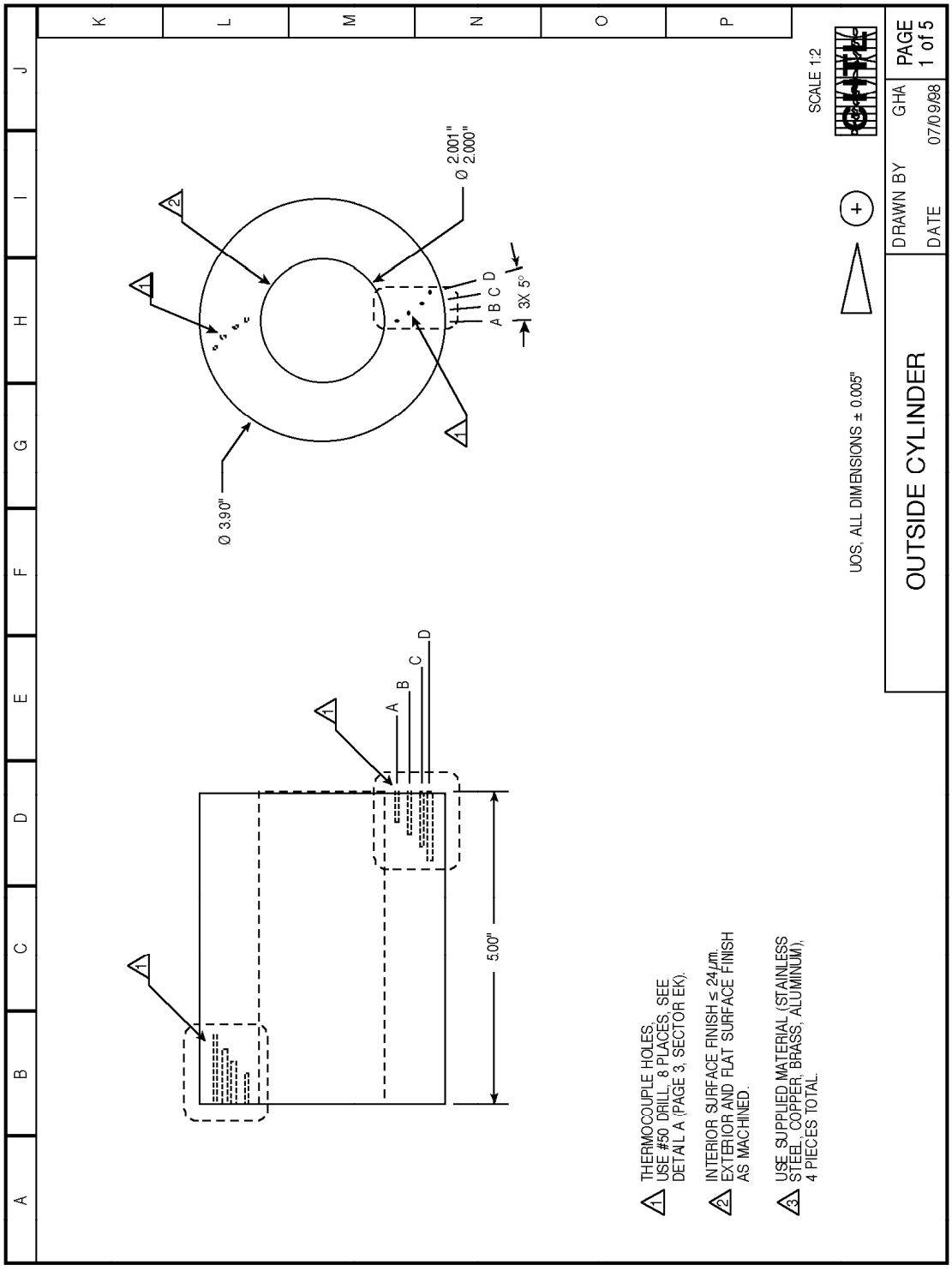
A
B
C
D
E
F
G
H
I
J
K
L
M
N
O
P
Ø 3.90"
5.00"
A B C D
3X 5°
Ø 2.001"
Ø 2.000"
A B C D
1 THERMOCOUPLE HOLES, USE #50 DRILL, 8 PLACES, SEE DETAIL A (PAGE 3, SECTOR EK).
2 INTERIOR SURFACE FINISH ≤ 24μm. EXTERIOR AND FLAT SURFACE FINISH AS MACHINED.
3 USE SUPPLIED MATERIAL (STAINLESS STEEL, COPPER, BRASS, ALUMINUM), 4 PIECES TOTAL.
UOS, ALL DIMENSIONS ± 0.005"
SCALE 1:2
OUTSIDE CYLINDER
DRAWN BY GHA
DATE 07/09/08
PAGE 1 of 5

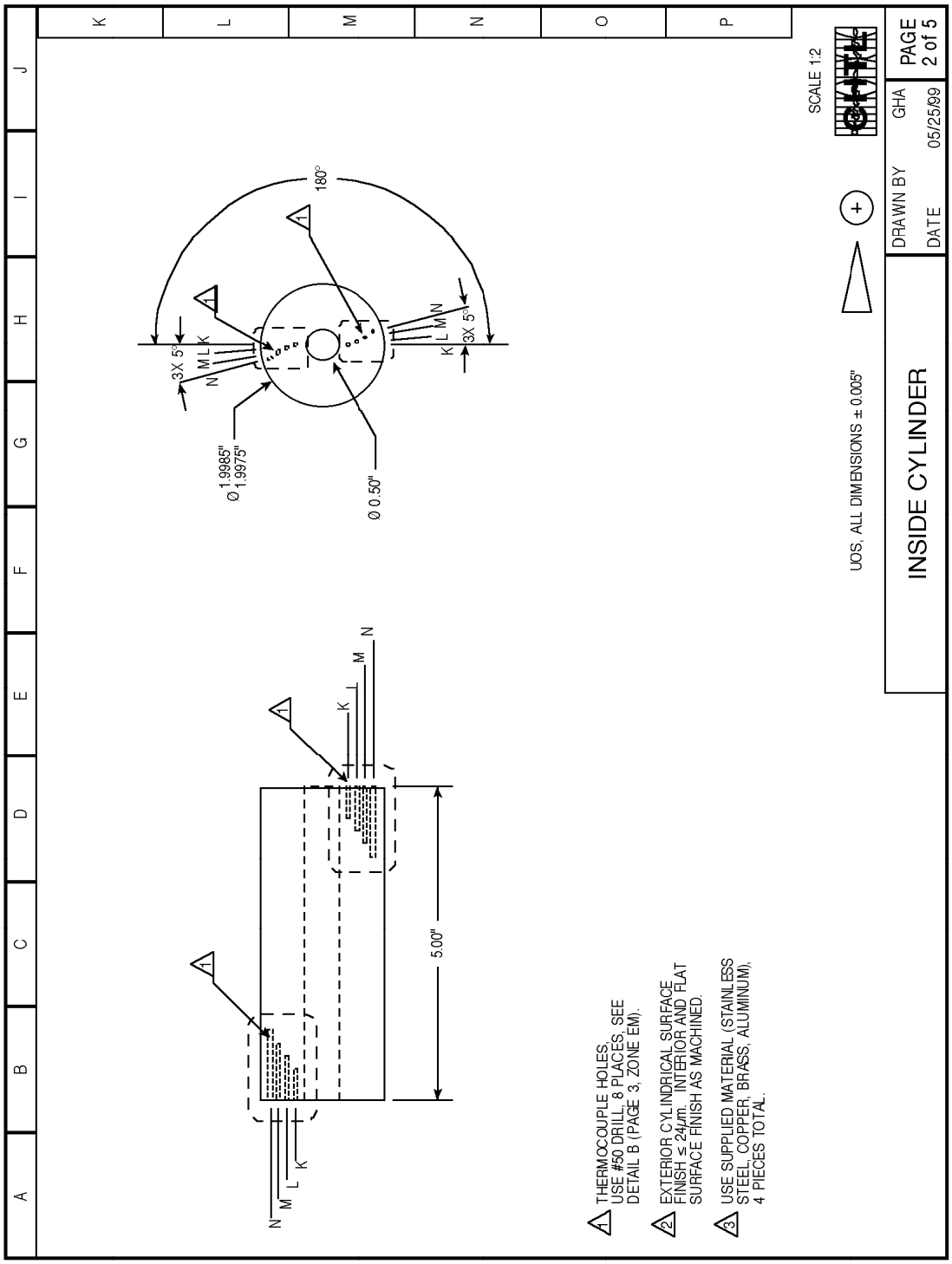
INSIDE CYLINDER
SCALE 1:2
UOS, ALL DIMENSIONS ± 0.005"
DRAWN BY GHA
DATE 05/25/99
PAGE 2 of 5
180°
3X 5°
Ø 1.9985"
1.9975"
Ø 0.50"
5.00"
1 THERMOCOUPLE HOLES, USE #50 DRILL, 8 PLACES, SEE DETAIL B (PAGE 3, ZONE EM).
2 EXTERIOR CYLINDRICAL SURFACE FINISH ≤ 24μm. INTERIOR AND FLAT SURFACE FINISH AS MACHINED.
3 USE SUPPLIED MATERIAL (STAINLESS STEEL, COPPER, BRASS, ALUMINUM), 4 PIECES TOTAL.

THERMOCOUPLE HOLE DETAIL A
PAGE 1, ZONE BL, HM

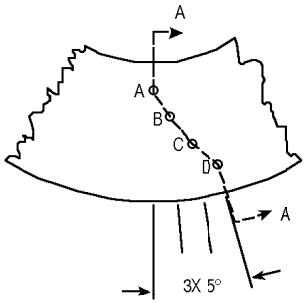

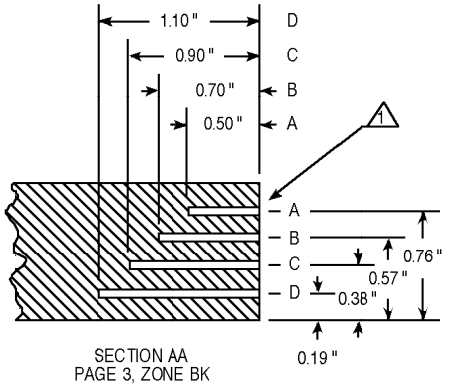

SECTION AA
PAGE 3, ZONE BK

THERMOCOUPLE HOLE DETAIL B
PAGE 2, ZONE BL, HM

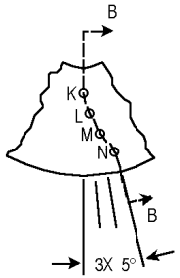

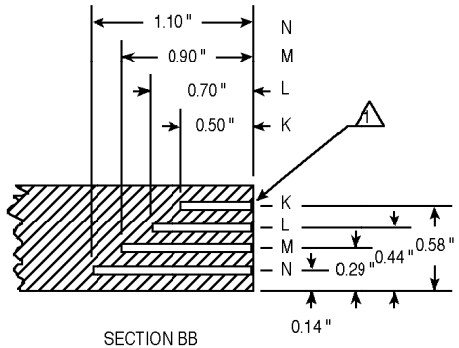

SECTION BB
PAGE 3, ZONE BP

SCALE 1:1

1 THERMOCOUPLE HOLES. USE #50 DRILL, 8 PLACES, DIMENSIONS ARE FROM OUTER DIAMETER AND END FACES OF CYLINDER.

UOS, ALL DIMENSIONS ± 0.005"

GHTL

CYLINDER DETAIL

DRAWN BY	GHA
DATE	07/20/98

PAGE 3 of 5

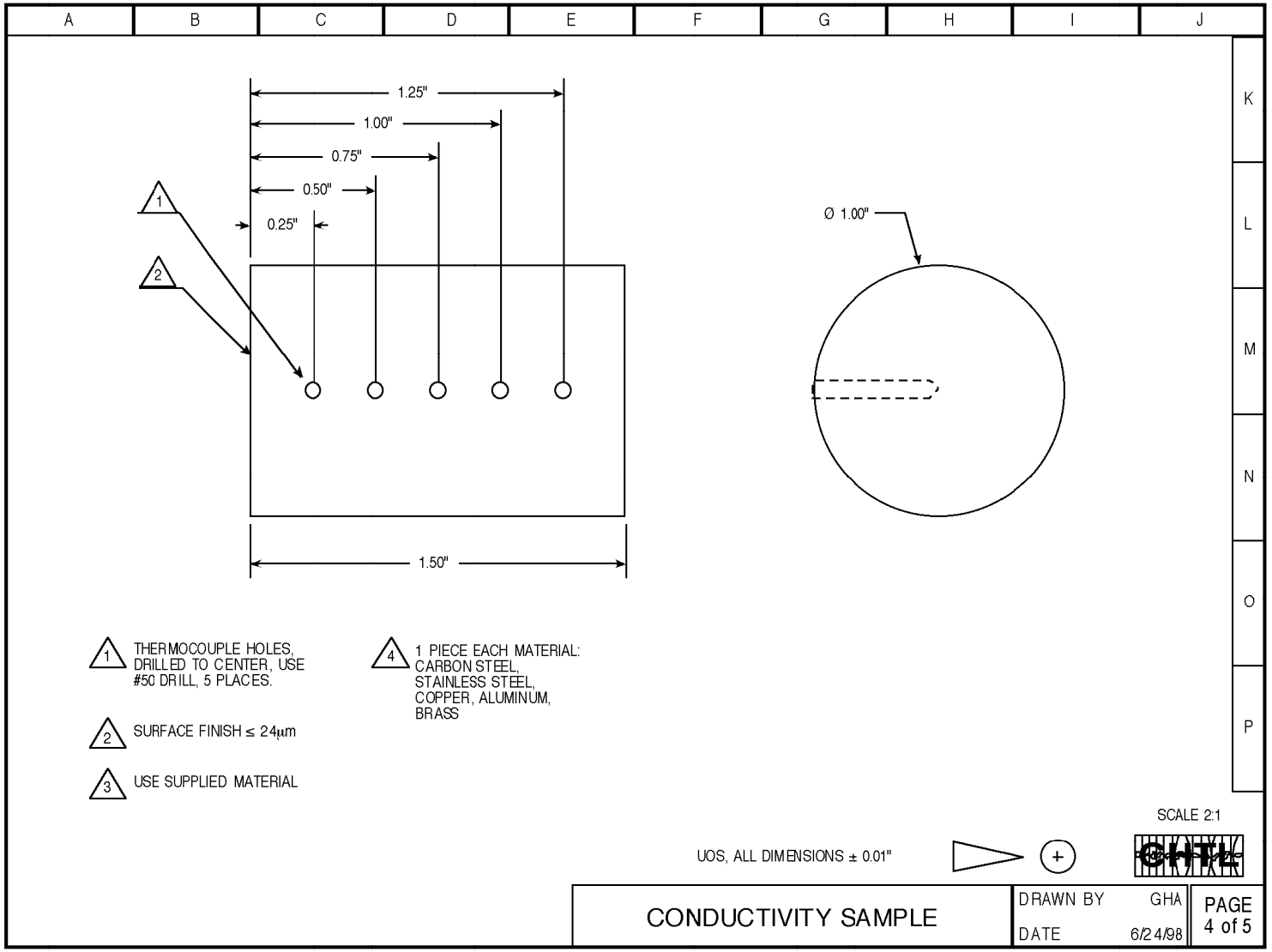
A
B
C
D
E
F
G
H
I
J
K
L
M
N
O
P
1.25"
1.00"
0.75"
0.50"
0.25"
1
2
Ø 1.00"
1.50"
1 THERMOCOUPLE HOLES, DRILLED TO CENTER, USE #50 DRILL, 5 PLACES.
2 SURFACE FINISH ≤ 24μm
3 USE SUPPLIED MATERIAL
4 1 PIECE EACH MATERIAL: CARBON STEEL, STAINLESS STEEL, COPPER, ALUMINUM, BRASS
SCALE 2:1
UOS, ALL DIMENSIONS ± 0.01"
CONDUCTIVITY SAMPLE
DRAWN BY GHA
DATE 6/24/98
PAGE 4 of 5

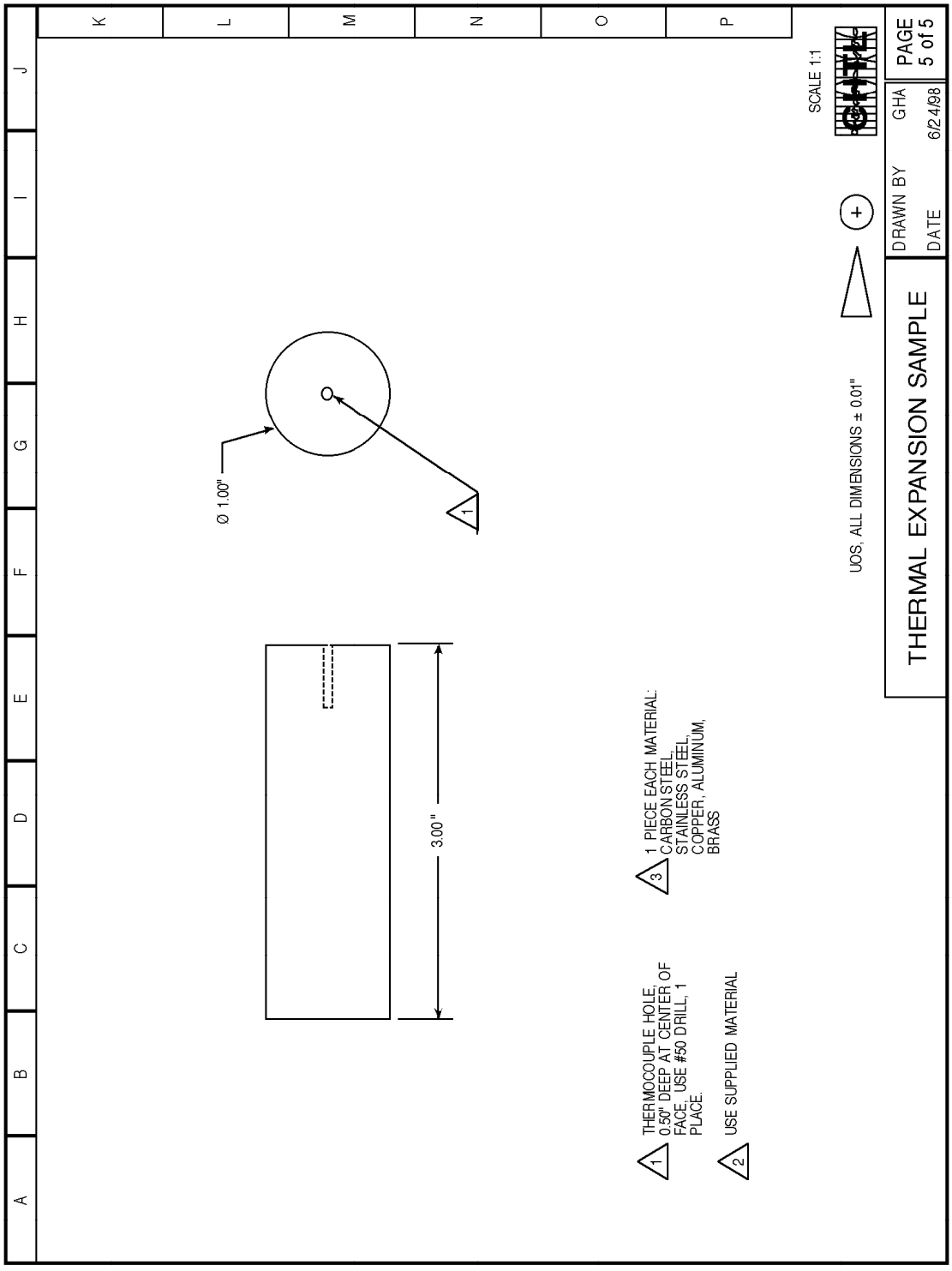
A
B
C
D
E
F
G
H
I
J
K
L
M
N
O
P
Ø 1.00"
1
3.00"
1 THERMOCOUPLE HOLE, 0.50" DEEP AT CENTER OF FACE, USE #50 DRILL, 1 PLACE.
2 USE SUPPLIED MATERIAL
3 1 PIECE EACH MATERIAL: CARBON STEEL, STAINLESS STEEL, COPPER, ALUMINUM, BRASS
UOS, ALL DIMENSIONS ± 0.01"
SCALE 1:1
THERMAL EXPANSION SAMPLE
DRAWN BY GHA
DATE 6/24/98
PAGE 5 of 5

APPENDIX B

DATA ACQUISITION PROGRAM

The diagram in Figure B.1 illustrates the data acquisition and experiment control algorithm used in the present study. As explained in Chapter III, the control program accepts input regarding the cylindrical shells used and the desired heater power settings prior to execution. Upon execution, the program initializes arrays for controlling the heater, storing cylindrical shell geometry and temperature-independent thermophysical properties, and calculating temperature-variable thermophysical properties. For each heater setting, the program write headers for the appropriate runtime and data files and initializes arrays that are used for tracking the variables that are used to indicate steady state conditions. Next, the sensors are polled and data written to the runtime file. The runtime file serves as a backup of sensor data in the case of a power failure or in the case where it is necessary to see the test conditions at a certain time. Appropriate variable displays on the screen are updated and runtime arrays are checked to see if steady state conditions have been met. Steady state is judged to have occurred if the variation of steady state indicating variables is within the prescribed limits for a 30 minute operation period. If steady state has not been reached, the program wait one sample interval (approximately three minutes) and re-enters the control loop at the point where sensors are polled.

Once steady state has been reached, appropriate data are sent to the runtime file and the output data file. If the current heater setting is not the last one in the queue, then the next heater setting is used in the program, which enters the control loop at the point

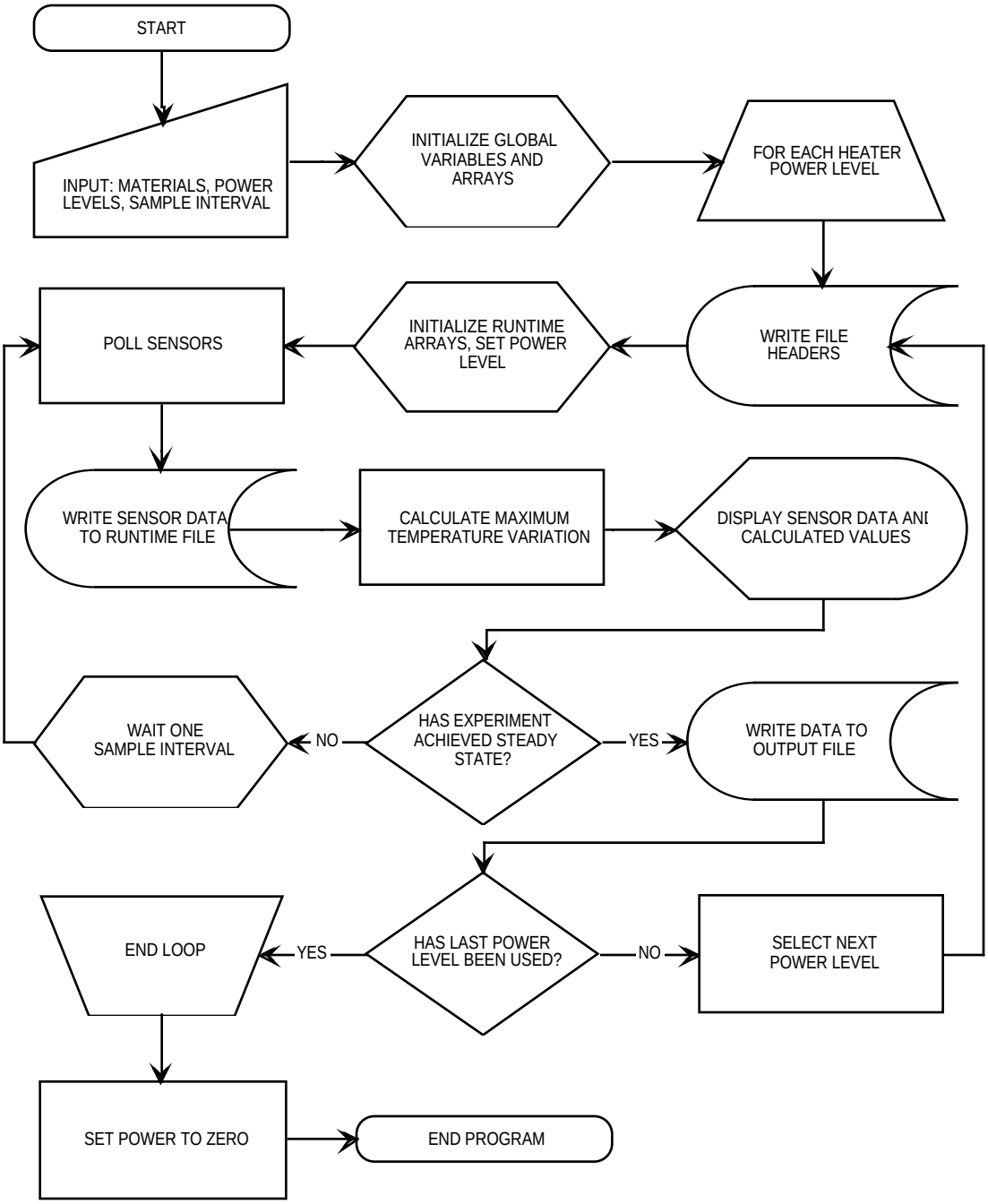

Figure B.1 – Flow chart of experiment control and data acquisition program.

where the runtime arrays are initialized. If the last heater setting in the queue has been used, then the heater is powered down and the program execution is halted.

PSEUDOCODE OF LABVIEW DAQ PROGRAM OPERATION

Input on front panel
- Cylinder materials,
- Desired power levels,
- Sample interval (default 3 min)

Operation - after program is started

- Before all testing begins
  - Determine the number of power levels,
  - Set heater to off (safety feature),
  - Initialize sensor error counter = 0
- For each power level
  - Initialize variables:
    - CTE values,
    - Conductivity values,
    - Cylinder temperatures,
    - Uncertainties,
    - Time-temperature-location array
      - Store 30 minutes worth of data for calculation for all radial locations, preloaded to ensure that temperature variation is greater than steady state limit for temperatures.
    - Geometry
      - Location of thermocouples and interfaces,
      - Labels for cylinder materials
  - Write runtime and data file headers;
  - Set heater power;
  - At every sample interval:
    - Log time;
    - While not in error condition, poll sensors:
      - Check for error reported by FieldPoint units,
      - Thermocouples - check for Over-Temperature, spurious data,
      - Strain gage bridge output - check for spurious data,
      - Strain gage bridge input - check for spurious data.
    - If (Over-Temperature)
      - Report condition,
      - Shut off heater,
      - Shut down program.

Calculate temperature parameters (for each cylinder):
- Average radial location temperature,
- Slope of log temperature distribution,
- Interface temperatures,
- Weighted, mean cylinder temperatures,
- Uncertainties.

Determine thermophysical properties at average temperatures;

Determine appropriate tolerance band;

Calculate interface heat flux;

Calculate thermal contact conductance;

Calculate corrected strain (for each gage array);

Test for steady state - all must be true
- Temperature variation within tolerance for each location?
- Variation of averaged interface heat rate within tolerance?
- At least 30 min have elapsed since setting heater power?

Calculate temperature change since last poll time;

Set steady state indicator colors;

Output runtime variables:
- Sample time,
- Heat rate through inner cylinder,
- Heat rate through outer cylinder,
- Average inner cylinder temperature,
- Average outer cylinder temperature,
- Interface temperature,
- Interface temperature difference,
- Corrected strain,
- Value of maximum temperature variation over last 30 min,
- Averaged temperatures for each radial location,
- Averaged interface heat flux

Output to screen:
- Calculate temperatures at each location;
- Output temperatures to temp-position graph;
- Output to time-temperature chart:
  - High temperature,
  - Inner cylinder temp,
  - Interface temp,
  - Outer cylinder temp,
  - Low temperature,
- Output strain and excitation voltage to time-strain chart;

Wait for next interval;

At reaching steady state:
While not in error condition, poll sensors:
Check for error reported by FieldPoint units,
Thermocouples - check for Over-Temperature, spurious data,
Strain gage bridge output - check for spurious data,
Strain gage bridge input - check for spurious data.

If (Over-Temperature):
Report condition,
Shut off heater,
Shut down program.

Calculate temperature parameters (for each cylinder):
Average radial location temperature,
Slope of log temperature distribution,
Interface temperatures,
Weighted, mean cylinder temperatures,
Uncertainties.

Determine thermophysical properties at average temperatures;

Determine appropriate tolerance band;

Calculate interface heat flux;

Calculate thermal contact conductance;

Calculate corrected strain (for each gage array);

Test for steady state - all must be true
Temperature variation within tolerance for each location?
Variation of averaged interface heat rate within tolerance?
At least 30 min have elapsed since setting heater power?

Calculate temperature change since last poll time;

Set steady state indicator colors;

Output runtime variables:
Sample time,
Heat rate through inner cylinder,
Heat rate through outer cylinder,
Average inner cylinder temperature,
Average outer cylinder temperature,
Interface temperature,
Interface temperature difference,
Corrected strain,
Value of maximum temperature variation over last 30 min,

Averaged temperatures for each radial location,
Averaged interface heat flux

Output to screen:
Calculate temperatures at each location;
Output temperatures to temp-position graph;
Output to time-temperature chart:
High temperature,
Inner cylinder temp,
Interface temp,
Outer cylinder temp,
Low temperature,
Output strain and excitation voltage to time-strain chart;

Write to data file

Determine gage uncertainties;
Output elapsed time;
Output header for temperature distribution;
Output (for each thermocouple in each cylinder):
Temperature,
Temperature uncertainty,
Radial location

Output (for each gage array):
Gage header,
Gage voltage,
Gage uncertainty,
Corrected strain,
Strain uncertainty,
Excitation voltage,
Excitation voltage uncertainty.

Output (for each cylinder):
Average cylinder temperature,
Average thermal conductivity,
Average CTE.

Output:
Interface temperature,
Interface temperature difference,
Inner cylinder heat rate,
Outer cylinder heat rate,
Averaged interface heat rate,
Interface heat flux,
Thermal contact conductance.

Output (for each cylinder):
Raw thermocouple data,
Averaged temperatures,
Raw thermocouple uncertainties.

Output:
Raw gage voltages,
Gage uncertainties,
Corrected strain,
Corrected strain error.

After all power levels have been used

Set heater to off (safety feature),
End Program;

APPENDIX C

EXPERIMENTAL DATA

The symbols in the tables within this appendix have the following meanings and units:

E'	Hertzian Elastic Modulus, Pa
E_e	Elastic Modulus, Pa
ζ	Elastic Conformity Modulus of Clausing and Chao (1964)
h*	Dimensionless Contact Conductance
h_c	Thermal Contact Conductance, W/m^2K
H_e	Effective Vickers Microhardness†, Pa
L*	Dimensionless Load
m_R	slope of effective roughness
m_W	slope of effective longitudinal waviness
m_q	slope of effective circumferential waviness
P*	dimensionless interface pressure
P_i	Calculated interface pressure, Pa
Ψ_G	Plasticity Index of Greenwood (1967)
Q	Nominal Heat Rate, W
Q"	Calculated Interface Heat Flux, W/m^2
R_e	Effective roughness, m
ξ	Waviness Number of Thomas and Sayles (1964)
W_e	effective longitudinal waviness, m
W_q	effective circumferential waviness

† RMS average of microhardness, as measured according to ASTM Standard E 92-82 (ASTM, 1997).

Table C.1 – Test Results for Composite Cylinder AA.

Inner Cylinder: Aluminum 6061

Outer Cylinder: Aluminum 6061

E', Pa	3.939E+10	R_e, m	6.909E-05
E_e, Pa	7.000E+10	m_R	1.484E-01
H_e, Pa	1.148E+09	W_e, m	6.097E-05
		m_W	2.236E-03
ζ	7.533E+02	W_θ, m	1.975E-05
ξ	4.205E+03	m_θ	2.384E-03
Ψ_G	5.091E+00		

Q, W	Q", W/m^2	P_i, Pa	P*	L*	h_c, W/m^{2}K	h*
3.000E+02	1.212E+04	5.339E+07	4.649E-02	7.587E-02	2.521E+02	6.973E-04
5.000E+02	1.836E+04	5.458E+07	4.752E-02	7.756E-02	3.794E+02	1.054E-03
6.000E+02	2.169E+04	5.508E+07	4.796E-02	7.827E-02	4.503E+02	1.253E-03
7.000E+02	2.445E+04	5.580E+07	4.859E-02	7.929E-02	5.093E+02	1.419E-03
7.500E+02	2.567E+04	5.588E+07	4.866E-02	7.941E-02	5.354E+02	1.492E-03
8.000E+02	2.701E+04	5.654E+07	4.923E-02	8.034E-02	5.633E+02	1.571E-03
8.500E+02	2.900E+04	5.641E+07	4.912E-02	8.017E-02	6.060E+02	1.691E-03
9.000E+02	3.042E+04	5.695E+07	4.959E-02	8.093E-02	6.372E+02	1.779E-03
9.500E+02	3.202E+04	5.680E+07	4.946E-02	8.071E-02	6.730E+02	1.881E-03
1.000E+03	3.344E+04	5.730E+07	4.990E-02	8.142E-02	7.040E+02	1.968E-03
5.010E+02	1.614E+04	5.474E+07	4.767E-02	7.779E-02	3.293E+02	9.145E-04

Table C.2 – Test Results for Composite Cylinder AB.

Inner Cylinder: Aluminum 6061

Outer Cylinder: Brass 360

E', Pa	4.838E+10	R_e, m	7.607E-05
E_e, Pa	8.556E+10	m_R	1.544E-01
H_e, Pa	1.148E+09	W_e, m	6.311E-05
		m_W	2.236E-03
ζ	6.220E+02	W_θ, m	1.831E-05
ξ	3.456E+03	m_θ	2.385E-03
Ψ_G	6.504E+00		

Q, W	Q", W/m^2	P_i, Pa	P*	L*	h_c, W/m^{2}K	h*
5.000E+02	3.052E+04	5.481E+07	4.773E-02	5.882E-02	8.537E+02	3.432E-03
7.500E+02	4.050E+04	6.123E+07	5.332E-02	6.571E-02	1.151E+03	4.618E-03
8.500E+02	4.481E+04	6.363E+07	5.540E-02	6.828E-02	1.285E+03	5.151E-03
9.000E+02	4.692E+04	6.506E+07	5.665E-02	6.982E-02	1.349E+03	5.404E-03
9.500E+02	4.919E+04	6.695E+07	5.830E-02	7.184E-02	1.661E+03	6.644E-03
1.000E+03	5.132E+04	6.798E+07	5.920E-02	7.295E-02	1.731E+03	6.921E-03
6.000E+02	3.518E+04	5.709E+07	4.971E-02	6.126E-02	9.988E+02	4.012E-03

Table C.3 – Test Results for Composite Cylinder AC.

Inner Cylinder: Aluminum 6061

Outer Cylinder: Copper 102

E', Pa	4.838E+10	R_e, m	4.826E-05
E_e, Pa	8.556E+10	m_R	1.991E-01
H_e, Pa	1.148E+09	W_e, m	6.015E-05
		m_W	1.414E-03
ζ	7.922E+02	W_θ, m	1.822E-05
ξ	4.401E+03	m_θ	2.385E-03
Ψ_G	8.388E+00		

Q, W	Q", W/m^2	P_i, Pa	P*	L*	h_c, W/m^{2}K	h*
3.000E+02	4.683E+03	9.544E+07	8.311E-02	3.662E-01	8.805E+01	9.115E-05
5.000E+02	6.865E+03	1.039E+08	9.047E-02	3.986E-01	1.238E+02	1.285E-04
6.000E+02	7.782E+03	1.076E+08	9.372E-02	4.129E-01	1.383E+02	1.437E-04
7.000E+02	8.513E+03	1.110E+08	9.662E-02	4.257E-01	1.496E+02	1.557E-04
7.500E+02	9.436E+03	1.132E+08	9.853E-02	4.341E-01	1.649E+02	1.716E-04
8.000E+02	1.020E+04	1.148E+08	1.000E-01	4.406E-01	1.773E+02	1.847E-04
8.500E+02	1.202E+04	1.163E+08	1.013E-01	4.463E-01	2.082E+02	2.170E-04
9.000E+02	1.178E+04	1.180E+08	1.028E-01	4.528E-01	2.029E+02	2.115E-04
9.500E+02	1.349E+04	1.194E+08	1.040E-01	4.581E-01	2.314E+02	2.413E-04
1.000E+03	1.408E+04	1.212E+08	1.055E-01	4.649E-01	2.404E+02	2.508E-04
5.010E+02	3.450E+03	9.299E+07	8.098E-02	3.568E-01	7.104E+01	7.354E-05

Table C.4 – Test Results for Composite Cylinder AS.

Inner Cylinder: Aluminum 6061

Outer Cylinder: Stainless Steel 304

E', Pa	5.750E+10	R_e, m	7.159E-05
E_e, Pa	1.027E+11	m_R	1.613E-01
H_e, Pa	1.148E+09	W_e, m	6.010E-05
		m_W	2.236E-03
ζ	1.570E+03	W_θ, m	1.823E-05
ξ	8.811E+03	m_θ	2.384E-03
Ψ_G	8.079E+00		

Q, W	Q", W/m^2	P_i, Pa	P*	L*	h_c, W/m^{2}K	h*
3.000E+02	1.513E+04	1.073E+08	9.347E-02	9.628E-02	4.189E+02	7.149E-03
5.000E+02	2.188E+04	1.355E+08	1.180E-01	1.215E-01	6.106E+02	1.032E-02
6.000E+02	2.998E+04	1.594E+08	1.388E-01	1.430E-01	8.051E+02	1.363E-02
7.000E+02	3.363E+04	1.652E+08	1.439E-01	1.482E-01	9.002E+02	1.521E-02
7.500E+02	3.541E+04	1.711E+08	1.490E-01	1.535E-01	9.426E+02	1.591E-02
8.000E+02	3.689E+04	1.779E+08	1.549E-01	1.596E-01	9.755E+02	1.646E-02
8.500E+02	3.841E+04	1.848E+08	1.609E-01	1.658E-01	1.010E+03	1.704E-02
9.000E+02	3.986E+04	1.930E+08	1.680E-01	1.731E-01	1.036E+03	1.746E-02
9.500E+02	4.135E+04	1.990E+08	1.733E-01	1.785E-01	1.073E+03	1.808E-02
1.000E+03	4.259E+04	1.951E+08	1.699E-01	1.750E-01	1.087E+03	1.832E-02
5.010E+02	2.415E+04	1.356E+08	1.181E-01	1.216E-01	6.303E+02	1.072E-02

Table C.5 – Test Results for Composite Cylinder BA.

Inner Cylinder: Brass 360

Outer Cylinder: Aluminum 6061

E', Pa	4.838E+10	R_e, m	1.053E-04
E_e, Pa	8.556E+10	m_R	2.885E-01
H_e, Pa	1.079E+09	W_e, m	3.494E-05
		m_W	6.633E-03
ζ	5.120E+03	W_θ, m	1.069E-05
ξ	2.844E+04	m_θ	3.658E-04
Ψ_G	1.294E+01		

Q, W	Q", W/m^2	P_i, Pa	P*	L*	h_c, W/m^{2}K	h*
5.000E+02	1.446E+04	5.003E+07	4.637E-02	1.979E-03	2.776E+02	7.962E-04
6.000E+02	2.138E+04	5.070E+07	4.699E-02	2.005E-03	4.138E+02	1.187E-03
7.000E+02	2.598E+04	5.097E+07	4.724E-02	2.016E-03	5.067E+02	1.453E-03
7.500E+02	2.857E+04	5.134E+07	4.758E-02	2.030E-03	5.595E+02	1.604E-03
8.000E+02	3.083E+04	5.146E+07	4.770E-02	2.035E-03	6.057E+02	1.736E-03
8.500E+02	3.289E+04	5.185E+07	4.806E-02	2.051E-03	6.491E+02	1.861E-03
9.000E+02	3.520E+04	5.199E+07	4.819E-02	2.056E-03	6.968E+02	1.997E-03
9.500E+02	3.782E+04	5.249E+07	4.865E-02	2.076E-03	7.523E+02	2.155E-03
1.000E+03	3.988E+04	5.250E+07	4.866E-02	2.077E-03	7.961E+02	2.280E-03
5.010E+02	1.673E+04	5.019E+07	4.652E-02	1.985E-03	3.206E+02	9.195E-04

Table C.6 – Test Results for Composite Cylinder BB.

Inner Cylinder: Brass 360

Outer Cylinder: Brass 360

E', Pa	6.268E+10	R_e, m	1.100E-04
E_e, Pa	1.100E+11	m_R	2.917E-01
H_e, Pa	1.079E+09	W_e, m	3.856E-05
		m_W	6.633E-03
ζ	4.484E+03	W_θ, m	7.726E-06
ξ	2.472E+04	m_θ	3.756E-04
Ψ_G	1.694E+01		

Q, W	Q", W/m^2	P_i, Pa	P*	L*	h_c, W/m^{2}K	h*
2.000E+02	6.359E+03	4.828E+07	4.475E-02	1.681E-03	1.624E+02	6.213E-04
4.000E+02	1.957E+04	6.111E+07	5.663E-02	2.127E-03	4.596E+02	1.749E-03
5.000E+02	2.554E+04	6.331E+07	5.868E-02	2.204E-03	5.949E+02	2.260E-03
6.500E+02	3.388E+04	7.271E+07	6.739E-02	2.531E-03	7.324E+02	2.772E-03
7.500E+02	3.879E+04	7.441E+07	6.896E-02	2.590E-03	8.413E+02	3.191E-03
8.000E+02	3.796E+04	7.817E+07	7.245E-02	2.721E-03	8.565E+02	3.232E-03
8.500E+02	4.506E+04	7.848E+07	7.273E-02	2.732E-03	1.017E+03	3.837E-03
9.000E+02	4.779E+04	7.581E+07	7.026E-02	2.639E-03	1.124E+03	4.243E-03
9.500E+02	5.048E+04	7.728E+07	7.163E-02	2.690E-03	1.183E+03	4.461E-03
1.000E+03	5.311E+04	7.900E+07	7.322E-02	2.750E-03	1.243E+03	4.682E-03
5.100E+02	2.434E+04	6.443E+07	5.971E-02	2.243E-03	5.511E+02	2.094E-03

Table C.7 – Test Results for Composite Cylinder BC.

Inner Cylinder: Brass 360

Outer Cylinder: Copper 102

E', Pa	6.268E+10	R_e, m	9.295E-05
E_e, Pa	1.100E+11	m_R	3.176E-01
H_e, Pa	1.079E+09	W_e, m	3.350E-05
		m_W	6.403E-03
ζ	5.888E+03	W_θ, m	7.518E-06
ξ	3.246E+04	m_θ	3.738E-04
Ψ_G	1.845E+01		

Q, W	Q", W/m^2	P_i, Pa	P*	L*	h_c, W/m^{2}K	h*
3.000E+02	1.384E+04	6.776E+07	6.281E-02	2.417E-03	3.736E+02	6.811E-04
5.000E+02	2.397E+04	6.963E+07	6.453E-02	2.484E-03	6.560E+02	1.192E-03
6.000E+02	2.850E+04	7.102E+07	6.582E-02	2.534E-03	7.799E+02	1.416E-03
7.000E+02	3.276E+04	7.199E+07	6.672E-02	2.568E-03	9.017E+02	1.635E-03
7.500E+02	3.415E+04	7.274E+07	6.742E-02	2.595E-03	9.381E+02	1.700E-03
8.000E+02	3.718E+04	7.315E+07	6.780E-02	2.610E-03	1.022E+03	1.851E-03
8.500E+02	3.877E+04	7.369E+07	6.829E-02	2.629E-03	1.066E+03	1.929E-03
9.000E+02	3.993E+04	7.410E+07	6.868E-02	2.644E-03	1.092E+03	1.976E-03
9.500E+02	4.146E+04	7.497E+07	6.948E-02	2.675E-03	1.129E+03	2.041E-03
1.000E+03	4.393E+04	7.546E+07	6.994E-02	2.692E-03	1.193E+03	2.155E-03
5.010E+02	2.525E+04	6.944E+07	6.436E-02	2.477E-03	7.031E+02	1.278E-03

Table C.8 – Test Results for Composite Cylinder BS.

Inner Cylinder: Brass 360

Outer Cylinder: Stainless Steel 304

E', Pa	7.889E+10	R_e, m	1.069E-04
E_e, Pa	1.401E+11	m_R	2.954E-01
H_e, Pa	1.079E+09	W_e, m	3.341E-05
		m_W	6.633E-03
ζ	9.551E+03	W_θ, m	7.533E-06
ξ	5.330E+04	m_θ	3.686E-04
Ψ_G	2.160E+01		

Q, W	Q", W/m^2	P_i, Pa	P*	L*	h_c, W/m^{2}K	h*
3.000E+02	1.508E+04	9.569E+07	8.868E-02	2.072E-03	4.151E+02	6.124E-03
5.000E+02	2.352E+04	1.205E+08	1.116E-01	2.609E-03	7.061E+02	1.021E-02
6.000E+02	2.780E+04	1.320E+08	1.224E-01	2.860E-03	8.076E+02	1.164E-02
7.000E+02	3.441E+04	1.451E+08	1.345E-01	3.142E-03	9.781E+02	1.411E-02
7.500E+02	3.596E+04	1.495E+08	1.386E-01	3.238E-03	1.001E+03	1.443E-02
8.000E+02	3.767E+04	1.494E+08	1.385E-01	3.237E-03	1.022E+03	1.471E-02
8.500E+02	4.001E+04	1.559E+08	1.445E-01	3.377E-03	1.157E+03	1.665E-02
9.000E+02	4.273E+04	1.621E+08	1.503E-01	3.511E-03	1.211E+03	1.740E-02
9.500E+02	4.464E+04	1.672E+08	1.549E-01	3.620E-03	1.265E+03	1.817E-02
1.000E+03	4.826E+04	1.722E+08	1.596E-01	3.731E-03	1.367E+03	1.962E-02
5.010E+02	2.337E+04	1.216E+08	1.127E-01	2.633E-03	6.940E+02	1.003E-02

Table C.9 – Test Results for Composite Cylinder CA.

Inner Cylinder: Copper 102

Outer Cylinder: Aluminum 6061

E', Pa	4.838E+10	R_e, m	8.835E-05
E_e, Pa	8.556E+10	m_R	1.796E-01
H_e, Pa	8.345E+08	W_e, m	9.617E-05
		m_W	2.828E-03
ζ	3.368E+02	W_θ, m	1.070E-05
ξ	1.871E+03	m_θ	2.782E-04
Ψ_G	1.041E+01		

Q, W	Q", W/m^2	P_i, Pa	P*	L*	h_c, W/m^{2}K	h*
3.000E+02	9.766E+03	4.938E+07	5.917E-02	6.912E-02	1.958E+02	4.075E-04
5.000E+02	1.222E+04	5.503E+07	6.594E-02	7.702E-02	2.250E+02	4.710E-04
6.000E+02	1.723E+04	5.803E+07	6.954E-02	8.123E-02	3.054E+02	6.409E-04
7.000E+02	1.600E+04	6.045E+07	7.244E-02	8.461E-02	2.750E+02	5.781E-04
7.500E+02	1.731E+04	6.139E+07	7.356E-02	8.593E-02	2.942E+02	6.189E-04
8.000E+02	1.894E+04	6.226E+07	7.461E-02	8.715E-02	3.187E+02	6.710E-04
8.500E+02	1.978E+04	6.311E+07	7.562E-02	8.833E-02	3.298E+02	6.947E-04
9.000E+02	2.042E+04	6.422E+07	7.695E-02	8.988E-02	3.371E+02	7.106E-04
9.500E+02	2.146E+04	6.504E+07	7.793E-02	9.103E-02	3.503E+02	7.389E-04
1.000E+03	2.211E+04	6.622E+07	7.935E-02	9.269E-02	3.565E+02	7.525E-04
5.010E+02	1.377E+04	5.493E+07	6.582E-02	7.689E-02	2.512E+02	5.256E-04

Table C.10 – Test Results for Composite Cylinder CB.

Inner Cylinder: Copper 102

Outer Cylinder: Brass 360

E', Pa	6.268E+10	R_e, m	9.391E-05
E_e, Pa	1.100E+11	m_R	1.846E-01
H_e, Pa	8.345E+08	W_e, m	9.754E-05
		m_W	2.828E-03
ζ	4.534E+02	W_θ, m	7.729E-06
ξ	2.500E+03	m_θ	2.909E-04
Ψ_G	1.386E+01		

Q, W	Q", W/m^2	P_i, Pa	P*	L*	h_c, W/m^{2}K	h*
4.000E+02	1.633E+04	8.892E+07	1.066E-01	9.019E-02	2.949E+02	9.706E-04
6.500E+02	2.522E+04	1.061E+08	1.271E-01	1.076E-01	4.090E+02	1.344E-03
8.500E+02	3.178E+04	1.197E+08	1.434E-01	1.214E-01	4.779E+02	1.567E-03
9.500E+02	3.487E+04	1.254E+08	1.502E-01	1.272E-01	5.057E+02	1.656E-03
1.000E+03	3.670E+04	1.285E+08	1.540E-01	1.303E-01	5.233E+02	1.713E-03
9.000E+02	3.360E+04	1.228E+08	1.471E-01	1.245E-01	4.957E+02	1.625E-03
7.500E+02	2.825E+04	1.133E+08	1.357E-01	1.149E-01	4.337E+02	1.424E-03
4.100E+02	1.588E+04	9.132E+07	1.094E-01	9.262E-02	2.786E+02	9.171E-04
2.000E+02	9.170E+03	7.567E+07	9.068E-02	7.675E-02	1.829E+02	6.019E-04
5.010E+02	2.381E+04	2.596E+05	3.111E-04	2.633E-04	3.901E+02	1.285E-03

Table C.11 – Test Results for Composite Cylinder CC.

Inner Cylinder: Copper 102

Outer Cylinder: Copper 102

E', Pa	6.268E+10	R_e, m	7.321E-05
E_e, Pa	1.100E+11	m_R	2.233E-01
H_e, Pa	8.345E+08	W_e, m	9.565E-05
		m_W	2.236E-03
ζ	2.944E+02	W_θ, m	7.522E-06
ξ	1.623E+03	m_θ	2.886E-04
Ψ_G	1.677E+01		

Q, W	Q", W/m^2	P_i, Pa	P*	L*	h_c, W/m^{2}K	h*
6.000E+02	9.615E+03	8.261E+07	9.898E-02	1.665E-01	2.069E+02	1.731E-04
7.000E+02	1.103E+04	8.421E+07	1.009E-01	1.697E-01	2.352E+02	1.971E-04
7.500E+02	1.178E+04	8.509E+07	1.020E-01	1.715E-01	2.501E+02	2.096E-04
8.000E+02	1.290E+04	8.533E+07	1.022E-01	1.720E-01	2.734E+02	2.294E-04
8.500E+02	1.393E+04	8.639E+07	1.035E-01	1.741E-01	2.941E+02	2.469E-04
9.000E+02	1.491E+04	8.723E+07	1.045E-01	1.758E-01	3.138E+02	2.636E-04
9.500E+02	1.608E+04	8.816E+07	1.056E-01	1.777E-01	3.364E+02	2.828E-04
1.000E+03	1.709E+04	8.911E+07	1.068E-01	1.796E-01	3.557E+02	2.992E-04
5.010E+02	7.479E+03	8.195E+07	9.820E-02	1.652E-01	1.605E+02	1.342E-04

Table C.12 – Test Results for Composite Cylinder CS.

Inner Cylinder: Copper 102

Outer Cylinder: Stainless Steel 304

E', Pa	7.889E+10	R_e, m	9.031E-05
E_e, Pa	1.401E+11	m_R	1.904E-01
H_e, Pa	8.345E+08	W_e, m	9.562E-05
		m_W	2.828E-03
ζ	7.124E+02	W_θ, m	7.537E-06
ξ	3.975E+03	m_θ	2.818E-04
Ψ_G	1.800E+01		

Q, W	Q", W/m^2	P_i, Pa	P*	L*	h_c, W/m^{2}K	h*
4.000E+02	2.069E+04	1.239E+08	1.485E-01	1.017E-01	5.051E+02	8.827E-03
5.000E+02	2.819E+04	1.642E+08	1.967E-01	1.348E-01	6.513E+02	1.128E-02
6.000E+02	3.053E+04	1.833E+08	2.196E-01	1.505E-01	7.103E+02	1.224E-02
7.000E+02	3.785E+04	2.074E+08	2.486E-01	1.703E-01	7.989E+02	1.374E-02
7.500E+02	3.973E+04	2.157E+08	2.585E-01	1.771E-01	8.156E+02	1.402E-02
8.500E+02	4.260E+04	2.334E+08	2.797E-01	1.916E-01	8.390E+02	1.441E-02
8.000E+02	4.158E+04	2.252E+08	2.699E-01	1.849E-01	8.346E+02	1.434E-02
9.000E+02	4.407E+04	2.431E+08	2.913E-01	1.996E-01	8.425E+02	1.447E-02
9.500E+02	4.647E+04	2.534E+08	3.037E-01	2.081E-01	8.655E+02	1.486E-02
1.000E+03	4.820E+04	2.623E+08	3.143E-01	2.154E-01	8.727E+02	1.498E-02
5.010E+02	2.150E+04	1.343E+08	1.609E-01	1.103E-01	5.423E+02	9.425E-03

Table C.13 – Test Results for Composite Cylinder SA.

Inner Cylinder: Stainless Steel 304

Outer Cylinder: Aluminum 6061

E', Pa	5.750E+10	R_e, m	7.736E-05
E_e, Pa	1.027E+11	m_R	1.557E-01
H_e, Pa	2.576E+09	W_e, m	3.771E-05
		m_W	2.828E-03
ζ	1.130E+03	W_θ, m	8.807E-06
ξ	6.341E+03	m_θ	1.887E-04
Ψ_G	3.477E+00		

Q, W	Q", W/m^2	P_i, Pa	P*	L*	h_c, W/m^{2}K	h*
3.000E+02	1.556E+04	3.669E+07	1.424E-02	8.107E-03	4.784E+02	9.030E-03
5.000E+02	2.383E+04	3.628E+07	1.409E-02	8.017E-03	8.422E+02	1.591E-02
6.000E+02	2.790E+04	3.741E+07	1.452E-02	8.266E-03	1.019E+03	1.928E-02
7.000E+02	3.077E+04	3.694E+07	1.434E-02	8.164E-03	1.162E+03	2.199E-02
7.500E+02	3.288E+04	3.676E+07	1.427E-02	8.124E-03	1.258E+03	2.381E-02
8.000E+02	3.419E+04	3.748E+07	1.455E-02	8.283E-03	1.327E+03	2.511E-02
8.500E+02	3.603E+04	3.732E+07	1.449E-02	8.248E-03	1.421E+03	2.689E-02
9.000E+02	3.790E+04	3.741E+07	1.452E-02	8.267E-03	1.514E+03	2.865E-02
9.500E+02	3.979E+04	3.796E+07	1.474E-02	8.388E-03	1.610E+03	3.048E-02
1.000E+03	4.165E+04	3.775E+07	1.465E-02	8.341E-03	1.714E+03	3.242E-02
5.010E+02	2.303E+04	3.654E+07	1.419E-02	8.075E-03	8.154E+02	1.541E-02
9.990E+02	4.115E+04	3.762E+07	1.461E-02	8.314E-03	1.709E+03	3.234E-02
4.990E+02	2.253E+04	3.686E+07	1.431E-02	8.146E-03	7.976E+02	1.507E-02

Table C.14 – Test Results for Composite Cylinder SB.

Inner Cylinder: Stainless Steel 304

Outer Cylinder: Brass 360

E', Pa	7.889E+10	R_e, m	8.366E-05
E_e, Pa	1.401E+11	m_R	1.614E-01
H_e, Pa	2.576E+09	W_e, m	4.108E-05
		m_W	2.828E-03
ζ	1.859E+03	W_θ, m	4.783E-06
ξ	1.038E+04	m_θ	2.071E-04
Ψ_G	4.944E+00		

Q, W	Q", W/m^2	P_i, Pa	P*	L*	h_c, W/m^{2}K	h*
3.000E+02	1.329E+04	8.301E+07	3.223E-02	1.411E-02	2.869E+02	5.991E-03
6.000E+02	3.011E+04	9.722E+07	3.775E-02	1.653E-02	6.547E+02	1.361E-02
7.500E+02	3.659E+04	1.043E+08	4.049E-02	1.773E-02	7.909E+02	1.637E-02
8.500E+02	4.067E+04	1.076E+08	4.175E-02	1.828E-02	8.757E+02	1.807E-02
9.500E+02	4.479E+04	1.128E+08	4.379E-02	1.917E-02	9.598E+02	1.972E-02
1.000E+03	4.695E+04	1.156E+08	4.487E-02	1.965E-02	1.002E+03	2.053E-02
9.000E+02	4.281E+04	1.100E+08	4.269E-02	1.869E-02	9.292E+02	1.913E-02
8.000E+02	3.840E+04	1.051E+08	4.079E-02	1.786E-02	8.431E+02	1.743E-02
6.010E+02	3.057E+04	9.722E+07	3.774E-02	1.653E-02	6.794E+02	1.414E-02
4.000E+02	2.186E+04	8.656E+07	3.361E-02	1.471E-02	4.942E+02	1.032E-02
2.000E+02	9.475E+03	7.706E+07	2.992E-02	1.310E-02	2.131E+02	4.449E-03

Table C.15 – Test Results for Composite Cylinder SC.

Inner Cylinder: Stainless Steel 304

Outer Cylinder: Copper 102

E', Pa	7.889E+10	R_e, m	5.950E-05
E_e, Pa	1.401E+11	m_R	2.046E-01
H_e, Pa	2.576E+09	W_e, m	3.638E-05
		m_W	2.236E-03
ζ	1.445E+03	W_θ, m	4.441-06
ξ	8.063E+03	m_θ	2.039E-04
Ψ_G	6.267E+00		

Q, W	Q", W/m^2	P_i, Pa	P*	L*	h_c, W/m^{2}K	h*
3.000E+02	6.048E+03	1.757E+05	6.820E-05	5.555E-05	1.845E+02	1.944E-03
5.000E+02	7.184E+03	7.570E+07	2.939E-02	2.394E-02	2.226E+02	2.349E-03
6.000E+02	9.996E+03	7.595E+07	2.948E-02	2.401E-02	3.204E+02	3.383E-03
7.000E+02	1.223E+04	7.660E+07	2.974E-02	2.422E-02	4.038E+02	4.267E-03
7.500E+02	1.113E+04	7.670E+07	2.978E-02	2.425E-02	3.730E+02	3.942E-03
8.000E+02	1.181E+04	7.691E+07	2.986E-02	2.432E-02	4.022E+02	4.253E-03
8.500E+02	1.285E+04	7.710E+07	2.993E-02	2.438E-02	4.443E+02	4.698E-03
9.000E+02	1.316E+04	7.706E+07	2.992E-02	2.437E-02	4.626E+02	4.892E-03
9.500E+02	1.410E+04	7.755E+07	3.011E-02	2.452E-02	5.037E+02	5.328E-03
1.000E+03	1.460E+04	7.766E+07	3.015E-02	2.456E-02	5.305E+02	5.612E-03
5.010E+02	7.618E+03	7.527E+07	2.922E-02	2.380E-02	2.442E+02	2.576E-03
3.010E+02	5.409E+03	7.482E+07	2.905E-02	2.366E-02	1.613E+02	1.700E-03

Table C.16 – Test Results for Composite Cylinder SS.

Inner Cylinder: Stainless Steel 304

Outer Cylinder: Stainless Steel 304

E', Pa	1.064E+11	R_e, m	7.960E-05
E_e, Pa	1.930E+11	m_R	1.681E-01
H_e, Pa	2.576E+09	W_e, m	3.629E-05
		m_W	2.828E-03
ζ	3.836E+03	W_θ, m	4.466E-06
ξ	2.186E+04	m_θ	1.941E-04
Ψ_G	6.944E+00		

Q, W	Q", W/m^2	P_i, Pa	P*	L*	h_c, W/m^{2}K	h*
2.000E+02	8.645E+03	1.011E+08	3.926E-02	1.072E-02	2.550E+02	8.770E-03
4.000E+02	1.573E+04	1.495E+08	5.805E-02	1.584E-02	3.825E+02	1.281E-02
5.000E+02	1.966E+04	1.886E+08	7.321E-02	1.998E-02	4.679E+02	1.549E-02
6.000E+02	2.524E+04	2.155E+08	8.368E-02	2.284E-02	5.734E+02	1.877E-02
6.500E+02	2.792E+04	2.239E+08	8.691E-02	2.372E-02	6.141E+02	2.014E-02
7.000E+02	2.783E+04	2.211E+08	8.585E-02	2.343E-02	6.288E+02	2.061E-02
7.500E+02	2.943E+04	2.332E+08	9.053E-02	2.471E-02	6.483E+02	2.116E-02
8.000E+02	3.038E+04	2.446E+08	9.497E-02	2.592E-02	6.365E+02	2.069E-02
8.500E+02	3.228E+04	2.541E+08	9.864E-02	2.692E-02	6.689E+02	2.165E-02
9.000E+02	4.029E+04	2.873E+08	1.115E-01	3.044E-02	8.189E+02	2.642E-02
9.500E+02	4.196E+04	2.759E+08	1.071E-01	2.923E-02	8.207E+02	2.642E-02
1.000E+03	4.332E+04	2.877E+08	1.117E-01	3.049E-02	8.149E+02	2.616E-02
5.010E+02	2.046E+04	1.785E+08	6.928E-02	1.891E-02	5.029E+02	1.677E-02

APPENDIX D

CALCULATION OF INTERFACE PRESSURE

One goal of this analysis is to use data collected in the experimental part of the present study to determine the contact pressures experienced by the compound cylindrical shells. Another goal is to develop a methodology to estimate the pressure experienced by other compound cylindrical shells from published data. An estimate of the interface pressure must be obtained so that the results of this study may be compared with previously published results (both flat and cylindrical thermal contact conductance) on the same basis. Due to the difficulty in placing reliable pressure measurement sensors at the interface without disrupting the flow of heat, we turn to the mathematical theory of elasticity in order to determine the interface pressure – specifically the theories associated with the Lamé problem. Through superposition, we can use the separate solutions for the thermally induced stress and the mechanically induced stress in conjunction with the experimental data and the initial geometry to determine the pressure exerted at the interface.

The material in this appendix is developed from material by Kozik (1997), Popov (1978), Boley (1997), and Timoshenko and Goodier (1951).

SUPERPOSITION OF STRESSES

The equations and boundary conditions for the stresses and displacements within the compound cylinder are linear. We may then divide the problem into two pieces, solve them separately, and calculate the displacements and stresses to be the sum of the two solutions. Posing this in mathematical terms:

$$\begin{aligned} \sigma_{total} &= \sigma_{mechanical} + \sigma_{thermal} \\ u(r)_{total} &= u(r)_{mechanical} + u(r)_{thermal} \end{aligned} \tag{D.1}$$

This analysis will first address the mechanical part of the problem, including the effects of the initial stress at the interface. The cases of negligible and full longitudinal restraint at the interface will be considered. Later, the thermal part of the problem will be addressed. The solutions for the two parts will be used together to obtain the solutions for the total problem.

MECHANICAL EFFECTS

As noted in Chapter IV, the cylindrical shells used in this study are thick-walled and have an initial clearance fit. The cylindrical shells are unrestrained, except by each other. Each cylindrical shell is instrumented with thermocouples at different radial locations, so the temperature distribution within each shell can be determined. Additionally, the outer shells are instrumented with 90° strain gage rosettes placed at the mid-plane. It is assumed that the stresses and the thermal distribution are axi-symmetric. It is not unreasonable to assume that the temperature distribution in our experimental facility is not going to be uniform. Instead, the radial temperature distribution due to the steady conduction is likely to be of the form:

$$\begin{aligned} T(r) &= \frac{T(r_i) - T(r_o)}{\ln(r_i/r_o)} \ln(r/r_o) + T(r_o) \\ &= \frac{T(r_i) - T(r_o)}{\ln(r_i/r_o)} [\ln(r) - \ln(r_o)] + T(r_o) \\ &= \left[\frac{T(r_i) - T(r_o)}{\ln(r_i/r_o)} \right] \ln(r) + \left[T(r_o) - \frac{T(r_i) - T(r_o)}{\ln(r_i/r_o)} \ln(r_o) \right] \\ &= m \ln(r) + b \end{aligned} \tag{D.2}$$

The axial temperature distribution should be uniform, with some possible variation near the ends.

The analysis of the compound cylinder begins with the analysis of a single cylindrical shell. From static equilibrium, the sum of forces upon an infinitesimal element of the cylinder must be zero. Following Popov (1978) and defining u(r) to be the radial displacement of any radial location, the resulting differential equation can be expressed in terms of radial displacements:

$$\frac{d^2u}{dr^2}+\frac{1}{r}\frac{du}{dr}-\frac{u}{r^2}=0 \tag{D.3}$$

The solution of this differential equation is of the form:

$$u(r)=A_1 r+\frac{A_2}{r} \tag{D.4}$$

where constants A_1 and A_2 are determined by the boundary conditions. The radial and tangential strains are defined in terms of u(r):

$$\varepsilon_r \equiv \frac{du}{dr}=A_1-\frac{A_2}{r^2} \tag{D.5}$$

$$\varepsilon_\theta \equiv \frac{u}{r}=A_1+\frac{A_2}{r^2} \tag{D.6}$$

From elastic theory, the deformation of a body is related to the stresses applied to that body. These relations are specialized forms of Hooke's law. In the case of cylindrical shells these relations are, for a body experiencing mechanical stresses alone:

$$\begin{aligned}
\varepsilon_r &= \frac{1}{E}\left(\sigma_r-\nu\sigma_\theta-\nu\sigma_z\right)\\
\varepsilon_\theta &= \frac{1}{E}\left(-\nu\sigma_r+\sigma_\theta-\nu\sigma_z\right)\\
\varepsilon_z &= \frac{1}{E}\left(-\nu\sigma_r-\nu\sigma_\theta+\sigma_z\right)
\end{aligned} \tag{D.7}$$

This last relation is further refined by the type of longitudinal boundary condition. For the case of a cylinder with axially restrained deformation, $\varepsilon_z = 0$. This case is termed plane strain. Similarly, the formulations for the stresses are obtained from elastic theory:

$$\begin{aligned}
\sigma_r &= \frac{E}{(1+\nu)(1-2\nu)}\left[(1-\nu)\varepsilon_r + \nu\varepsilon_\theta + (1-\nu)\varepsilon_z\right] \\
\sigma_\theta &= \frac{E}{(1+\nu)(1-2\nu)}\left[\nu\varepsilon_r + (1-\nu)\varepsilon_\theta + (1-\nu)\varepsilon_z\right] \\
\sigma_z &= \frac{E}{(1+\nu)(1-2\nu)}\left[(1-\nu)\varepsilon_r + (1-\nu)\varepsilon_\theta + \nu\varepsilon_z\right]
\end{aligned} \tag{D.8}$$

Analogously, in the case of plane stress, no stress is exerted upon the cylinder in the axial direction (e.g. as in a thin, annular disk). These two cases give rise to two different solutions to the differential equation expressed in Equation D.3 – however, in either case, the relations for the radial and tangential stresses are in the forms:

Table D.1 – Summary of Constants for Mechanical Problem.

	Plane stress	Plane strain
A_1	$\frac{(1-\nu)}{E}\frac{P_i r_i^2 - P_o r_o^2}{r_o^2 - r_i^2}$	$\frac{(1+\nu)(1-2\nu)}{E}\frac{P_i r_i^2 - P_o r_o^2}{r_o^2 - r_i^2}$
A_2	$\frac{1+\nu}{E}\frac{(P_i - P_o) r_i^2 r_o^2}{r_o^2 - r_i^2}$	$\frac{1+\nu}{E}\frac{(P_i - P_o) r_i^2 r_o^2}{r_o^2 - r_i^2}$
C_1	$\frac{P_i r_i^2 - P_o r_o^2}{r_o^2 - r_i^2}$	$\frac{(1-\nu)}{(1+\nu)(1-2\nu)}\frac{P_i r_i^2 - P_o r_o^2}{r_o^2 - r_i^2}$
C_2	$\frac{(P_i - P_o) r_i^2 r_o^2}{r_o^2 - r_i^2}$	$\frac{1}{(1-2\nu)}\frac{(P_i - P_o) r_i^2 r_o^2}{r_o^2 - r_i^2}\frac{1}{r^2}$
z	$\varepsilon_z = \frac{\nu}{E}(\sigma_r + \sigma_\theta)$ $= \frac{2\nu}{E} C_1$	$\sigma_z = \nu(\sigma_r + \sigma_\theta)$ $= 2\nu C_1$

$$\sigma_r(r) = C_1 - \frac{C_2}{r^2} \tag{D.9}$$

$$\sigma_\theta(r) = C_1 + \frac{C_2}{r^2} \tag{D.10}$$

where C_1 and C_2 are determined through substitution of the displacement function into stress-strain relations with the appropriate boundary conditions. The relations defining the displacement, strain and stress constants in equations D.4, D.5, D.6, D.9, and D.10 are presented in Table D.1, along with relations for the appropriate axial stress or strain.

Let $u_M(r)$ be the radial displacement at any radial location of the cylindrical shell, due to mechanical stresses. If an applied longitudinal stress, σ_L, were to exist, then the radial displacement of any location within the shell is:

$$u_M(r) = A_1 r + \frac{A_2}{r} - \left(\frac{\nu \sigma_L r}{E}\right) \tag{D.11}$$

The plane stress form of this is:

$$u_M(r) = \left(\frac{1-\nu}{E}\right)\left(\frac{r_i^2 P_i - r_o^2 P_o}{r_o^2 - r_i^2}\right) r + \left(\frac{1+\nu}{E}\right)\left(\frac{P_i - P_o}{r_o^2 - r_i^2}\right)\left(\frac{r_i^2 r_o^2}{r}\right) - \left(\frac{\nu \sigma_L r}{E}\right) \tag{D.12}$$

Initial Clearance

Since the cylinders were designed for room-temperature assembly, a clearance exists at the interface. Many analyses of compound cylinder problems assume that the adjacent cylindrical shells are in contact with each other and superpose an initial pre-stress due to an interference fit upon the problem (e.g. Lemczyk and Yovanovich, 1987). However, by stipulating that the interface radii are the same (neglecting the plane separation from the contact conductance analysis), we account for the stress required to bring the surfaces into contact:

$$r_{o,B} + u_B(r_{o,B}) = r_{i,A} + u_A(r_{i,A}) \tag{D.13}$$

If the initial interference fit is given, but not the initial, unassembled interface radii, the assembled radii can be used as in Hsu and Tam (1978) to determine the contact pressure.

Longitudinal Restraint

Consider now two cylindrical shells that initially are placed in load contact with each other and then heated. Consider then steady state conditions and assume that the radial displacements at the interface are the same. However, the longitudinal displacements (along the axis of the shells) need not be the same. Thus, the value of σ_L can be zero if there is no longitudinal restraint, or a significant value if the longitudinal displacements are the same. Since the cylindrical shells are assembled with a clearance fit, we must assume that the actual displacement is somewhere between the no restraint and full restraint conditions, and thus both analyses must be done. Obviously, for the plane strain case, this

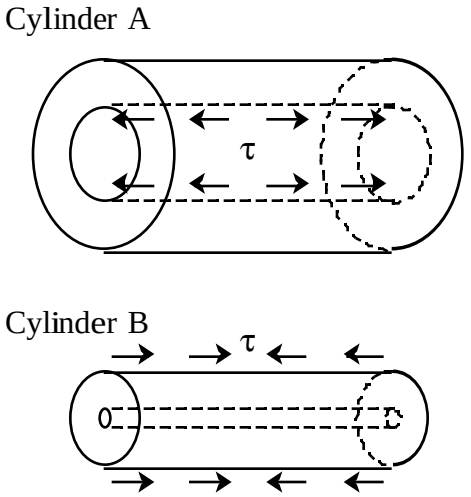

Figure D.1 – Stress states at the interface of cylindrical shells A and B.

analysis is moot.

Consider the loading on the cylindrical shells at the interface (Figure D.1). In addition to the radial stresses, there may be shear stresses exerted between the cylindrical shells. For equilibrium to be maintained, the shear stresses acting at the interfacial surface of each cylindrical shell must sum to zero. Further, the stresses exerted on shell A by shell B must be equal and opposing.

Consider now the free bodies of the cylindrical shells (Figure D.2). At equilibrium, the shear stress, τ, acting over the interfacial surface of each shell must be countered by the longitudinal stress, σ_L, acting within the wall of the cylindrical shell. However, these shear stresses are generally functions of the axial distance, z. It then follows that the longitudinal stress within the shell would also be a function of z. For the equilibrium condition to be satisfied:

$$\sigma_{L,A}\,\pi\left(r_{o,A}^2 - r_{i,A}^2\right) = 2\pi\, r_{i,A} \int_0^{L/2} \tau\, dz \tag{D.14}$$

$$\sigma_{L,B}\,\pi\left(r_{o,B}^2 - r_{i,B}^2\right) = 2\pi\, r_{o,B} \int_0^{L/2} \tau\, dz \tag{D.15}$$

and from equilibrium,

$$\sigma_{L,A}\,\pi\left(r_{o,A}^2 - r_{i,A}^2\right) = \sigma_{L,B}\,\pi\left(r_{o,B}^2 - r_{i,B}^2\right) \tag{D.16}$$

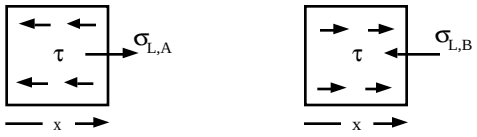

Figure D.2 – Free body diagrams of cylindrical shells A and B.

thus,

$$\sigma_{L,B} = \sigma_{L,A} \frac{\left(r_{o,A}^2 - r_{i,A}^2\right)}{\left(r_{o,B}^2 - r_{i,B}^2\right)} \tag{D.17}$$

For the purposes of this discussion, the variation of τ as a function of z will be assumed to be nearly constant. Thus, the longitudinal stresses within the cylindrical shells can be assumed to be constants. Considering the resulting deformation of cylindrical shells A and B, let L' be the deformed lengths, let w represent the axial displacement of the cylindrical shell, and let Δw represent the change in length due to load. The deformed lengths due to both load and thermal expansion are expressed as

$$\begin{aligned} L'_A &= L + \alpha_A \Delta T_A \left(r_{i,A}\right) L + \Delta w_A = L + \varepsilon_{z,A} L \\ L'_B &= L + \alpha_B \Delta T_B \left(r_{o,B}\right) L + \Delta w_B = L + \varepsilon_{z,B} L \end{aligned} \tag{D.18}$$

The axial strain, ε_z, is given as:

$$\varepsilon_z \equiv \frac{\partial w}{\partial z} \tag{D.19}$$

From elastic theory,

$$\begin{aligned} \varepsilon_{z,A} &= \frac{\sigma_{L,A}}{E_A} - \frac{\nu_A}{E_A}\left(\sigma_{r,A} + \sigma_{\theta,A}\right) + \alpha_A \Delta T_A \left(r_{i,A}\right) \\ \varepsilon_{z,B} &= -\frac{\sigma_{L,B}}{E_B} - \frac{\nu_B}{E_B}\left(\sigma_{r,B} + \sigma_{\theta,B}\right) + \alpha_B \Delta T_B \left(r_{o,B}\right) \end{aligned} \tag{D.20}$$

but, from inspection,

$$\begin{aligned} \sigma_{r,A} + \sigma_{\theta,A} &= \frac{2 r_{i,A}^2 \sigma}{r_{o,A}^2 - r_{i,A}^2} \\ \sigma_{r,B} + \sigma_{\theta,B} &= -\frac{2 r_{o,B}^2 \sigma}{r_{o,B}^2 - r_{i,B}^2} \end{aligned} \tag{D.21}$$

Thus,

$$\varepsilon_{z,A} = \frac{\sigma_{L,A}}{E_A} - \frac{\nu_A}{E_A}\left(\frac{2r_{i,A}^2\sigma}{r_{o,A}^2 - r_{i,A}^2}\right) + \alpha_A \Delta T_A\left(r_{i,A}\right)$$
$$\varepsilon_{z,B} = -\frac{\sigma_{L,B}}{E_B} + \frac{\nu_B}{E_B}\left(\frac{2r_{o,B}^2\sigma}{r_{o,B}^2 - r_{i,B}^2}\right) + \alpha_B \Delta T_B\left(r_{o,B}\right) \qquad \text{(D.22)}$$

Since at the interface $L'_A = L'_B$, $\varepsilon_{x,A} = \varepsilon_{x,B}$, and we can set the two relations in D.22 equal to each other and solve for the longitudinal stresses:

$$\frac{\sigma_{L,A}}{E_A} + \frac{\sigma_{L,B}}{E_B} = 2\sigma\left[\frac{\nu_B}{E_B}\left(\frac{r_{o,B}^2}{r_{o,B}^2 - r_{i,B}^2}\right) + \frac{\nu_A}{E_A}\left(\frac{r_{i,A}^2}{r_{o,A}^2 - r_{i,A}^2}\right)\right] + \left(\alpha_B \Delta T_B\left(r_{o,B}\right) - \alpha_A \Delta T_A\left(r_{i,A}\right)\right) \qquad \text{(D.23)}$$

Substituting Equation D.19 for $\sigma_{L,B}$ and rearranging slightly:

$$\sigma_{L,A}\left[1 + \frac{E_A}{E_B}\frac{\left(r_{o,A}^2 - r_{i,A}^2\right)}{\left(r_{o,B}^2 - r_{i,B}^2\right)}\right] = 2\sigma\left[\frac{E_A}{E_B}\left(\frac{\nu_B r_{o,B}^2}{r_{o,B}^2 - r_{i,B}^2}\right) + \left(\frac{\nu_A r_{i,A}^2}{r_{o,A}^2 - r_{i,A}^2}\right)\right] + \left(\alpha_B \Delta T_B\left(r_{o,B}\right) - \alpha_A \Delta T_A\left(r_{i,A}\right)\right) E_A \qquad \text{(D.24)}$$

Solving for $\sigma_{L,A}$,

$$\sigma_{L,A} = 2\sigma\frac{\left[\left(\frac{\nu_A r_{i,A}^2}{r_{o,A}^2 - r_{i,A}^2}\right) + \frac{E_A}{E_B}\left(\frac{\nu_B r_{o,B}^2}{r_{o,B}^2 - r_{i,B}^2}\right)\right]}{\left[1 + \frac{E_A}{E_B}\frac{\left(r_{o,A}^2 - r_{i,A}^2\right)}{\left(r_{o,B}^2 - r_{i,B}^2\right)}\right]} + \frac{\left(\alpha_B \Delta T_B\left(r_{o,B}\right) - \alpha_A \Delta T_A\left(r_{i,B}\right)\right) E_A}{\left[1 + \frac{E_A}{E_B}\frac{\left(r_{o,A}^2 - r_{i,A}^2\right)}{\left(r_{o,B}^2 - r_{i,B}^2\right)}\right]} \qquad \text{(D.25)}$$

This may in turn be substituted into Equation D.12 (or into Equation D.17 then into Equation D.12, depending on the cylindrical shell) and used to eventually find the interface contact stress.

THERMAL EFFECTS

Timoshenko and Goodier (1951) pose the stress and deformation equations as:

$$u_T(r) = \frac{1+\nu}{1-\nu}\frac{\alpha}{r}\int_{r_i}^{r}\Delta T(r)\,r\,dr \; + D_1 r + \frac{D_2}{r} \tag{D.26}$$

$$\sigma_{r,T}(r) = -\frac{\alpha E}{1-\nu}\frac{1}{r^2}\int_{r_i}^{r}\Delta T(r)\,r\,dr \; + \frac{E}{1+\nu}\left(\frac{D_1}{1-2\nu} - \frac{D_2}{r^2}\right) \tag{D.27}$$

$$\sigma_{\theta,T}(r) = \frac{\alpha E}{1-\nu}\frac{1}{r^2}\int_{r_i}^{r}\Delta T(r)\,r\,dr \; - \frac{\alpha E\,\Delta T(r)}{1-\nu} + \frac{E}{1+\nu}\left(\frac{D_1}{1-2\nu} + \frac{D_2}{r^2}\right) \tag{D.28}$$

$$\sigma_{z,T}(r) = -\frac{\alpha E\,\Delta T(r)}{1-\nu} + \frac{2\nu E D_1}{(1+\nu)(1-2\nu)} \tag{D.29}$$

Taking into account the appropriate boundary conditions for the thermal stress problem (radial stresses are zero on the curved surfaces), we solve for constants D_1 and D_2:

$$\sigma_{r,T}(r_i) = \left(\frac{D_1}{1-2\nu} - \frac{D_2}{r_i^2}\right) = 0 \tag{D.30}$$

$$\sigma_{r,T}(r_o) = -\frac{\alpha E}{1-\nu}\frac{1}{r_o^2}\int_{r_i}^{r}\Delta T(r)\,r\,dr \; + \frac{E}{1+\nu}\left(\frac{D_1}{1-2\nu} - \frac{D_2}{r_o^2}\right) = 0 \tag{D.31}$$

Solving these for useful groupings:

$$\frac{E D_2}{1+\nu} = \frac{\alpha E}{1-\nu}\frac{r_i^2}{r_o^2 - r_i^2}\int_{r_i}^{r}\Delta T(r)\,r\,dr \tag{D.32}$$

$$\frac{E\,D_1}{(1+\nu)(1-2\nu)} = \frac{\alpha E}{1-\nu}\frac{1}{r_o^2 - r_i^2}\int_{r_i}^{r} \Delta T(r)\,r\,dr \qquad (D.33)$$

Substituting these into Equations D.26 – D.29, we obtain the following expressions for the stresses and radial displacement:

$$u_T(r) = \frac{1+\nu}{1-\nu}\frac{\alpha}{r_o^2 - r_i^2}\left[\left((1-2\nu)r + \frac{r_i^2}{r}\right)\int_{r_i}^{r} \Delta T(r)\,r\,dr \; + \frac{r_o^2 - r_i^2}{r}\int_{r_i}^{r} \Delta T(r)\,r\,dr \right] \qquad (D.34)$$

$$\sigma_{r,T}(r) = \frac{\alpha E}{1-\nu}\frac{1}{r^2}\left[\frac{r^2 - r_i^2}{r_o^2 - r_i^2}\int_{r_i}^{r} \Delta T(r)\,r\,dr \; - \int_{r_i}^{r} \Delta T(r)\,r\,dr \right] \qquad (D.35)$$

$$\sigma_{\theta,T}(r) = \frac{\alpha E}{1-\nu}\frac{1}{r^2}\left[\frac{r^2 + r_i^2}{r_o^2 - r_i^2}\int_{r_i}^{r} \Delta T(r)\,r\,dr \; + \int_{r_i}^{r} \Delta T(r)\,r\,dr \; - \Delta T(r)\,r^2 \right] \qquad (D.36)$$

$$\sigma_{z,T}(r) = \frac{\alpha E}{1-\nu}\left[\frac{2}{r_o^2 - r_i^2}\int_{r_i}^{r} \Delta T(r)\,r\,dr \; - \Delta T(r)\right] \qquad (D.37)$$

These, in turn, may be substituted into Equations D.7 to obtain relations for the thermal strains.

INTERFACE STRESSES

There are two approaches to determining the contact pressure available in this study – relying upon the temperature distributions within the cylinders, and using the temperature distributions in conjunction with the strain reported by gages placed on the outer surface of the outer cylinder at the mid-plane.

Case I – Without Longitudinal Restraint

Starting with the thermal displacement equation, (Equation D.34), when evaluated at the inner and outer radii, it is reduced to:

$$u_T(r_i) = \frac{2\alpha r_i}{r_o^2 - r_i^2}(1+\nu)\int_{r_i}^{r_o} \Delta T(r)\, r\, dr$$
$$u_T(r_o) = \frac{2\alpha r_o}{r_o^2 - r_i^2}(1+\nu)\int_{r_i}^{r_o} \Delta T(r)\, r\, dr \tag{D.38}$$

and defining new inner and outer radius values,

$$\hat{r} \equiv r + u_T(r) \tag{D.39}$$

the resulting radii may be substituted into the mechanical displacement equations to solve for the stresses necessary to make the interface radii the same:

$$\hat{r}_{o,B} + u_{M,B}(\hat{r}_{o,B}) = \hat{r}_{i,A} + u_{M,A}(\hat{r}_{i,A}) \tag{D.40}$$

Expanding,

$$\begin{aligned} &\hat{r}_{o,B} + \left(\frac{-r_{o,B}^2}{r_{o,B}^2 - \hat{r}_{i,B}^2}\right)\left[\left(\frac{1-\nu_B}{E_B}\right) r_{o,B} + \left(\frac{1+\nu_B}{E_B}\right)\left(\frac{r_{i,B}^2}{r_{o,B}}\right)\right]\sigma - \left(\frac{\nu_B \sigma_{L,B} r_{o,B}}{E_B}\right) \\ &= \hat{r}_{i,A} + \left(\frac{r_{i,A}^2}{r_{o,A}^2 - r_{i,A}^2}\right)\left[\left(\frac{1-\nu_A}{E_A}\right) r_{i,A} + \left(\frac{1+\nu_A}{E_A}\right)\left(\frac{r_{o,A}^2}{r_{i,A}}\right)\right]\sigma - \left(\frac{\nu_A \sigma_{L,A} r_{i,A}}{E_A}\right) \end{aligned} \tag{D.41}$$

neglecting the longitudinal stress terms and solving for interface stress $\sigma = \sigma_I$:

$$\sigma_I = \frac{\hat{r}_{o,B} - \hat{r}_{i,A}}{\left\{\left(\frac{r_{i,A}^2}{\hat{r}_{o,A}^2 - \hat{r}_{i,A}^2}\right)\left[\left(\frac{1-\nu_A}{E_A}\right) r_{i,A} + \left(\frac{1+\nu_A}{E_A}\right)\left(\frac{r_{o,A}^2}{r_{i,A}}\right)\right]\right\} + \left\{\left(\frac{r_{o,B}^2}{r_{o,B}^2 - r_{i,B}^2}\right)\left[\left(\frac{1-\nu_B}{E_B}\right) r_{o,B} + \left(\frac{1+\nu_B}{E_B}\right)\left(\frac{r_{i,B}^2}{r_{o,B}}\right)\right]\right\}} \tag{D.42}$$

Case II – With Longitudinal Restraint

Returning to Equation D.41 and recall the relations for the longitudinal stresses from the discussion of longitudinal restraint, Equations D.17 and D.25, the relations for the longitudinal stresses may be substituted into Equation D.41 to obtain:

$$
\begin{aligned}
&\hat{r}_{o,B}+\left(\frac{-r_{o,B}^2}{r_{o,B}^2-r_{i,B}^2}\right)\left[\left(\frac{1-\nu_B}{E_B}\right)\hat{r}_{o,B}+\left(\frac{1+\nu_B}{E_B}\right)\left(\frac{r_{i,B}^2}{r_{o,B}}\right)\right]\sigma \\
&\quad-\left(\frac{\nu_B r_{o,B}}{E_B}\right)\frac{\left(r_{o,A}^2-r_{i,A}^2\right)}{\left(r_{o,B}^2-r_{i,B}^2\right)}\left[2\frac{\left[\left(\frac{\nu_A r_{i,A}^2}{r_{o,A}^2-r_{i,A}^2}\right)+\frac{E_A}{E_B}\left(\frac{\nu_B r_{o,B}^2}{r_{o,B}^2-r_{i,B}^2}\right)\right]}{\left[1+\frac{E_A}{E_B}\frac{\left(r_{o,A}^2-r_{i,A}^2\right)}{\left(r_{o,B}^2-r_{i,B}^2\right)}\right]}\right]\sigma \\
&\quad-\left(\frac{\nu_B r_{o,B}}{E_B}\right)\frac{\left(r_{o,A}^2-r_{i,A}^2\right)}{\left(r_{o,B}^2-r_{i,B}^2\right)}\frac{\left(\alpha_B\Delta T_B\left(r_{o,B}\right)-\alpha_A\Delta T_A\left(r_{i,B}\right)\right)E_A}{\left[1+\frac{E_A}{E_B}\frac{\left(r_{o,A}^2-r_{i,A}^2\right)}{\left(r_{o,B}^2-r_{i,B}^2\right)}\right]} \\
&\qquad=r_{i,A}+\left(\frac{r_{i,A}^2}{r_{o,A}^2-\hat{r}_{i,A}^2}\right)\left[\left(\frac{1-\nu_A}{E_A}\right)r_{i,A}+\left(\frac{1+\nu_A}{E_A}\right)\left(\frac{r_{o,A}^2}{r_{iA}}\right)\right]\sigma \\
&\quad-\left[2\left(\frac{\nu_A r_{i,A}}{E_A}\right)\frac{\left[\left(\frac{\nu_A r_{i,A}^2}{r_{o,A}^2-r_{i,A}^2}\right)+\frac{E_A}{E_B}\left(\frac{\nu_B r_{o,B}^2}{r_{o,B}^2-r_{i,B}^2}\right)\right]}{\left[1+\frac{E_A}{E_B}\frac{\left(r_{o,A}^2-r_{i,A}^2\right)}{\left(r_{o,B}^2-r_{i,B}^2\right)}\right]}\right]\sigma \\
&\quad-\left(\frac{\nu_A r_{i,A}}{E_A}\right)\frac{\left(\alpha_B\Delta T_B\left(r_{o,B}\right)-\alpha_A\Delta T_A\left(r_{i,B}\right)\right)E_A}{\left[1+\frac{E_A}{E_B}\frac{\left(r_{o,A}^2-r_{i,A}^2\right)}{\left(r_{o,B}^2-r_{i,B}^2\right)}\right]}
\end{aligned}
\tag{D.43}
$$

Defining a thermal expansion term (due to the longitudinal stress term):

$$
\Phi_L\equiv\left[\left(\frac{\nu_A r_{i,A}}{E_A}\right)-\left(\frac{\nu_B r_{o,B}}{E_B}\right)\frac{\left(r_{o,A}^2-r_{i,A}^2\right)}{\left(r_{o,B}^2-r_{i,B}^2\right)}\right]\frac{\left(\alpha_B\Delta T_B\left(r_{o,B}\right)-\alpha_A\Delta T_A\left(r_{i,B}\right)\right)E_A}{\left[1+\frac{E_A}{E_B}\frac{\left(r_{o,A}^2-r_{i,A}^2\right)}{\left(r_{o,B}^2-r_{i,B}^2\right)}\right]}
\tag{D.44}
$$

and solving for interface stress $\sigma = \sigma_{II}$:

$$\sigma_{II} = \frac{\hat{r}_{o,B} - \hat{r}_{i,A} + \Phi_L}{\left\{\begin{array}{l} \left(\frac{r_{i,A}^2}{r_{o,A}^2 - r_{i,A}^2}\right)\left[\left(\frac{1-\nu_A}{E_A}\right)r_{i,A} + \left(\frac{1+\nu_A}{E_A}\right)\left(\frac{r_{o,A}^2}{r_{i,A}}\right)\right] \\ + \left(\frac{r_{o,B}^2}{r_{o,B}^2 - r_{i,B}^2}\right)\left[\left(\frac{1-\nu_B}{E_B}\right)r_{o,B} + \left(\frac{1+\nu_B}{E_B}\right)\left(\frac{r_{i,B}^2}{r_{o,B}}\right)\right] \\ - \left[2\left(\frac{\nu_A r_{i,A}}{E_A}\right) - \frac{\left[\left(\frac{\nu_A r_{i,A}^2}{r_{o,A}^2 - r_{i,A}^2}\right) + \frac{E_A}{E_B}\left(\frac{\nu_B r_{o,B}^2}{r_{o,B}^2 - r_{i,B}^2}\right)\right]}{\left[1 + \frac{E_A}{E_B}\frac{\left(r_{o,A}^2 - r_{i,A}^2\right)}{\left(r_{o,B}^2 - r_{i,B}^2\right)}\right]}\right] \\ + \left(\frac{\nu_B r_{o,B}}{E_B}\right)\frac{\left(r_{o,A}^2 - r_{i,A}^2\right)}{\left(r_{o,B}^2 - r_{i,B}^2\right)}\left[2\frac{\left[\left(\frac{\nu_A r_{i,A}^2}{r_{o,A}^2 - r_{i,A}^2}\right) + \frac{E_A}{E_B}\left(\frac{\nu_B r_{o,B}^2}{r_{o,B}^2 - r_{i,B}^2}\right)\right]}{\left[1 + \frac{E_A}{E_B}\frac{\left(r_{o,A}^2 - r_{i,A}^2\right)}{\left(r_{o,B}^2 - r_{i,B}^2\right)}\right]}\right] \end{array}\right\}} \quad \text{(D.45)}$$

Case III – Strain Gage Formulation

Since we assume that the displacement of the outer radius is due to the temperature distribution and the effect of the expansion of the inner cylinder:

$$\varepsilon_\theta = \frac{\Delta\theta}{\theta} = \frac{\Delta r_{o,A}\, 2\pi}{r_{o,A}\, 2\pi} = \frac{u(r_{o,A})}{r_{o,A}} = \frac{u_T(r_{o,A})}{r_{o,A}} + \frac{u_M(r_{o,A})}{r_{o,A}} \quad \text{(D.46)}$$

Solving for the mechanical displacement, the relation can be subsequently solved for the interface pressure. The reported expansion less that accounted for by thermal expansion is:

$$\frac{\Delta\theta}{\theta} r_{o,A} - u_T(r_{o,A}) = u_M(r_{o,A}) \quad \text{(D.47)}$$

Recall that

$$u_M(r) = \left(\frac{1-\nu}{E}\right)\left(\frac{r_i^2 P_i - r_o^2 P_o}{r_o^2 - r_i^2}\right) r + \left(\frac{1+\nu}{E}\right)\left(\frac{P_i - P_o}{r_o^2 - r_i^2}\right)\left(\frac{r_i^2 r_o^2}{r}\right) - \left(\frac{\nu \sigma_L r}{E}\right) \tag{D.12}$$

Thus, neglecting longitudinal stresses:

$$\frac{\Delta\theta}{\theta} r_{o,A}^{\circ} + r_{o,A} - \hat{r}_{o,A} = \sigma\left[\left(\frac{1-\nu_A}{E_A}\right) r_{o,A} + \left(\frac{1+\nu_A}{E_A}\right)\left(\frac{r_{i,A}^2}{r_{o,A}}\right)\right]\left(\frac{r_{o,A}^2}{r_{o,A}^2 - r_{i,A}^2}\right) \tag{D.48}$$

Solving for $\sigma = \sigma_{III}$

$$\sigma_{III} = \frac{\frac{\Delta\theta}{\theta} r_{o,A}^{\circ} + r_{o,A} - \hat{r}_{o,A}}{\left[\left(\frac{1-\nu_A}{E_A}\right) r_{o,A} + \left(\frac{1+\nu_A}{E_A}\right)\left(\frac{r_{i,A}^2}{r_{o,A}}\right)\right]\left(\frac{r_{o,A}^2}{r_{o,A}^2 - r_{i,A}^2}\right)} \tag{D.49}$$

APPENDIX E

SAMPLE CALCULATIONS AND ANALYSIS OF UNCERTAINTY

The experimental data used in this appendix are taken from the aluminum 6061-stainless steel 304 compound cylinder dataset, at the 750 W experiment. The uncertainty analysis takes advantage of the work of Kline and McKlintock (1953). Given some function, f, of n variables, the uncertainty of the function for a set of parameters is:

$$KM(f) \equiv U_f = \left[\sum_{i=1}^{n} \left(\frac{\partial f}{\partial x_i} U_{x_i} \right)^2 \right]^{\frac{1}{2}} \tag{E.1}$$

The uncertainties calculated in this appendix are valid for this data point only, but are representative of the uncertainties for all data in the study, which (in extreme cases) may take values between one half and two and a half times the values calculated here. A table of the calculated values and relevant uncertainties for the data of this experiment can be found at the end of this appendix.

GEOMETRIC DATA

Cylindrical Shell Geometry

Table E.1 details the length, inner radius, outer radius of the AL-6061 and SS-304 cylindrical shells that form the composite cylinder used to acquirmahe the experimental data used in this sample calculation. These radii were obtained through measurements taken in the laboratory, and measurements taken at the Providence, RI facility of Mahr-Federal, Inc.. From these radii are determined the nominal interface radius:

$$r_i = \frac{r_{i,A} + r_{o,B}}{2} \tag{E.2}$$

and nominal interface area:

$$A_i = 2\pi L r_i \tag{E.3}$$

Defining an average error of the interface radii:

$$U_r = \left[U_{r_{i,A}}^2 + U_{r_{o,B}}^2\right]^{\frac{1}{2}} \tag{E.4}$$

The uncertainties of the nominal radius and nominal area are

$$U_{r_i} = \left[\left(\frac{U_r}{2}\right)^2 + \left(\frac{U_r}{2}\right)^2\right]^{\frac{1}{2}} \tag{E.5}$$

and

$$U_{A_i} = \left[\left(2\pi L U_r\right)^2 + \left(2\pi r U_L\right)^2\right]^{\frac{1}{2}} \tag{E.6}$$

Cylindrical Waviness

Linear surface parameters are supplied by the SurfAnalyzer and by Mahr-Federal after characterization of the cylindrical shells. Circumferential waviness parameters are not.

Table E.1 – Relevant Cylindrical Shell Dimensions

Cylinder	Length (m)	Inner Radius (m)	Outer Radius (m)
B AL-6061	0.1270 ± 0.00127	0.00635 ± 7.6E-4	0.0253824 ± 3.4E-05
A SS-304	0.1270 ± 0.00127	0.0253958 ± 6.4284E-06	0.049399 ± 6.35E-5

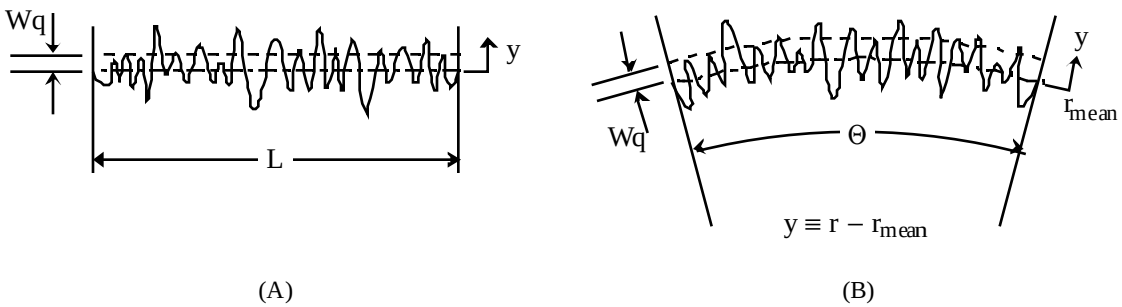

Figure E.1 – Waviness for (A) a nominally flat surface, and (B) a curved surface.

However, partially processed sensor output was included with the roundness and cylindricity data. The sensor output consisted of 4096 data points taken at each of the four locations of the cylindrical scans. Waviness for the cylindrical surface is calculated in the same manner as for a flat surface. For a flat surface, assuming a uniform sample density:

$$Wq = \left[\frac{1}{L}\int_0^L \left|y^2\right| dx\right]^{\frac{1}{2}} \approx \left[\frac{1}{n}\sum_{i=1}^{n} y_i^2\right]^{\frac{1}{2}} \tag{E.7}$$

Similarly for a cylindrical surface:

$$Wq_\theta = \left[\frac{1}{\Theta}\int_0^\Theta \left|y^2\right| d\theta\right]^{\frac{1}{2}} \approx \left[\frac{1}{n}\sum_{i=1}^{n} y_i^2\right]^{\frac{1}{2}} \tag{E.8}$$

Radius of Curvature

If the isotropic surface waviness (or roughness) is assumed to take the shape of a sinusoidal waveform:

$$S(x) = A\sin(Bx) \tag{E.9}$$

and taking advantage of the natural symmetry of the trigonometric functions, the average slope is calculated as

$$m = \left|\tan(\theta)\right| = \frac{2}{\pi B}\int_{0}^{\frac{\pi}{2B}} \left|AB\cos(Bx)\right| dx \tag{E.10}$$

After some manipulation,

$$\left|\tan(\theta)\right| = \frac{2AB}{\pi} \tag{E.11}$$

a relation between the reported amplitude, reported waviness slope, and radius of curvature at the tip can be constructed. Recall that the radius of curvature for a plane curve in Cartesian coordinates is:

$$\rho(x) = \frac{\left[1 + S_x(x)^2\right]^{\frac{3}{2}}}{\left|S_{xx}(x)\right|} \tag{E.12}$$

or

$$\rho(x) = \frac{\left[1 + \left(AB\cos(Bx)\right)^2\right]^{\frac{3}{2}}}{\left|AB^2\sin(Bx)\right|} = \frac{4A}{\left(\pi\left|\tan(\theta)\right|\right)^2} \tag{E.13}$$

Note that both A and $\left|\tan(\theta)\right|$ are parameters obtained through the surface metrology, where A is either the roughness (σ_{RMS}) or the waviness (W_{RMS})of the surface.

EXPERIMENTAL DATA

Measurement Uncertainty

Characterization of the thermocouple wire consisted of comparing the indicated temperatures of eight thermocouple junctions with that of a NIST-traceable mercury thermometer. The thermocouples were installed in a single copper block, which was submerged in a constant-temperature circulating bath along with the thermometer. The

bath temperature was varied between 260 K and 560 K, and temperature readings were taken at least two hours after the bat temperature was changed. Thermocouple readings were obtained through a FieldPoint program, which was written to take 300 samples at a rate of four per second. The thermometer was read three times. Average readings were compared. The thermocouple uncertainty was calculated at each of the five temperatures as

$$U_{T/C} = \left\{ \sum_{j=1}^{8} \left(\frac{U_{\bar{T}_j}}{8} \right)^2 + \left(T_{average} - T_{NIST} \right)^2 \right\}^{\frac{1}{2}} \tag{E.14}$$

which is the sum of the square of the average thermocouple channel measurement uncertainty and the square of the difference between the average thermocouple temperature and the NIST-traceable thermometer temperature.

Temperature Data

The recorded thermocouple readings within the AL-6061/SS-304 composite cylinder at steady state for the 750 W heater setting are tabulated in Table E.2. Similarly, The recorded thermocouple readings within the AL-6061/SS-304 composite cylinder at steady state for the 300 W heater setting are tabulated in Table E.3. The listed temperature uncertainties are those obtained through multiple polling of the thermocouples.

Temperature uncertainties used in these calculations are a combination of the systemic uncertainty of ± 0.003 K (due to the resolution of the FieldPoint temperature module), the thermocouple uncertainty of ± 0.3 K (obtained through comparison of a readings of a NIST traceable thermometer with multiple measurements of samples immersed in a constant temperature bath), and the measurement uncertainty obtained through multiple polling of the thermocouples.

$$U_T = \left[U_{system}^2 + U_{T/C}^2 + U_M^2 \right]^{\frac{1}{2}} \tag{E.15}$$

Table E.2 – Location-Temperature Data Acquired in the AL-6061/SS-304 Composite Cylinder at a Nominal Heater Power of 750 W

	r, m	T, K	U_T, K
Cylinder B	0.01016	377.198	0.0403
	0.01397	376.829	0.0529
	0.01778	376.652	0.0470
	0.02159	376.223	0.0380
Cylinder A	0.03048	326.046	0.0480
	0.03556	313.210	0.0370
	0.04064	306.153	0.0442
	0.04572	300.312	0.0534

Temperature Distribution

Under steady, one-dimensional conduction conditions (without internal generation), the temperature distribution within a cylindrical shell is a function of radial location only. Knowing the inner and outer temperatures and radii, this relation is expressed as:

$$T(r) = T_{out} + \frac{T_{in} - T_{out}}{\ln(r_{in}/r_{out})}\left[\ln\left(\frac{r}{r_{out}}\right)\right] = \left[\frac{T_{in} - T_{out}}{\ln(r_{in}/r_{out})}\right]\ln(r) + \left[T_{out} - \frac{T_{in} - T_{out}}{\ln(r_{in}/r_{out})}\ln(r_{out})\right] \quad \text{(E.16)}$$
$$= m\ln(r) + b$$

Table E.3 – Location-Temperature Data Acquired in the AL-6061/SS-304 Composite Cylinder at a Nominal Heater Power of 300 W

	r, m	T, K	U_T, K
Cylinder B	0.01016	349.010	0.0276
	0.01397	348.886	0.0313
	0.01778	348.896	0.0240
	0.02159	348.935	0.0225
Cylinder A	0.03048	305.552	0.0196
	0.03556	298.895	0.0135
	0.04064	295.370	0.0128
	0.04572	292.194	0.0116

By changing the independent variable from the radial location to the natural log of the radial location, this relation is reduced to a linear form. The standard error of the correlation of the correlation is the expected error of the predicted value, and is calculated as:

$$SE_T = \left[\frac{\sum_{i=1}^{n} T(r_i) - (m \ln(r_i) + b)}{n-2} \right] \tag{E.17}$$

The uncertainty of the mean interface temperature is:

$$\begin{aligned} T_i &= \frac{T_{i,A} + T_{o,B}}{2} \\ U_{T_i} &= \left[\left(\frac{SE_{TA}}{2} \right)^2 + \left(\frac{SE_{TB}}{2} \right)^2 \right]^{\frac{1}{2}} \end{aligned} \tag{E.18}$$

and interface temperature discontinuity are found to be:

$$\begin{aligned} \Delta T_i &= T_{o,B} - T_{i,A} \\ U_{\Delta T_i} &= \left[SE_{TA}^2 + SE_{TB}^2 \right]^{\frac{1}{2}} \end{aligned} \tag{E.19}$$

The uncertainty in the least-squares slope is determined by solving Equation E.16 for the slope and using the resulting relation to find the uncertainty:

$$U_m = \left[\frac{2}{\ln\left(\frac{r_i}{r_o}\right)^2} SE_T^2 + \frac{(T_i - T_o)^2}{\ln\left(\frac{r_i}{r_o}\right)^4} \left(\frac{1}{r_i^2} + \frac{1}{r_o^2} \right) U_r^2 \right]^{\frac{1}{2}} \tag{E.20}$$

A least squares technique is used to determine the parameters m and b for the best-fit line through the data. The uncertainty of the parameter, b, is taken to be the standard error.

Average Shell Temperature

Since the temperature distribution within the shells is likely to be non-linear with respect to r, the appropriate average temperature for each shell must be the integral-averaged temperature:

$$\overline{T} = \frac{1}{r_o^2 - r_i^2} \int_{r_i}^{r_o} (m\ln(\rho) + b)\rho \, d\rho \tag{E.21}$$

This is the average shell temperature that will be used to determine the value of temperature-dependent thermophysical properties. The uncertainty for this average temperature may be obtained by symbolically evaluating the expression for the average temperature and then applying the KM operator:

$$U_{\overline{T}} = \left\{ \begin{array}{l} \left[\frac{r_o^2}{\left(r_o^2 - r_i^2\right)} SE_T \right]^2 + \left[\frac{\left(T_o^2 - T_i^2\right)}{\left(r_i^2 - r_o^2\right)} \frac{U_m}{2} \right]^2 + \left[2 r_o r_i^2 \frac{\left(T_o^2 - T_i^2\right)}{\left(r_o^2 - r_i^2\right)^2} U_r \right]^2 \\ + \left[\frac{r_i^2}{\left(r_o^2 - r_i^2\right)} SE_T \right]^2 + \left[2 r_i r_o^2 \frac{\left(T_o^2 - T_i^2\right)}{\left(r_i^2 - r_o^2\right)^2} U_r \right]^2 \end{array} \right\} \tag{E.22}$$

THERMOPHYSICAL PROPERTIES

Although the room temperature thermophysical properties of the materials used in the present study interest are tabulated in Table 3.1, the conductivity and coefficient of thermal expansion have a significant dependence on temperature. Fifth order polynomial expressions have been obtained for the conductivity and coefficient of thermal expansion. One common practice (adopted here) has been to assume that handbook values and derived polynomial expressions for thermophysical values have a fixed uncertainty on the order of (and probably less than) five percent, unless otherwise specified. The inclusion of the

temperature uncertainty negligibly affects the value of the uncertainty of the fifth order polynomial expression for the thermophysical properties. For an arbitrary property Ψ:

$$\Psi(T) = \sum_{i=0}^{5} a_i T^i$$
$$U_\Psi = \left\{ \left[\left(\sum_{i=0}^{5} i\, a_i T^{i-1} \right) U_{\bar{T}} \right]^2 + \left[\left(\sum_{i=0}^{5} a_i T^i \right) 0.05 \right]^2 \right\}^{\frac{1}{2}} \tag{E.23}$$

Taking, for example, the thermal conductivity of the aluminum inner shell, the increase in the percentage uncertainty is 0.003%, and is negligible.

Interface Heat Flux

From conduction theory, the expressions for the heat rate and heat flux through a cylindrical shell at the nominal interface radius is

$$q_i = -2\pi L\, k m$$
$$q_i'' = -\frac{k}{r_i} m \tag{E.24}$$

The corresponding uncertainty relation for the interface heat flux is:

$$U_{q_i''} = \left\{ \left[\frac{k}{r_i} U_m \right]^2 + \left[\frac{m}{r_i} (0.05k) \right]^2 + \left[\frac{km}{r_i^2} U_{r_i} \right]^2 \right\}^{\frac{1}{2}} \tag{E.25}$$

The histogram in Figure E.2 illustrates the distribution of the uncertainty in the value of the interface heat flux on a percentage basis.

The Effect of Temperature Drift on the Heat Flux Calculation

If the interface heat flux is divided by thermal conductivity (appropriate to the other parameters used to determine the interface heat flux), the resulting expression has the units of temperature. The uncertainty of the heat flux-conductivity ratio is expressed as:

$$U_{\frac{q_i''}{k}} = \left\{ \left[\frac{U_m}{r_i} \right]^2 + \left[\frac{m}{r_i^2} U_{r_i} \right]^2 \right\}^{\frac{1}{2}} \tag{E.26}$$

expanding the uncertainty for the least squares slope, and using the formulation for the outer cylinder:

$$U_{\frac{q_i''}{k}} = \left\{ \frac{2}{\ln\left(\frac{r_i}{r_o}\right)^2} \frac{SE_T^2}{r_i^2} + \frac{(T_i - T_o)^2}{\ln\left(\frac{r_i}{r_o}\right)^4} \left(\frac{1}{r_i^2} + \frac{1}{r_o^2} \right) \frac{U_r^2}{r_i^2} + \frac{m^2}{r_i^4} U_{r_i}^2 \right\}^{\frac{1}{2}} \tag{E.27}$$

Taking the uncertainty of the temperature to be equal to the allowed temperature drift and holding all else constant, a relation between the temperature drift tolerance and the uncertainty in the calculated heat flux can be obtained. Figure E.3 relates the change in the calculated heat flux to the heat flux-thermal conductivity ratio as a function of the temperature drift tolerance.

Thermal Contact Conductance

The thermal contact conductance is the ratio of the heat flux to the temperature discontinuity at the interface:

$$h_c = \frac{q_i''}{\Delta T_i} \tag{E.28}$$

$$U_{h_c} = \left[\left(\frac{U_{q_i''}}{\Delta T_i} \right)^2 + \left(\frac{q_i''}{\Delta T_i^2} U_{\Delta T} \right)^2 \right]^{\frac{1}{2}} \tag{E.29}$$

Figure E.4 illustrates the distribution of the percent uncertainty in the thermal contact conductance calculation.

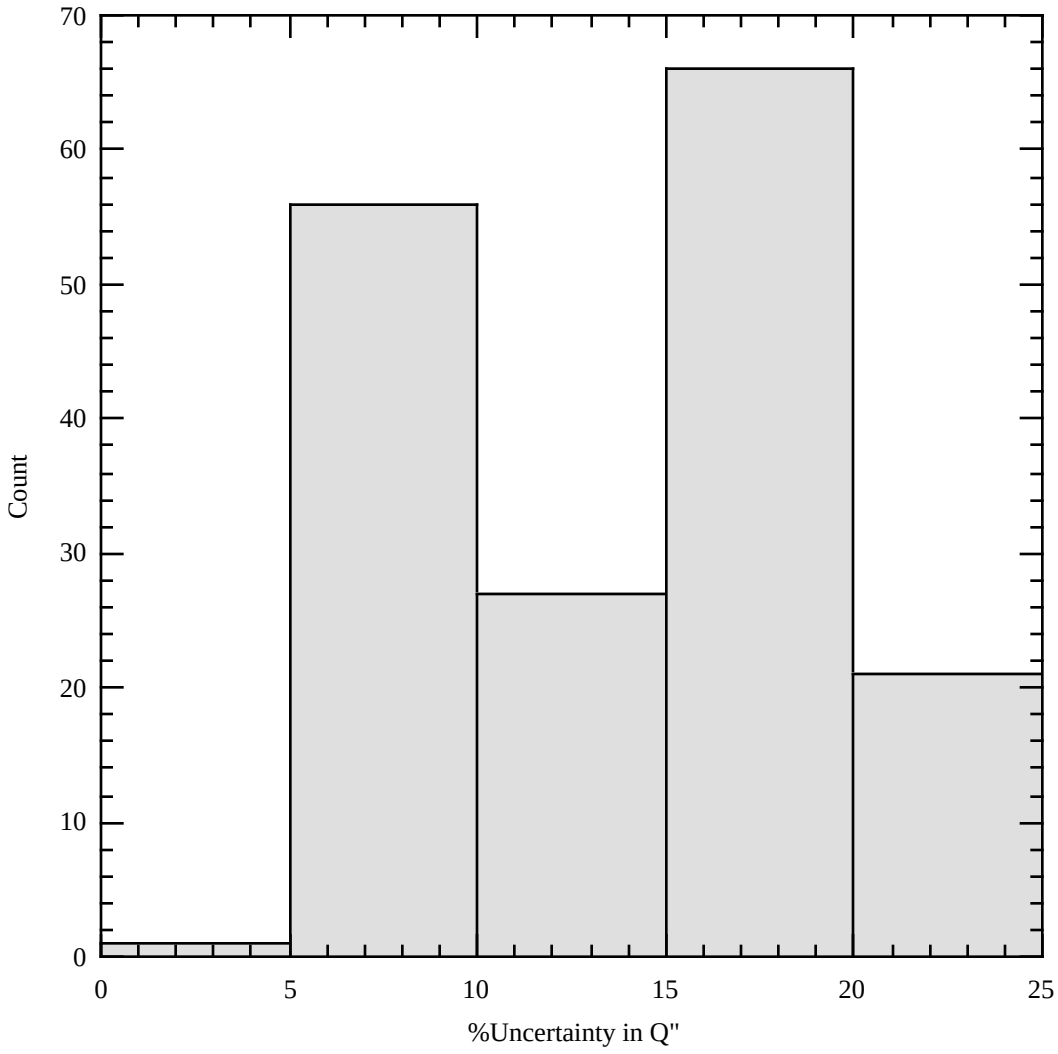

Figure E.2 – Histogram of the percentage uncertainty in the value of the interface heat flux for the 170 data points used in this study.

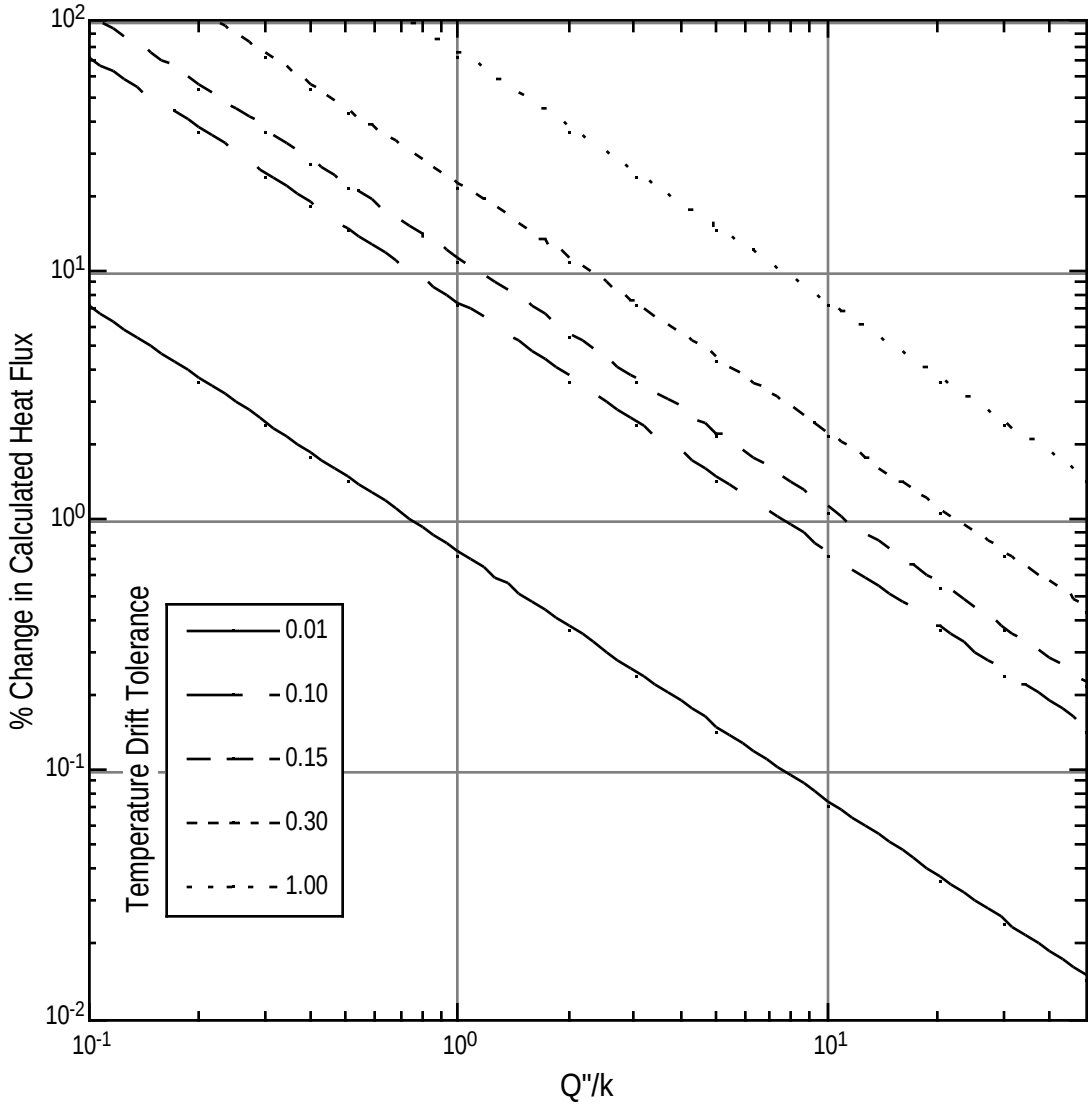

Figure E.3 — The effect of temperature drift tolerance on heat flux uncertainty.

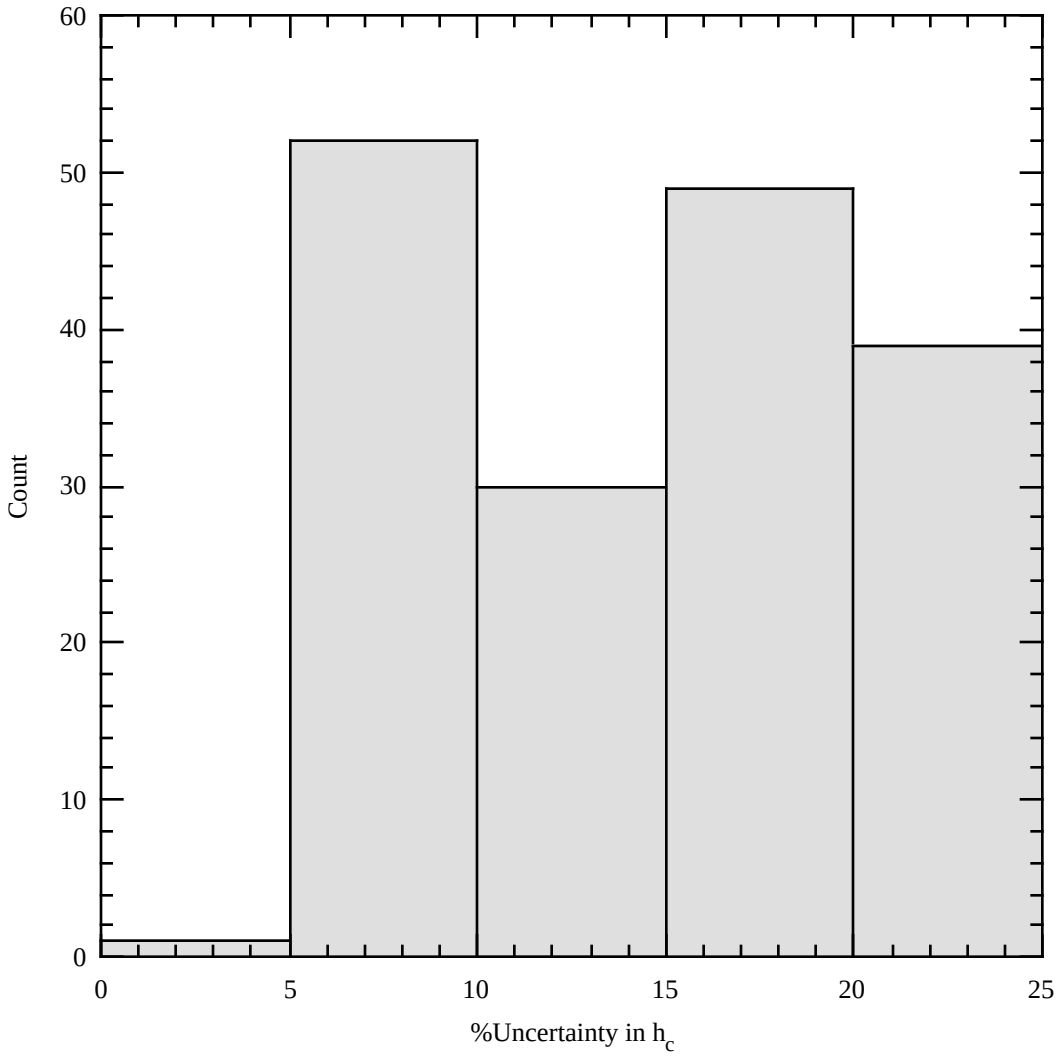

Figure E.4 – Histogram of the percentage uncertainty in the value of the thermal contact conductance for the 170 data points used in this study.

Radiation View Factor and Heat Loss

If the radiation shield and exposed end surfaces of the cylindrical shells are approximated as parallel annular rings, the radiation view factor (and subsequently the radiation heat loss from the ends) may be determined. Following the method of Example 6-8 in Siegel and Howell (1992), the view factor from shells A and B to the radiation shield is at least:

$$\begin{aligned} F_{A\to S} &\geq 0.7090 \\ F_{B\to S} &\geq 0.7303 \end{aligned} \tag{E.30}$$

The radiation heat transfer from the inner shell is expressed as

$$\begin{aligned} q_{rad} &= q_{rad,\,A} + q_{rad\,B} \\ &= 2\left[\begin{array}{l} \varepsilon_A A_A \sigma\left[1-\dfrac{(1-\varepsilon_S)A_A F_{A\to S}^2}{A_S}\right]\left(T_A^4 - T_\infty^4\right) \\ +\varepsilon_B A_B \sigma\left[1-\dfrac{(1-\varepsilon_S)A_B F_{B\to S}^2}{A_S}\right]\left(T_B^4 - T_\infty^4\right) \end{array}\right] \end{aligned} \tag{E.31}$$

The uncertainty of the radiation heat loss calculation is

$$\frac{U_{q_{rad}}}{q_{rad}} = 2\left\{\begin{aligned}&\left[\frac{U_{\varepsilon_A}}{\varepsilon_A}\right]^2+\left[\left(\frac{A_S-2A_AF_{A\to S}^2(1+\varepsilon_S)}{A_S-A_AF_{A\to S}^2(1+\varepsilon_S)}\right)\frac{U_{A_A}}{A_A}\right]^2\\&+\left[\frac{A_AF_{A\to S}^2}{A_S-A_AF_{A\to S}^2(1+\varepsilon_S)}U_{\varepsilon_S}\right]^2+\left[\frac{-2A_A(1-\varepsilon_S)F_{A\to S}}{A_S-A_AF_{A\to S}^2(1+\varepsilon_S)}U_{F_{A\to S}}\right]^2\\&+\left[\frac{A_A(1-\varepsilon_S)F_{A\to S}^2}{A_S\left(A_S-A_AF_{A\to S}^2(1+\varepsilon_S)\right)}U_{A_S}\right]^2+\left[\frac{4T_A^3}{T_A^4-T_\infty^4}SE_{TA}\right]^2\\&+\left[\frac{4T_\infty^3}{T_A^4-T_\infty^4}U_{T_\infty}\right]^2+\left[\frac{U_{\varepsilon_B}}{\varepsilon_B}\right]^2+\left[\left(\frac{A_S-2A_BF_{B\to S}^2(1+\varepsilon_S)}{A_S-A_BF_{B\to S}^2(1+\varepsilon_S)}\right)\frac{U_{A_B}}{A_B}\right]^2\\&+\left[\frac{A_BF_{A\to S}^2}{A_S-A_BF_{B\to S}^2(1+\varepsilon_S)}U_{\varepsilon_S}\right]^2+\left[\frac{-2A_B(1-\varepsilon_S)F_{B\to S}}{A_S-A_BF_{B\to S}^2(1+\varepsilon_S)}U_{F_{B\to S}}\right]^2\\&+\left[\frac{A_B(1-\varepsilon_S)F_{B\to S}^2}{A_S\left(A_S-A_BF_{B\to S}^2(1+\varepsilon_S)\right)}U_{A_S}\right]^2+\left[\frac{4T_B^3}{T_B^4-T_\infty^4}SE_{TB}\right]^2\\&+\left[\frac{4T_\infty^3}{T_B^4-T_\infty^4}U_{T_\infty}\right]^2\end{aligned}\right\}^{\frac{1}{2}} \qquad \text{(E.32)}$$

Strain

Taking the initial test results, with heater power set to zero, as the unstrained condition, and all subsequent ones as strained, we can determine the change in strain for each set of test parameters. The partially corrected strain reported by the gage is expressed as:

$$\hat{\varepsilon} = \frac{\left\{\left[\frac{-4V_r}{K'(1+2V_r)}\right]-\left[\frac{2}{K_g}\sum_{i=0}^{n}a_iT^i+(\alpha_B-\alpha_A)(T-T_s)\right]\right\}\left[1+\frac{2R_{lw}}{R_g'}\right]}{\left[1+\frac{\Delta GF(T)\%}{100}\right]} \qquad \text{(E.33)}$$

However, we must further correct the strain for transverse sensitivity:

$$\varepsilon_i = \frac{1-\nu_0 K_t}{1-K_t^2}\left(\varepsilon_i^{'} - K_t \varepsilon_j^{'}\right) \tag{E.34}$$

The results reported from the 90° strain gage rosettes can then be used to determine the interface stress. Strain and related uncertainties in the longitudinal and circumferential directions are calculated and corrected according to methods recommended by Omega Engineering, Inc. (1995) and Measurements Group, Inc. (1999b). Embedded within the uncertainty calculation are uncertainties in measured output voltage and gage thermal output.

INTERFACE PRESSURE

Thermal Expansion

From Equation D.38, the thermal displacement of the inner radius of shell A is

$$u_T(r_{i,A}) = \frac{2\alpha r_{i,A}}{r_{o,A}^2 - r_{i,A}^2}(1+\nu)\int_{r_{i,A}}^{r_{o,A}} \Delta T(r)\, r\, dr \tag{E.35}$$

Similarly, the thermal displacement of the outer radius of Shell B is

$$u_T(r_{o,B}) = \frac{2\alpha r_{o,B}}{r_{o,B}^2 - r_{i,B}^2}(1+\nu)\int_{r_{i,B}}^{r_{o,B}} \Delta T(r)\, r\, dr \tag{E.36}$$

Since these displacements are approximately four orders of magnitude less than the undisplaced radii, the uncertainties of the displaced radii are assumed to be those of the undisplaced radii.

Case I

The mechanical restraint due to the contacting cylinders are imposed on the displaced radii. For the interface radii to be the same, the interface stresses must be as well. From Appendix D (Equation D.42):

$$\sigma_I = \frac{\hat{r}_{o,B} - \hat{r}_{i,A}}{\left\{\left(\frac{r_{i,A}^2}{\hat{r}_{o,A}^2 - \hat{r}_{i,A}^2}\right)\left[\left(\frac{1-\nu_A}{E_A}\right)r_{i,A} + \left(\frac{1+\nu_A}{E_A}\right)\left(\frac{r_{o,A}^2}{r_{i,A}}\right)\right]\right\} + \left\{\left(\frac{r_{o,B}^2}{r_{o,B}^2 - r_{i,B}^2}\right)\left[\left(\frac{1-\nu_B}{E_B}\right)r_{o,B} + \left(\frac{1+\nu_B}{E_B}\right)\left(\frac{r_{i,B}^2}{r_{o,B}}\right)\right]\right\}} \tag{E.37}$$

To facilitate an uncertainty analysis, this relation is broken into pieces:

$$\sigma_I = \frac{AA}{DI}$$
$$DI \equiv BB\ CC + DD\ EE \tag{E.38}$$

$$AA = \hat{r}_{o,B} - \hat{r}_{i,A}$$
$$U_{AA} = \sqrt{2}U_r \tag{E.39}$$

$$BB = \frac{r_{i,A}^2}{r_{o,A}^2 - r_{i,A}^2}$$

$$U_{BB} = \left\{\left[\frac{2r_{i,A}^2 r_{o,A}}{\left(r_{o,A}^2 - r_{i,A}^2\right)^2}U_r\right]^2 + \left[\frac{2r_{i,A}^3}{\left(r_{o,A}^2 - r_{i,A}^2\right)^2}U_r\right]^2 + \left[\frac{2r_{i,A}}{\left(r_{o,A}^2 - r_{i,A}^2\right)}U_r\right]^2\right\}^{\frac{1}{2}} \tag{E.40}$$

$$CC = \left(\frac{1-\nu_A}{E_A}\right)r_{i,A} + \left(\frac{1+\nu_A}{E_A}\right)\left(\frac{r_{o,A}^2}{r_{i,A}}\right)$$

$$U_{CC} = \left\{\begin{array}{l}\left[\left(\frac{-r_{i,A}}{E_A}\right) + \left(\frac{1}{E_A}\right)\left(\frac{r_{o,A}^2}{r_{i,A}}\right)\right]^2 U_{\nu_A}^2 + \left[-\frac{(1-\nu_A)}{E_A^2}r_{i,A} - \left(\frac{1+\nu_A}{E_A^2}\right)\left(\frac{r_{o,A}^2}{r_{i,A}}\right)\right]^2 U_{E_A}^2 \\ + \left[\left(\frac{1-\nu_A}{E_A}\right) - \left(\frac{1+\nu_A}{E_A}\right)\left(\frac{r_{o,A}^2}{r_{i,A}^2}\right)\right]^2 U_r^2 + \left[2\left(\frac{1+\nu_A}{E_A}\right)\left(\frac{r_{o,A}}{r_{i,A}}\right)U_r\right]^2\end{array}\right\}^{\frac{1}{2}} \tag{E.41}$$

$$DD = \frac{r_{o,B}^2}{r_{o,B}^2 - r_{i,B}^2}$$

$$U_{DD} = \left\{ \left[\frac{2 r_{o,B}^2 r_{i,B}}{\left(r_{o,B}^2 - r_{i,B}^2\right)^2} U_r \right]^2 + \left[\frac{2 r_{o,B}^3}{\left(r_{o,B}^2 - r_{i,B}^2\right)^2} U_r \right]^2 + \left[\frac{2 r_{o,B}}{\left(r_{o,B}^2 - r_{i,B}^2\right)} U_r \right]^2 \right\}^{\frac{1}{2}} \quad \text{(E.42)}$$

$$EE = \left(\frac{1 - \nu_B}{E_B} \right) r_{o,B} + \left(\frac{1 + \nu_B}{E_B} \right) \left(\frac{r_{i,B}^2}{r_{o,B}} \right)$$

$$U_{EE} = \left\{ \begin{array}{l} \left[\left[\left(\frac{-r_{o,B}}{E_B} \right) + \left(\frac{1}{E_A} \right) \left(\frac{r_{i,B}^2}{r_{o,B}} \right) \right]^2 U_{\nu_B}^2 + \left[-\frac{(1 - \nu_B)}{E_B^2} r_{i,A} - \left(\frac{1 + \nu_B}{E_B^2} \right) \left(\frac{r_{i,B}^2}{r_{o,B}} \right) \right]^2 U_{E_B}^2 \right. \\ \left. + \left[\left(\frac{1 - \nu_B}{E_B} \right) - \left(\frac{1 + \nu_B}{E_B} \right) \left(\frac{r_{i,B}^2}{r_{o,B}^2} \right) \right]^2 U_r^2 + \left[2 \left(\frac{1 + \nu_B}{E_B} \right) \left(\frac{r_{i,B}}{r_{o,B}} \right) U_r \right]^2 \right\}^{\frac{1}{2}} \end{array} \quad \text{(E.43)}$$

The uncertainty of the interface pressure relation is then:

$$U_{\sigma_I} = \left\{ \begin{array}{l} \left[\frac{U_{AA}}{DI} \right]^2 + \left[\frac{AA\ CC}{DI^2} U_{BB} \right]^2 + \left[\frac{AA\ BB}{DI^2} U_{CC} \right]^2 \\ + \left[\frac{AA\ EE}{DI^2} U_{DD} \right]^2 + \left[\frac{AA\ DD}{DI^2} U_{EE} \right]^2 \end{array} \right\}^{\frac{1}{2}} \quad \text{(E.44)}$$

Case II

Similarly, when the effects of the longitudinal stress are included, (Equation D.45):

$$\sigma_{II} = \frac{\hat{r}_{o,B} - \hat{r}_{i,A} + \Phi_L}{\left\{ \begin{array}{l} \left(\frac{r_{i,A}^2}{r_{o,A}^2 - r_{i,A}^2}\right)\left[\left(\frac{1-\nu_A}{E_A}\right) r_{i,A} + \left(\frac{1+\nu_A}{E_A}\right)\left(\frac{r_{o,A}^2}{r_{i,A}}\right)\right] \\ + \left(\frac{r_{o,B}^2}{r_{o,B}^2 - r_{i,B}^2}\right)\left[\left(\frac{1-\nu_B}{E_B}\right) r_{o,B} + \left(\frac{1+\nu_B}{E_B}\right)\left(\frac{r_{i,B}^2}{r_{o,B}}\right)\right] \\ - \left[2\left(\frac{\nu_A r_{i,A}}{E_A}\right) \frac{\left[\left(\frac{\nu_A r_{i,A}^2}{r_{o,A}^2 - r_{i,A}^2}\right) + \frac{E_A}{E_B}\left(\frac{\nu_B r_{o,B}^2}{r_{o,B}^2 - r_{i,B}^2}\right)\right]}{\left[1 + \frac{E_A}{E_B}\frac{\left(r_{o,A}^2 - r_{i,A}^2\right)}{\left(r_{o,B}^2 - r_{i,B}^2\right)}\right]} \right] \\ + \left(\frac{\nu_B r_{o,B}}{E_B}\right)\frac{\left(r_{o,A}^2 - r_{i,A}^2\right)}{\left(r_{o,B}^2 - r_{i,B}^2\right)} \left[2 \frac{\left[\left(\frac{\nu_A r_{i,A}^2}{r_{o,A}^2 - r_{i,A}^2}\right) + \frac{E_A}{E_B}\left(\frac{\nu_B r_{o,B}^2}{r_{o,B}^2 - r_{i,B}^2}\right)\right]}{\left[1 + \frac{E_A}{E_B}\frac{\left(r_{o,A}^2 - r_{i,A}^2\right)}{\left(r_{o,B}^2 - r_{i,B}^2\right)}\right]} \right] \end{array} \right\}} \tag{E.45}$$

To facilitate an uncertainty analysis, this is broken into pieces:

$$\sigma_{II} = \frac{FF}{DII}$$
$$DII = BB\ CC + DD\ EE - GG\ HH + GG\ II\ JJ \tag{E.46}$$

$$FF = \hat{r}_{o,B} - \hat{r}_{i,A} + \Phi_L$$
$$U_{FF} = \left\{ U_{AA}^2 + U_{\Phi_L}^2 \right\}^{\frac{1}{2}} \tag{E.47}$$

Recalling that the longitudinal thermal expansion term is defined in Equation D.44,

$$\Phi_L \equiv \left[\left(\frac{\nu_A r_{i,A}}{E_A}\right) - \left(\frac{\nu_B r_{o,B}}{E_B}\right)\frac{\left(r_{o,A}^2 - r_{i,A}^2\right)}{\left(r_{o,B}^2 - r_{i,B}^2\right)}\right] \frac{\left(\alpha_B \Delta T_B(r_{o,B}) - \alpha_A \Delta T_A(r_{i,B})\right) E_A}{\left[1 + \frac{E_A}{E_B}\frac{\left(r_{o,A}^2 - r_{i,A}^2\right)}{\left(r_{o,B}^2 - r_{i,B}^2\right)}\right]} \tag{E.48}$$

Again, to facilitate an uncertainty analysis, this relation is broken into pieces:

$$\Phi_L \equiv \frac{LA\,LB}{LC} \tag{E.49}$$

$$LA = \left(\frac{\nu_A r_{i,A}}{E_A}\right) - \left(\frac{\nu_B r_{o,B}}{E_B}\right)\frac{\left(r_{o,A}^2 - r_{i,A}^2\right)}{\left(r_{o,B}^2 - r_{i,B}^2\right)}$$

$$U_{LA} = \left\{ \begin{array}{l} \left[\frac{r_{i,A}}{E_A} U_{\nu_A}\right]^2 + \left[\frac{\nu_A r_{i,A}}{E_A^2} U_{E_A}\right]^2 + \left[\left(\frac{\nu_A}{E_A}\right) + \left(\frac{\nu_B r_{o,B}}{E_B}\right)\frac{r_{i,A}}{\left(r_{o,B}^2 - r_{i,B}^2\right)}\right]^2 U_r^2 \\ + \left[\left(\frac{\nu_B r_{o,B}}{E_B}\right)\frac{r_{o,A}}{\left(r_{o,B}^2 - r_{i,B}^2\right)} U_r\right]^2 + \left[\left(\frac{r_{o,B}}{E_B}\right)\frac{\left(r_{o,A}^2 - r_{i,A}^2\right)}{\left(r_{o,B}^2 - r_{i,B}^2\right)} U_{\nu_B}\right]^2 \\ + \left[\left(\frac{\nu_B r_{o,B}}{E_B^2}\right)\frac{\left(r_{o,A}^2 - r_{i,A}^2\right)}{\left(r_{o,B}^2 - r_{i,B}^2\right)} U_{E_B}\right]^2 + \left[2\left(\frac{\nu_B r_{o,B}}{E_B}\right)\frac{\left(r_{o,A}^2 - r_{i,A}^2\right)}{\left(r_{o,B}^2 - r_{i,B}^2\right)^2} r_{i,B} U_r\right]^2 \\ + \left[-\left(\frac{\nu_B}{E_B}\right)\frac{\left(r_{o,A}^2 - r_{i,A}^2\right)}{\left(r_{o,B}^2 - r_{i,B}^2\right)} + \left(\frac{2\nu_B r_{o,B}^2}{E_B}\right)\frac{\left(r_{o,A}^2 - r_{i,A}^2\right)}{\left(r_{o,B}^2 - r_{i,B}^2\right)^2}\right]^2 U_r^2 \end{array} \right\}^{\frac{1}{2}} \tag{E.50}$$

$$LB = \left(\alpha_B \Delta T_B\left(r_{o,B}\right) - \alpha_A \Delta T_A\left(r_{i,B}\right)\right) E_A$$

$$U_{LB} = \left\{ \begin{array}{l} \left[E_A \Delta T_B\left(r_{o,B}\right) U_{\alpha_B}\right]^2 + \left[E_A \alpha_B SE_{TB}\right]^2 \\ \left[E_A \Delta T_A\left(r_{i,A}\right) U_{\alpha_A}\right]^2 + \left[E_A \alpha_A SE_{TA}\right]^2 \\ + \left[\left(\alpha_B \Delta T_B\left(r_{o,B}\right) - \alpha_A \Delta T_A\left(r_{i,B}\right)\right) U_{E_A}\right]^2 \end{array} \right\}^{\frac{1}{2}} \tag{E.51}$$

$$LC = \left[1 + \frac{E_A}{E_B}\frac{\left(r_{o,A}^2 - r_{i,A}^2\right)}{\left(r_{o,B}^2 - r_{i,B}^2\right)}\right]$$

$$U_{LC} = \left\{\begin{aligned}&\left[\frac{1}{E_B}\frac{\left(r_{o,A}^2 - r_{i,A}^2\right)}{\left(r_{o,B}^2 - r_{i,B}^2\right)}U_{E_A}\right]^2 + \left[\frac{E_A}{E_B^2}\frac{\left(r_{o,A}^2 - r_{i,A}^2\right)}{\left(r_{o,B}^2 - r_{i,B}^2\right)}U_{E_B}\right]^2 \\ &+\left[\frac{2E_A}{E_B}\frac{r_{o,A}}{\left(r_{o,B}^2 - r_{i,B}^2\right)}U_r\right]^2 + \left[\frac{2E_A}{E_B}\frac{r_{i,A}}{\left(r_{o,B}^2 - r_{i,B}^2\right)}U_r\right]^2 \\ &+\left[\frac{2E_A}{E_B}\frac{\left(r_{o,A}^2 - r_{i,A}^2\right)}{\left(r_{o,B}^2 - r_{i,B}^2\right)^2}r_{o,B}U_r\right]^2 + \left[\frac{2E_A}{E_B}\frac{\left(r_{o,A}^2 - r_{i,A}^2\right)}{\left(r_{o,B}^2 - r_{i,B}^2\right)^2}r_{i,B}U_r\right]^2\end{aligned}\right\} \tag{E.52}$$

$$U_{\Phi_L} = \left\{\left[\frac{LB}{LC}U_{LA}\right]^2 + \left[\frac{LA}{LC}U_{LB}\right]^2 + \left[\frac{LALB}{LC^2}U_{LC}\right]^2\right\}^{\frac{1}{2}} \tag{E.53}$$

$$GG = \frac{\left(\frac{\nu_A r_{i,A}^2}{r_{o,A}^2 - r_{i,A}^2}\right) + \frac{E_A}{E_B}\left(\frac{\nu_B r_{o,B}^2}{r_{o,B}^2 - r_{i,B}^2}\right)}{LC}$$

$$U_{GG} = \left\{\begin{aligned}&\left[\frac{r_{i,A}^2}{r_{o,A}^2 - r_{i,A}^2}\frac{U_{\nu_A}}{LC}\right]^2 + \left[\frac{2\nu_A r_{i,A}^2 r_{o,A}}{\left(r_{o,A}^2 - r_{i,A}^2\right)^2}\frac{U_r}{LC}\right]^2 + \left[\frac{2\nu_A r_{o,A}^2 r_{i,A}}{\left(r_{o,A}^2 - r_{i,A}^2\right)^2}\frac{U_R}{LC}\right]^2 \\ &+\left[\frac{\nu_B}{E_B}\frac{r_{o,B}^2}{r_{o,B}^2 - r_{i,B}^2}\frac{U_{E_A}}{LC}\right]^2 + \left[\frac{E_A}{E_B^2}\frac{\nu_B r_{o,B}^2}{r_{o,B}^2 - r_{i,B}^2}\frac{U_{E_B}}{LC}\right]^2 + \left[\frac{E_A}{E_B}\frac{r_{o,B}^2}{r_{o,B}^2 - r_{i,B}^2}\frac{U_{\nu_B}}{LC}\right]^2 \\ &+\left[2\frac{E_A}{E_B}\frac{\nu_B r_{o,B} r_{i,B}^2}{\left(r_{o,B}^2 - r_{i,B}^2\right)^2}\frac{U_R}{LC}\right]^2 + \left[2\frac{E_A}{E_B}\frac{\nu_B r_{i,B} r_{o,B}^2}{\left(r_{o,B}^2 - r_{i,B}^2\right)^2}\frac{U_r}{LC}\right]^2 + \left[\frac{GG}{LC}U_{LC}\right]^2\end{aligned}\right\}^{\frac{1}{2}} \tag{E.54}$$

$$HH = 2\left(\frac{\nu_A r_{i,A}}{E_A}\right)$$

$$U_{HH} = \left\{\left[\frac{2r_{i,A}}{E_A}U_{\nu_A}\right]^2 + \left[\frac{2\nu_A}{E_A}U_r\right]^2 + \left[\frac{\nu_A r_{i,A}}{E_A^2}U_{E_A}\right]^2\right\}^{\frac{1}{2}} \tag{E.55}$$

$$II = 2\left(\frac{\nu_B r_{o,B}}{E_B}\right)$$

$$U_{II} = \left\{\left[\frac{2r_{o,B}}{E_B}U_{\nu_B}\right]^2 + \left[\frac{2\nu_B}{E_B}U_r\right]^2 + \left[\frac{\nu_B r_{o,B}}{E_B^2}U_{E_B}\right]^2\right\}^{\frac{1}{2}} \tag{E.56}$$

$$JJ = \frac{\left(r_{o,A}^2 - r_{i,A}^2\right)}{\left(r_{o,B}^2 - r_{i,B}^2\right)}$$

$$U_{JJ} = \left\{\begin{array}{l}\left[\frac{2r_{o,A}}{r_{o,B}^2 - r_{i,B}^2}U_R\right]^2 + \left[\frac{2r_{i,A}}{r_{o,B}^2 - r_{i,B}^2}U_r\right]^2 \\ + \left[2\frac{\left(r_{o,A}^2 - r_{i,A}^2\right)}{\left(r_{o,B}^2 - r_{i,B}^2\right)^2}r_{o,B}U_r\right]^2 + \left[2\frac{\left(r_{o,A}^2 - r_{i,A}^2\right)}{\left(r_{o,B}^2 - r_{i,B}^2\right)^2}r_{i,B}U_R\right]^2\end{array}\right\}^{\frac{1}{2}} \tag{E.57}$$

The uncertainty of σ_{II} is then:

$$U_{\sigma_{II}} = \left\{\begin{array}{l}\left[\frac{U_{FF}}{DII}\right]^2 + \left[\frac{FF\ CC}{DII^2}U_{BB}\right]^2 + \left[\frac{FF\ BB}{DII^2}U_{CC}\right]^2 \\ + \left[\frac{FF\ EE}{DII^2}U_{DD}\right]^2 + \left[\frac{FF\ DD}{DII^2}U_{EE}\right]^2 + \left[\frac{FF(II\ JJ - HH)}{DII^2}U_{GG}\right]^2 \\ + \left[\frac{FF\ GG}{DII^2}U_{HH}\right]^2 + \left[\frac{FF\ GG\ II}{DII^2}U_{JJ}\right]^2 + \left[\frac{FF\ GG\ JJ}{DII^2}U_{II}\right]^2\end{array}\right\}^{\frac{1}{2}} \tag{E.58}$$

Case III

As developed in Equation D.49, the stress at the interface due to differential thermal expansion of the two shells can be determined using the known temperature distribution in the outer cylinder and the corrected strains in the circumferential and longitudinal directions:

$$\sigma_{III} = \frac{\frac{\Delta\theta}{\theta} r^{\circ}_{o,A} + r_{o,A} - \hat{r}_{o,A}}{\left[\left(\frac{1-\nu_A}{E_A}\right) r_{o,A} + \left(\frac{1+\nu_A}{E_A}\right)\left(\frac{r^2_{i,A}}{r_{o,A}}\right)\right]\left(\frac{r^2_{o,A}}{r^2_{o,A} - r^2_{i,A}}\right)} \tag{E.59}$$

or

$$\sigma_{III} = \frac{KK}{LL\ MM} \tag{E.60}$$

by parts:

$$\begin{aligned} KK &= \varepsilon_\theta\, r^{\circ}_{o,A} + r_{o,A} - \hat{r}_{o,A} \\ U_{KK} &= \left\{\left[r^{\circ}_{o,A} U_{\varepsilon_\theta}\right]^2 + \left[2 + \varepsilon^2_\theta\right] U^2_R\right\}^{\frac{1}{2}} \end{aligned} \tag{E.61}$$

$$\begin{aligned} LL &= \frac{r^2_{o,A}}{r^2_{o,A} - r^2_{i,A}} \\ U_{LL} &= \left\{\left[\frac{2 r_{o,A}}{r^2_{o,A} - r^2_{i,A}} - \frac{2 r^3_{o,A}}{\left(r^2_{o,A} - r^2_{i,A}\right)}\right]^2 U^2_R + \left[\frac{2 r^2_{o,A}\, r_{i,A}}{\left(r^2_{o,A} - r^2_{i,A}\right)^2} U_r\right]^2\right\}^{\frac{1}{2}} \end{aligned} \tag{E.62}$$

$$MM = \left(\frac{1-\nu_A}{E_A}\right) r_{o,A} + \left(\frac{1+\nu_A}{E_A}\right)\left(\frac{r_{i,A}^2}{r_{o,A}}\right)$$

$$U_{MM} = \left\{ \begin{array}{l} \left[\left(\frac{-r_{o,A}}{E_A}\right) + \left(\frac{1}{E_A}\right)\left(\frac{r_{o,A}^2}{r_{i,A}}\right)\right]^2 U_{\nu_A}^2 + \left[-\frac{(1-\nu_A)}{E_A^2} r_{o,A} - \left(\frac{1+\nu_A}{E_A^2}\right)\left(\frac{r_{o,A}^2}{r_{i,A}}\right)\right]^2 U_{E_A}^2 \\ + \left[\left(\frac{1-\nu_A}{E_A}\right) + 2\left(\frac{1+\nu_A}{E_A}\right)\left(\frac{r_{o,A}}{r_{i,A}}\right)\right]^2 U_R^2 + \left[\left(\frac{1+\nu_A}{E_A}\right)\left(\frac{r_{o,A}^2}{r_{i,A}^2}\right) U_r\right]^2 \end{array} \right\}^{\frac{1}{2}} \quad \text{(E.63)}$$

Thus,

$$U_{\sigma_{III}} = \left\{\left[\frac{U_{KK}}{LL}\right]^2 + \left[\frac{KK\, U_{LL}}{LL^2\, MM}\right]^2 + \left[\frac{KK\, U_{MM}}{LL\, MM^2}\right]^2\right\}^{\frac{1}{2}} \quad \text{(E.64)}$$

Table E.4 – Calculated Values and Associated Uncertainties for AL-6061 - SS-304 700W Test

Parameter	Value	Absolute Uncertainty	Percent Uncertainty
r_i	2.5380E-02	5.2480E-05	0.207%
A_i	2.0250E-02	7.9844E-04	3.943%
SE_{TA}	1.7982E+00	—	—
SE_{TB}	9.9000E-02	—	—
T_i	3.5619E+02	9.0047E-01	0.253%
ΔT_i	3.9862E+01	1.8010E+00	4.518%
m_A	-6.2899E+01	4.9715E+00	7.904%
b_A	1.0519E+02	1.7982E+00	1.709%
m_B	-1.2205E+00	1.4843E-01	12.161%
b_B	3.7162E+02	9.9000E-02	0.027%
$\overline{T}_A$	3.1080E+02	3.8025E+00	1.223%
$\overline{T}_B$	3.7660E+02	1.3263E-01	0.035%
q''_i	3.5467E+04	2.9974E+03	8.451%
h_c	8.8976E+02	8.5267E+01	9.583%
q_{rad}	3.5247E+00	1.3431E-01	3.811%
$\Delta\varepsilon_\theta$	9.5710E-05	3.5834E-05	37.439%
$\Delta\varepsilon_z$	-1.6974E-04	5.6185E-05	33.100%
σ_I	7.2478E+07	8.1790E+06	11.285%
σ_{II}	5.0203E+07	7.2747E+06	14.491%
Φ_L	-8.5829E-06	1.1791E-06	13.738%
σ_{III}	1.3474E+07	6.4256E+06	47.689%
AA	4.0354E-05	4.2992E-06	10.654%
BB	3.5904E-01	1.3135E-04	0.037%
CC	7.4144E-13	3.7491E-14	5.057%
DD	1.0668E+00	7.0177E-05	0.007%
EE	2.7237E-13	1.4759E-14	5.419%

Table E.4 (continued)

Parameter	Value	Absolute Uncertainty	Percent Uncertainty
FF	3.1771E-05	4.4580E-06	14.032%
GG	1.1912E-01	1.1950E-02	10.032%
HH	8.0267E-14	5.6757E-15	7.071%
II	2.4274E-13	1.7164E-14	7.071%
JJ	2.9619E+00	9.5725E-04	0.032%
KK	1.5161E-05	4.3028E-06	28.381%
LL	1.3590E+00	1.3135E-04	0.010%
MM	8.2792E-13	4.1560E-14	5.020%
LA	3.1934E-13	2.5577E-14	8.009%
LB	2.4636E+08	2.2699E+07	9.214%
LC	9.1726E+00	2.5592E-14	8.009%

Table E.5 – Calculated Values and Associated Uncertainties for AL-6061 - SS-304 300W Test

Parameter	Value	Absolute Uncertainty	Percent Uncertainty
r_i	2.5380E-02	5.2480E-05	0.207%
A_i	2.0250E-02	7.9844E-04	3.943%
SE_{TA}	5.5899E-02	—	—
SE_{TB}	9.1365E-01	—	—
T_i	3.2986E+02	4.5768E-01	0.139%
ΔT_i	3.8049E+01	9.1536E-01	2.406%
m_A	-3.2534E+01	2.5453E+00	7.824%
b_A	1.913E+02	5.5899E-02	0.029%
m_B	-1.0133E-01	5.7762E-02	57.001%
b_B	3.4851E+02	9.1365E-01	0.262%
$\overline{T}_A$	2.9768E+02	1.9431E+00	0.652%
$\overline{T}_B$	3.4892E+02	6.6407E-02	0.002%
q''_i	5.6847E+01	1.8033E+04	31722%
h_c	1.4940E+00	4.7394E+02	31722%
q_{rad}	1.7254E+00	7.8005E-02	4.521%
$\Delta\varepsilon_\theta$	-5.0739E-06	8.3765E-06	165.089%
$\Delta\varepsilon_z$	-9.6557E-05	8.4121E-06	8.712%
σ_I	1.5993E+07	4.0868E+06	25.554%
σ_{II}	1.6044E+07	4.0961E+06	25.530%
Φ_L	3.6018E-08	2.0991E-07	582.790%
σ_{III}	-1.1777E+06	1.3822E+06	117.363%
AA	1.3652E-05	4.2992E-06	31.491%
BB	3.5924E-01	1.3146E-04	0.004%
CC	2.0727E-12	1.0500E-13	5.066%
DD	1.0668E+00	7.0226E-05	0.007%
EE	1.0225E-13	5.4477E-15	5.328%

Table E.5 (continued)

Parameter	Value	Absolute Uncertainty	Percent Uncertainty
FF	1.3688E-05	4.3043E-06	31.446%
GG	1.1465E-01	7.0882E-03	6.183%
HH	2.4233E-13	1.7135E-14	7.071%
II	2.0304E-14	5.678E-15	7.071%
JJ	2.9663E+00	9.5952E-04	0.032%
KK	-3.6835E-06	4.3191E-06	117.255%
LL	1.3592E+00	1.3146E-04	0.010%
MM	2.3010E-12	1.1559E-13	5.0234%
LA	2.0618E-15	1.2014E-14	582.693%
LB	3.6264E+07	3.6275E+06	10.003%
LC	2.0759E+00	7.6080E-02	3.660%

VITA

George Harold Ayers

3015 N 103rd Avenue

Avondale, AZ 85323

George Harold Ayers was born in Buffalo, New York and grew up west of Phoenix, Arizona in Maricopa County. He attended Pendergast Elementary School and Tolleson Union High School before being admitted to Arizona State University in the Department of Mechanical and Aerospace Engineering. There, he earned a Batchelor of Science degree (1990) and a Master of Science degree (1993), both in mechanical engineering with an emphasis in heat transfer and thermodynamics.